Pontifícia Universidade Católica
do Rio de Janeiro

Tálita Coffler Botti Braz

Effect of Interfacial Rheology on the Stability of Water-Oil Emulsion

Tese de Doutorado

Thesis presented to the Programa de Pós–graduação em Engenharia Mecânica of PUC-Rio in partial fulfillment of the requirements for the degree of Doutor em Engenharia Mecânica.

Advisor : Prof. Márcio da Silveira Carvalho
Co-advisor: Ph.D. Anthony Pierre Jack Hutin

Rio de Janeiro
August 2022

Pontifícia Universidade Católica
do Rio de Janeiro

Tálita Coffler Botti Braz

Effect of Interfacial Rheology on the Stability of Water-Oil Emulsion

Thesis presented to the Programa de Pós–graduação em Engenharia Mecânica of PUC-Rio in partial fulfillment of the requirements for the degree of Doutor em Engenharia Mecânica. Approved by the Examination Committee.

Prof. Márcio da Silveira Carvalho
Advisor
Departamento de Engenharia Mecânica – PUC-Rio

Ph.D. Anthony Pierre Jack Hutin
Co-advisor
Laboratório de Microhidrodinâmica e Escoamento em Meios Porosos (LMMP) – PUC-Rio

Prof. Aurora Pérez Gramatges
Departamento de Química – PUC-Rio

Prof. Cari Dutcher
University of Minnesota –

Prof. Paulo Roberto de Souza Mendes
Departamento de Engenharia Mecânica – PUC-Rio

Prof. Roney Leon Thompson
Departamento de Engenharia Mecânica – UFRJ

Rio de Janeiro, August the 18th, 2022

Tálita Coffler Botti Braz

Tálita Botti graduated in Petroleum Engineer at the Universidade Federal do Espírito Santo (UFES) in 2011. In 2014, she earned a Master's degree in Mechanical Engineering from the Pontifícia Universidade Católica of Rio de Janeiro (PUC-Rio). Since 2014, she has been working in the Laboratory of Microhydrodynamics and Flow in Porous Media (LMMP) at PUC-Rio involved in projects with Equinor, Sintef and Petrobras.

Bibliographic data

Braz, Tálita Coffler Botti

Effect of Interfacial Rheology on the Stability of Water-Oil Emulsion / Tálita Coffler Botti Braz; advisor: Márcio da Silveira Carvalho; co-advisor: Anthony Pierre Jack Hutin. - 2022.

118 f.: il. color. ; 30 cm

Tese (doutorado) - Pontifícia Universidade Católica do Rio de Janeiro, Departamento de Engenharia Mecânica, 2022

Inclui bibliografia

1. Engenharia Mecânica – Teses. 2. Estabilidade de Emulsões. 3. Reologia Interfacial. 4. Coalescência. 5. Emulsificação Espontânea. 6. Desestabilização de Emulsões. I. Carvalho, Márcio da Silveira. II. Hutin, Anthony Pierre Jack. III. Pontifícia Universidade Católica do Rio de Janeiro. Departamento de Engenharia Mecânica. IV. Título.

CDD: 621

I dedicate this work to God and
to my family (Wanderson, Liz, Samuel and Clara), with love.

Acknowledgments

First of all, I would like to thank God, the author of my life and who gives me strength every day to keep going.

I also thank my husband and my children, to be my daily motivation, my support, inspiration and love.

To my parents, my sister and brother-in-law, to their love and support.

I would like to thank my advisor, Professor Márcio, for all encouragement and academic support during this time.

I also thank my co-advisor, Ph.D. Anthony, for sharing his technical knowledge and his time in the lab with me.

To my friends at LMMP, I thank you to share great moments, talks, help and knowledge, each one of you contributed to the succesfull of this thesis. I also thank to my friends from the Ph.D program to share with me this journey.

To my community friends who supported me in prayer, it is very good to always be able to count on you.

To CNPq, PUC-Rio and Petrobras, for the financial support. This study was financed in part by the Coordenação de Aperfeiçoamento de Pessoal de Nível Superior - Brasil (CAPES) - Finance Code 001.

To everyone who were present during this period and contributed in some way to my journey.

Abstract

Braz, Tálita Coffler Botti; Carvalho, Márcio da Silveira (Advisor); Hutin, Anthony Pierre Jack (Co-Advisor). **Effect of Interfacial Rheology on the Stability of Water-Oil Emulsion**. Rio de Janeiro, 2022. 118p. Tese de doutorado – Departamento de Engenharia Mecânica, Pontifícia Universidade Católica do Rio de Janeiro.

Several studies have been conducted to understand emulsions formation and stability. In some situations, it is desirable to have stable emulsions; in others, phase separation through drop coalescence is beneficial. In both cases, it is important to understand the mechanisms associated to the coalescence process. The present work investigates the relationship between rheological properties of oil-water interfaces and the drainage time of a thin oil film between two aqueous drops. Interfacial tension and dilatational rheology were measured using the axisymmetric drop shape analysis. We evaluated different concentrations of a nonionic surfactant (Span 80) dissolved in mineral oil (Primol 352) phase. The results indicate a direct relationship between the properties of the structure formed at the oil-water interface and the absence of droplet coalescence. For low surfactant concentrations, below the critical micelle concentration (CMC), the interface is weakly elastic (fluid-like) and the coalescence process always occurs; the draining time is not to related to the aging time of the interface. For surfactant concentrations above CMC, the elastic and viscous moduli showed significant changes with aging leading to the formation of a solid-like film at the interface preventing further coalescence. We used a drop/drop coalescence experiments to evaluate the effect of interfacial rheology on the coalescence dynamics. To better understand the phenomenon of non-coalescence, we study the structure of interfacial film microscopically and observe the appearance of small water droplets formed at the interface by spontaneous emulsification. We found that the emergence rate of these microdroplets is directly related to the surfactant concentration. As the surfactant concentration increases, faster the spontaneous emulsification process occurs, which confirms the results obtained with the interfacial rheology. Finally, a new method to promote emulsion destabilization by imposing a perturbation of the interfacial film by flowing the drops through constricted capillaries is proposed and tested.

Keywords

Emulsions Stability Interfacial Rheology Coalescence Spontaneous Emulsification Emulsion Destabilization

Resumo

Braz, Tálita Coffler Botti; Carvalho, Márcio da Silveira; Hutin, Anthony Pierre Jack. **Efeito da Reologia Interfacial na Estabilidade de Emulsões Água-Óleo**. Rio de Janeiro, 2022. 118p. Tese de Doutorado – Departamento de Engenharia Mecânica, Pontifícia Universidade Católica do Rio de Janeiro.

Inúmeros estudos têm sido realizados para melhor entender a formação e estabilidade de emulsões. Em algumas situações, é desejável ter emulsões estáveis; em outros, a separação de fases por coalescência de gotas é benéfica. Em ambos os casos, é importante entender os mecanismos associados ao processo de coalescência. O presente trabalho investiga a relação entre as propriedades reológicas das interfaces óleo-água e o tempo de drenagem de um filme fino de óleo entre duas gotas aquosas. A tensão interfacial e a reologia dilatacional interfacial foram medidas usando a análise axissimétrica da forma da gota. Foram avaliadas diferentes concentrações de um tensoativo não iônico (Span 80) dissolvido em óleo mineral (Primol 352). Os resultados indicam uma relação direta entre as propriedades da estrutura formada na interface óleo-água e a ausência de coalescência das gotas. Para concentrações de surfactante abaixo da concentração micelar crítica (CMC), a interface é fracamente elástica (fluid-like) e o processo de coalescência sempre ocorre; o tempo de drenagem não está relacionado ao tempo de envelhecimento da interface. Para concentrações de surfactante acima da CMC, os módulos elástico e viscoso mostraram mudanças significativas com o envelhecimento, levando à formação de um filme sólido na interface, impedindo a coalescência entre as gotas. Usamos experimentos de coalescência gota/gota para avaliar o efeito da reologia interfacial na dinâmica de coalescência. Para entender melhor o fenômeno da não coalescência, estudamos microscopicamente a estrutura do filme interfacial e observamos o aparecimento de pequenas gotas de água formadas na interface através de emulsificação espontânea. Descobrimos que a taxa de surgimento dessas microgotículas está diretamente relacionada à concentração de surfactante. À medida que a concentração de surfactante aumenta, mais rápido ocorre o processo de emulsificação espontânea, o que confirma os resultados obtidos com a reologia interfacial. Finalmente, um novo método para promover a desestabilização da emulsão impondo uma perturbação do filme interfacial pelo escoamento das gotas através de capilares constritos é proposto e testado.

Palavras-chave

Estabilidade de Emulsões Reologia Interfacial Coalescência Emulsificação Espontânea Desestabilização de Emulsões

Table of contents

1 Introduction **17**
1.1 Motivation 17
1.2 Objectives 20
1.3 Outline 21

2 Background and Literature Review **22**
2.1 Emulsions 22
2.2 Surfactants 23
2.3 Emulsion Stability 25
2.3.1 Literature Review of the Coalescence Process 26
2.3.1.1 Coalescence in the absence of surfactant 30
2.3.1.2 Coalescence in the presence of surfactant 34
2.4 Interfacial Rheology 38
2.4.1 Shear Rheology 39
2.4.2 Dilatational Rheology 40

3 Materials and Interfacial Rheological Properties **42**
3.1 Materials 42
3.2 Interfacial Rheological Experiments 43
3.2.1 Pendant Drop Technique 43
3.2.2 IFT measurements 46
3.3 Results of the Interfacial Rheological Characterization 48
3.3.1 Interfacial tension 49
3.3.2 Interfacial Dilatational Rheology 53
3.4 Brief conclusions 57

4 Relationship between interfacial properties and drop coalescence **59**
4.1 Experimental Procedure 59
4.1.1 Coalescence between two drops 59
4.1.2 Emulsion stability 64
4.2 Results and Discussion 67
4.2.1 Coalescence of two drops 67
4.2.2 Stability of emulsions 73
4.3 Brief conclusions 76

5 Structure of the film formed at the oil-water interface **78**
5.1 Observation of the structure formed at the interface of water drops 78
5.2 Spontaneous emulsification 79
5.3 Experimental Procedure 82
5.4 Results 84
5.5 Brief conclusions 89

6 Destabilization of water-oil emulsion breaking the interfacial structure **91**
6.1 Experimental Procedures 91

6.2 Results and Discussion 94
6.2.1 Behavior of a single drop passing through a constriction 94
6.2.2 Evaluation of interface cleanliness for produced emulsions 100
6.3 Brief conclusions 103

7 Final remarks and suggestions for future work **104**

Bibliography **107**

List of figures

Figure 1.1 Projected energy demand. 17
Figure 1.2 Water injection scheme. 18
Figure 1.3 Example of separator system. 19
Figure 1.4 Example of coalescence process between two droplets 20

Figure 2.1 Classification of emulsions. 22
Figure 2.2 Graphic representation of a generic surfactant molecule. 23
Figure 2.3 Position of the different groups of surfactants on the scale HLB. 24
Figure 2.4 Surface tension as a function of surfactant concentration, highlighting the schematic cross-section through a spherical micelle both in water and in oil phases. 25
Figure 2.5 Instability mechanisms in the emulsion systems. 26
Figure 2.6 Microscale analysis of the coalescence process: (a) coalescence between a drop and a flat interface, (b) coalescence between two droplets of the same size, and (c)coalescence between two droplets using a microdevice. 27
Figure 2.7 Stages of coalescence process between drop-drop: (a) approaching of two drops and forming a film between them; (b) surfactant mass balance at the film interface; (c) balance of tangential stresses at the film interface 28
Figure 2.8 Coalescence process between a drop and a flat interface. 29
Figure 2.9 a) Droplet radius plotted as a function of Ohnesorge number for a combination of different fluids and (b) example of partial coalescence of a drop of water at the air/water interface. 30
Figure 2.10 (a) Experimental apparatus (b) sequence of images that show the growth of this bridge. 31
Figure 2.11 Photo sequences recording coalescence events for different fluid pairs with different ratio between surface tension: (a) $R = 1.09$; (b) $R = 0.91$ and (c) $R = 0.30$. In (a) a daughter drop was formed and downward moved. In (b) complete coalescence was observed and (c) a small daughter droplet was ejected upwards. 32
Figure 2.12 Three different channel configurations for droplet coalescence. 33
Figure 2.13 (a) Geometry of the drop melting device. On the left, the drops are generated and on the right, part of the channel that promotes their coalescence. (b) Representation of the three types of coalescence that occurs in this device. 33
Figure 2.14 Sequence images over time showing the destabilization of a pair of drops passing through a channel with an expansion: collision, relaxation, separation and fusion. 34
Figure 2.15 Film formats computed at four different time steps during film draining to: (a) clean interface and (b) surfactant interface. 35

Figure 2.16 Representative scheme of the influence of Marangoni stresses on the coalescence of droplets with different compositions. 36
Figure 2.17 Scheme of the interaction between asphaltene molecules and interface of the (a) water and (b) oil. 36
Figure 2.18 Schematic of the microfluidic device used by: (a) Li et al 2018; (b) Dudek et al 2019; and (c) Narayan et al (2020). 37

Figure 3.1 Molecule of the surfactant Span 80. 42
Figure 3.2 (a) Surface curvature of the droplet and (b) Coordinates of a point M of the drop surface. 44
Figure 3.3 Evolution of the area and the surface tension of a drop undergoing a sinusoidal variation. 45
Figure 3.4 Tracker Teclis tensiometer. 46
Figure 3.5 Dynamic interfacial tension for 1.5 %wt. of Span 80, during the oscillation of the drop volume at frequency of 0.05 Hz. (IFT: interfacial tension) 47
Figure 3.6 Example of repeatability of interfacial rheological tests conducted at 0.05 Hz and 10% amplitude for 0.5 and 1.5 %wt. Span 80 (E': elastic modulus, E": viscous modulus). 48
Figure 3.7 Droplet interface aging for different surfactant concentrations showing the formation of the solid-like interface. 49
Figure 3.8 Dynamic interfacial tension as a function of Span 80 concentration: a) low surfactant concentrations (b) high surfactant concentration. 51
Figure 3.9 Equilibrium interfacial tension as a function of Span 80 concentration (dash black lines simply guide the eye). 52
Figure 3.10 Interfacial tension and interfacial dilatational moduli E' and E" (10 % volume amplitude and 0.05 Hz frequency) for different Span 80 concentrations over the CMC. 54
Figure 3.11 Influence of oscillation frequencies on elastic modulus for 2 wt%. Span 80. 56
Figure 3.12 Influence of aging time on the interfacial properties of 2 %wt. Span 80. Oscillations of the interface are started after 0 min (squares), 10 min (circles), and 20 min (triangles) of aging. 57

Figure 4.1 Scheme for the experimental setup for the coalescence study. 60
Figure 4.2 Experimental set-up of the droplet coalescence, including: (A) pressure transducer, (B) syringe pump, (C) cuvette, (D) high speed system, (E) lift, and (F) computer. 60
Figure 4.3 (a) 3D printed base and (b) example of the experiments with this base inserted into the cuvette. 61
Figure 4.4 Sequence of images representing the process: starting with the drops formation (a-f), then they are let in rest to aging the interface (f), after that they are put in contact (g), and finally when the oil film between them is drainage occurs the rupture of the interfaces and the drops coalescence (h-l). 62

Figure 4.5 Diagram representing the steps of the coalescence process: (1) formation of the first droplet; (2) formation of the second droplet and aging time of the interfaces; (3) approximation of the drops and oil film drainage time between them and (4) droplet coalescence. 62
Figure 4.6 Pressure data representing all the steps since the droplets formation until the coalescence process: (1) water drop formation, (2) aging time, (3) contact of the 2 drops, (4) drainage phase, (5) coalescence. 63
Figure 4.7 (a) Turbiscan LAB and (b) representation of the photos entering in the sample showing the difference between BS and T signal for a dispersion. 64
Figure 4.8 Representation of the phenomenon and the backscattering profile (ΔBS) corresponding. 66
Figure 4.9 Representation of mean free path l and l^*. 67
Figure 4.10 Separation of two water droplets that have not coalesced over time. 68
Figure 4.11 Drainage time for the Span 80 concentrations analyzed (lines simply guide the eye). 69
Figure 4.12 Frame sequences of coalescence experiment for 1) 2 $\%wt$. Span 80: (a) drops aging, (b) no coalescence after contact and (c-f) volume increase evidencing a solid-like "skin" without coalescence; and for 2) 1 $\%wt$. Span 80: (a) drops formation, (b) drops approximation after one hour of drops aging and, (c-f) coalescence phenomenon evidencing a fluid-like film. 71
Figure 4.13 Comparison between t_1, t_2, and the critical non-coalescence time t_c. 72
Figure 4.14 Turbidity over time for different Span 80 concentrations. Blue refers to the signal measured in transmission (T) for the transparent areas and orange to the backscattering (BS) for the opaque areas. 74
Figure 4.15 1 day picture of 30/70 water-in-oil emulsions at different Span 80 concentrations. 75
Figure 4.16 Average size of water drops over time for different Span 80 concentration. 76

Figure 5.1 Evidence of a skin on the experiments performed during the evaluation of the coalescence of the droplets. 78
Figure 5.2 Preliminary result showing the emergence of smaller droplets at the interface of the water drop along the time (0.25$\%wt$. of surfactant concentration). The left image shows a drop at the begin of experiment and the right image shows the drop after one day of aging. 79
Figure 5.3 (A) Schematic transversal view of the sample cell, top view image of the initial stage of the process and time evolution of the spontaneous crystalline structure formed on the spherical interface. (B) Schematic representation of the transversal view of the sample cell and an optical microscope image of the structure at the water–oil interface. 81

Figure 5.4 (a-c) images representing the results from the SE for low surfactant concentrations: shape of the water droplet at time $t = 19000s$, enlargement of the interface, and quantitative view of the interface structure, respectively. (d-f) the same sequence of images for the large concentrations of surfactant. 81
Figure 5.5 Schematic drawing of co-flow microfluidic device used to produce the droplets. 82
Figure 5.6 Experimental set-up for producing the droplets to evaluate the structure formed at the surface. 83
Figure 5.7 (a) microscope slide with a single depression cavity and (b) monitoring of the changes at the surface in a single water droplet. 83
Figure 5.8 (a-h) Images from different focal planes used to reconstruct a 3D image of the droplet and (i) final image. 84
Figure 5.9 Time evolution of the SE presented at the interface of the water droplet immersed in a oil solution with 0.25%wt. of Span 80. 85
Figure 5.10 Time evolution of the SE presented at the interface of the water droplet immersed in a oil solution with 0.50%wt. of Span 80. 85
Figure 5.11 Time evolution of the SE presented at the interface of the water droplet immersed in a oil solution with 2.0%wt. of Span 80. 86
Figure 5.12 Optical microscope image of the droplets detached from the original drop for all surfactant concentration studied, 24 h after sample preparation. 87
Figure 5.13 Time evolution of the SE presented at the interface of the water droplet immersed in a oil solution with 2.0%wt. of Span 80 varying the drop size. From the left for the right, the initial droplet size is 193, 394 and 650μm. 87
Figure 5.14 Time evolution of the SE presented at the interface of an emulsion with monodisperse water droplets of size around 400 μm, immersed in an oil phase of surfactant concentration equal 0.5 $\%wt$. 88
Figure 5.15 Drops from a monodispersed emulsion with water drops of size around 400 μm, immersed in an oil phase of surfactant concentration equal 0.5 $\%wt$. 88
Figure 5.16 A simplified schematic of the process proposed by Gonzales and Arauz (2007). (a) a multilayer of surfactant forms at the oil-water interface at the beginning of the process. (b) The film of surfactant swells and forms liquid bridges. (c) Those bridges undergoes an instability transition and breaks off in small water droplets, reducing the internal energy. 89

Figure 6.1 Scheme of the coaxial flow microfluidic device connected to the capillary with constriction. In this scheme is represented the cases enumerated in the text: case 1 - collection right after the production; case 2 - collection after the emulsions passing through a long line to allow the aging of the droplets; and case 3 - collection after the drops of the second case passing through the capillary with constriction. 92
Figure 6.2 Experimental set-up for the production and collection of the emulsions to evaluate their stability, including: (A) syringe pumps, (B) the coaxial flow microfluidic device, (C) an inverted optical microscope, (D) lines for collection and (E) a vial for collection of the emulsions produced. 93
Figure 6.3 Evolution of the drop position and behavior as it flows through the constriction. Surfactant concentration of 0.5%$wt.$ and drop without aging of the interface. 96
Figure 6.4 Evolution of the drop position and behavior as it flows through the constriction. Surfactant concentration of 0.5%$wt.$ and drop with one hour aging of the interface. 97
Figure 6.5 Evolution of the drop position and behavior as it flows through the constriction. Surfactant concentration of 0.5%$wt.$ and drop with two hour aging of the interface. 98
Figure 6.6 Drop position at capillary downstream showing its interface clean. Surfactant concentration of 0.5%$wt.$. 99
Figure 6.7 Evolution of the drop position and behavior as it flows through the constriction. Surfactant concentration of 0.5%$wt.$ and drop with 24 hours aging of the interface. The image from the left shows one drop passing through the constriction while the image from the right shows two drops that arrive together but are not connected. 99
Figure 6.8 Emulsions produced with surfactant concentration of 0.5%$wt.$. (C1) represents the collection of the drops right after the production. (C2) represents the condition of drop interface aging of one hour. And (C3) is a continuation of case 2, but drops pass through by a constriction before being collected. 100
Figure 6.9 Emulsions produced with surfactant concentration of 0.25%$wt.$. Case 1 represents the collection of the drops right after the production. Case 2 represents the condition of drop interface aging of one hour. And Case 3 is a continuation of case 2, but drops pass through by a constriction before being collected. 101
Figure 6.10 Emulsions produced with surfactant concentration of 2.0 %$wt.$. C1 represents the collection of the drops right after the production. And in the C3 the drops passed through by a constriction before being collected. 102

List of tables

Table 3.1 Properties of fluids measured at 23 ^oC. 43
Table 3.2 Density of fluids measured at 23 ^oC. 48
Table 3.3 γ_{eq} for concentrations below the CMC determined from long time experimental data and from Ward and Tordai fit. 52
Table 3.4 Characteristic times t_1 and t_2 of changes in modulus of elasticity as a function of Span 80 concentration. 55

Table 5.1 Formation flow rates for each drop size desired and surfactant concentration, Q_o (ml/h) and Q_w ($\mu l/min$). 83

Table 6.1 Formation flow rates for each surfactant concentration of emulsions analyzed and mean diameter obtained for each condition. 94
Table 6.2 Residence time for each case analyzed. 94

1
Introduction

1.1
Motivation

The modern history of oil and gas industry started in the 19^{th} century and is still today thriving despite competition from renewable sources of energy (Fig. 1.1). Oil is mainly used in the form of automotive fuels, such as gasoline and diesel oil, and is also burned in the operation of thermoelectric plants. In addition, it is an important raw material used in the manufacture of plastics, paints, synthetic rubbers, and many other products.

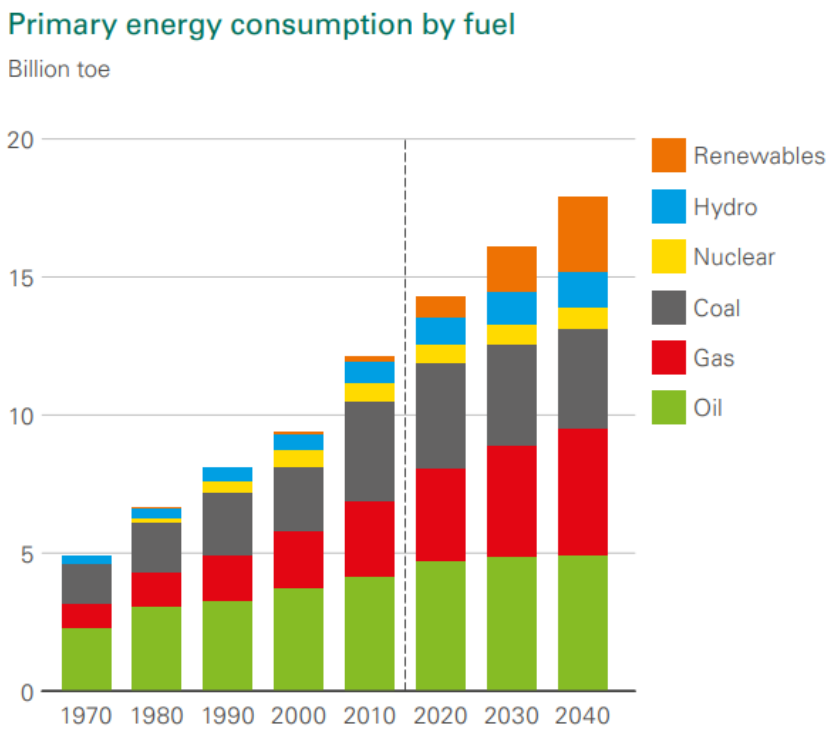

Figure 1.1: Projected energy demand [1].

Crude oil is found in association with gas and saline formation water [2] and the recovery process can occur by three main steps: primary, secondary, and tertiary. The primary one results from the displacement of the oil by

the natural energy existing in the reservoir. However, this process normally recovers only a small part of the initial oil, making it necessary to apply secondary recovery processes. This, in turn, results from the maintenance or increase of the natural energy of the reservoir through the injection of water or gas. The tertiary recovery methods nowadays can be used out of this chronological order according to the need and are better known as enhance oil recovery (EOR). Some examples of this technique are: thermal methods, such as steam injection or in situ combustion; miscible methods such as CO_2, natural gas and nitrogen injection; chemical methods such as injection of polymers, surfactants, and alkali.

Water injection is the most used secondary recovery technique, and consists of injecting water into wells located at the ends of the reservoirs. The injected water displaces the oil from the reservoir towards the producing well, as sketched in Fig. 1.2. After a certain time, the injected water starts to be produced. Although the fractions of water produced over the years increases, the growing energy demand justifies the greater exploitation of these reservoirs, even in those with large water cuts, until when the water production is so high that becomes economically unfeasible.

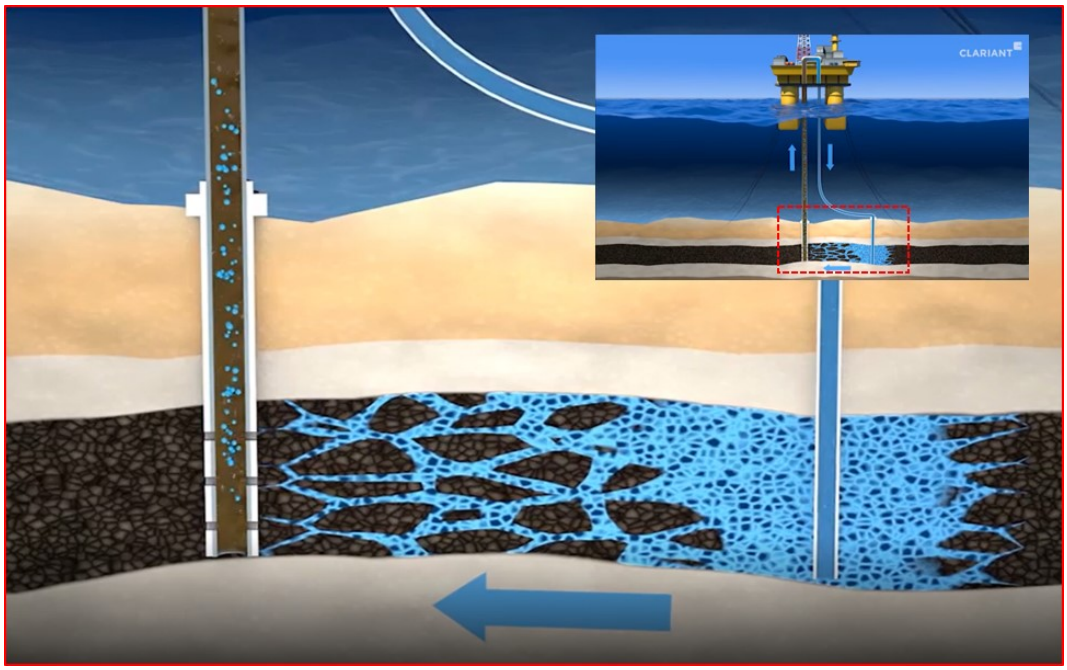

Figure 1.2: Water injection scheme [3].

The multiple phase flow of oil and water can result in the generation of emulsions (water-in-oil, w/o, or oil-in-water, o/w) during all the production

process [2, 4]. Emulsions are formed in the two-phase flow in reservoirs and through tubes, pumps, and valves [5]. These emulsions may cause several problems from production to refining, such as scale formation in ducts, storage tanks and pumps, loss of conversion efficiency of catalytic processes, and decrease in commercial value of the heavier fractions [6]. In addition, studies show that the viscosity of the w/o emulsions is substantially higher than the viscosity of the continuous hydrocarbon phase [7, 8], which leads to much higher pressure drops during flow [9, 10].

Crude oil emulsions are stabilized by the presence of complex molecules in the oil phase such as asphaltenes, resins, naphthenic acids, and clay nanoparticles [11, 12]. The adsorption of these components at the oil-water interface may lead to the formation of a gel phase at the water/oil interfaces [13, 14]. This behavior can result in a strong stabilization of the emulsions, making it very hard to separate both phases [15].

The final process of recovery is the phase separation of the produced fluids. The first step of this separation occurs in a specialized equipment that comprises large vessels called separators (Fig. 1.3). The first step of the phase separation is associated to the different densities of fluids (crude oil, water and gas). However, the residence time of the fluids in the separators may not be sufficient to ensure complete phase separation [16]. For this reason, other kind of separation systems need to be used, for example hydrocyclones [17] or floaters [18]. Meantime, emulsion separation is extremely sensitive to droplet size and these sophisticated methods can present low efficiency at the separation of small droplets.

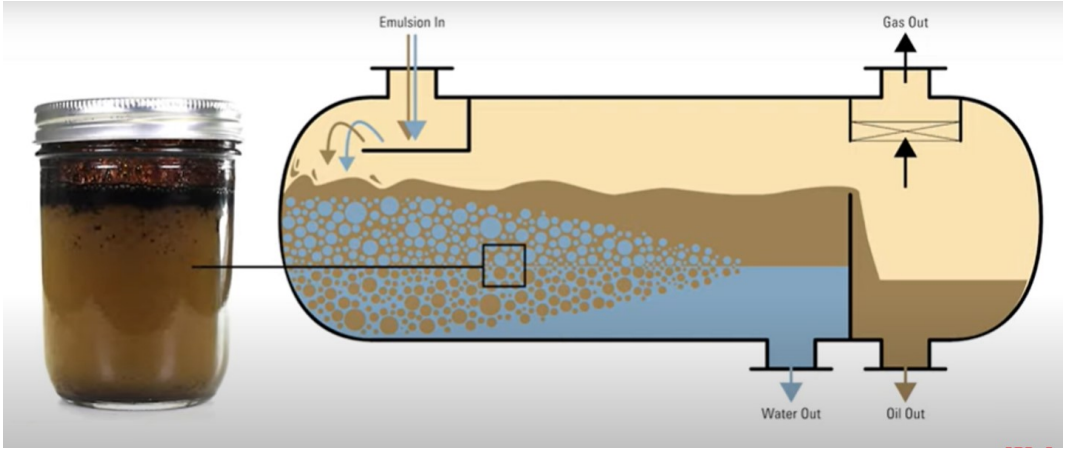

Figure 1.3: Example of separator system [19].

The separation of very small droplets is usually possible by adding

large amounts of chemical additives at high temperatures and with long residence times and/or applying electrostatic fields. In electric fields, due to the electrostatic forces, such as dipole-dipole interaction and dielectrophoretic force, small water droplets move towards each other or collide with each other. As a result, the merging (coalescence) of those droplets will increase the droplet size and eventually lead to settling and separation of water from the oil phase avoiding long residence times [20]. However, these techniques can imply high operational costs and technological challenges.

Another important issue in separation processes is that the separation rate of o/w emulsions is different from that of w/o emulsions, even if the droplet size distribution is the same. Bochner de Araujo et al. (2017) showed that in the case of oil droplets, the coalescence times measured were very short when in comparison with the water droplets. They attributed this behavior to the arrangement of asphaltene molecules at the oil/water interface and the resulting interface interactions [15].

Thus, it is essential to understand the mechanisms by which dispersed drops in a continuous phase coalesce. The coalescence process consists of the fusion of two or more drops to form a single larger drop. When two drops come close to contact, the thin film between them drains until the drops merge into a single drop, as sketched in Fig. 1.4 [21]. This phenomenon is governed by hydrodynamics, surface rheology, surface forces, and thermal fluctuations.

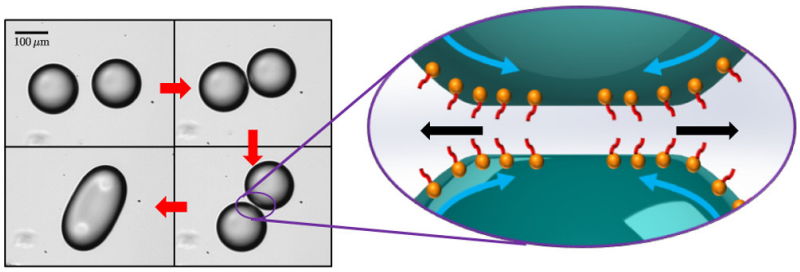

Figure 1.4: Example of coalescence process between two droplets [22].

1.2 Objectives

As discussed, the presence of emulsions during oil production may cause numerous problems and presents important technological challenges to be overcome. The production of stable emulsions in the reservoir and throughout production tubes makes the water/oil separation step extremely complex, both for the selection of the separation method and for the positioning of the

separation equipment. Furthermore, the flow of emulsions can damage various pieces of equipment, which leads to production stoppages, among other other cost increases.

The complex molecules present in crude oil can migrate towards the water/oil interfaces and form interfacial structures that play an important role in formation and stability of emulsions. The adsorption of surface active species at the water/oil interface reduces the interfacial tension (IFT), which eases the formation of the emulsion while the strengthening of the films formed delays or inhibits the separation process [23, 24]. So, a fundamental understanding of the role of these complex molecules in the coalescence of water and oil emulsion droplets, which is currently lacking, can provide the fundamental knowledge necessary for optimizing coalescence process.

The literature reports that different types of emulsifiers, such as amphiphilic proteins, small molecule surfactants (e.g., sorbitan esters), phospholipids, and particles [11, 25], can provide similar behaviors to those observed with the components present in crude oil. So, due to the complexity and limitations of some experimental techniques in the use of crude oil, this work focuses on the study of emulsions formed by an oil phase composed by a mineral oil with a nonionic surfactant and milliQ water as a model system.

This thesis examines different aspects of the behavior of water-oil emulsions. First, the effect of interfacial rheology on the coalescence behavior of two water drops is examined. The nature and structure of the oil-water interface that leads to the complex rheological interface behavior is examined in detail. Finally, as a way to enhance coalescence and promote phase separation by disturbing the interfacial film is explored.

1.3 Outline

The structure of the thesis is divided in 6 chapters. Following this Introduction Chapter, we present in Chapter 2 important concepts associated with this work and a literature review on the subject. In Chapter 3, the materials and methodologies used to perform the experiments are described. The experimental results are divided in three Chapters. Chapter 4 discusses the relationship between the interfacial properties and drop coalescence process. Chapter 5 presents the search for a better understanding of the structures formed at the droplet interface that hinders coalescence. Chapter 6 shows an attempt to promote coalescence by disturbing the interface structure. Finally, Chapter 7 presents conclusions and suggestions for future works.

2
Background and Literature Review

2.1
Emulsions

An emulsion is defined as a mixture of two immiscible liquid phases, in which one of the phases is dispersed as droplets in the other one. In the presence of interfacial active materials (surfactant molecules, amphiphilic polymers and solid particles), these emulsions which are usually thermodynamically unstable, can be stable systems for long periods of time. Usually, a large input of energy (generally by mechanical means) is required to form these systems. However, in some cases, normally when the interfacial tension between oil and water is low enough, emulsification process can start spontaneously without shaking, stirring, or homogenizing.

Simple emulsions can be categorized as water-in-oil (w/o) or oil-in-water (o/w) (Fig. 2.1. However, the phase configurations can be more complex, such as multiple water-in-oil-in-water (W/O/W) or oil-water-in-oil(O/W/O) emulsions [26], also sketched in Fig. 2.1.

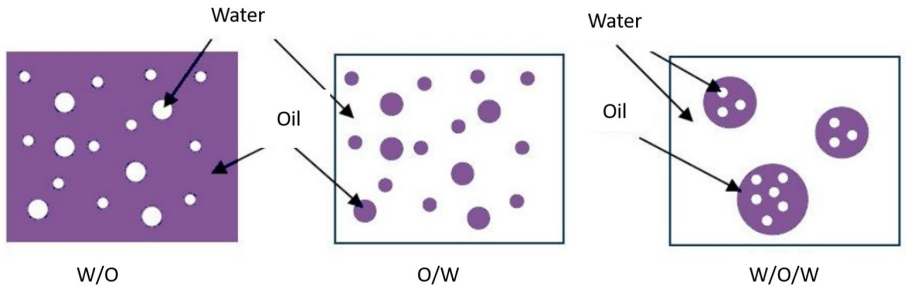

Figure 2.1: Classification of emulsions.

2.2 Surfactants

Also known as surface active agents, surfactants are amphiphilic molecules that consist of a hydrophilic group, referred to as the head, which has a tendency to interact with water, and a hydrophobic group, referred to as the tail, that has an affinity towards oil (Fig. 2.2) [26, 27]. When adsorbed at the interface they acts as IFT reducers [28].

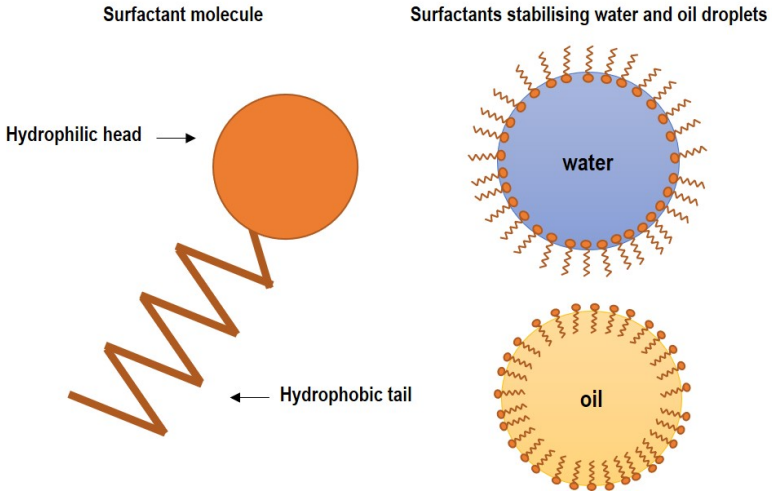

Figure 2.2: Graphic representation of a generic surfactant molecule.

The hydrophobic group consists of linear or branched hydrocarbons and may also contain some aromatic groups and haloalkanes. The surfactant head can be classified according to their polarity as anionic, cationic, zwitterionic, or nonionic [27].

The selection of the appropriate surfactant is an important step in the formulation of emulsions. In this work the surfactant used is nonionic. This kind of surfactant has no charges, they are not originated from dissociated salts and do not ionize in aqueous solution [28].

An essential characteristic of the nonionic surfactants is the hydrophilic–lipophilic balance (HLB), which influences the type of emulsion formed, o/w or w/o [29]. HLB indicates the tendency of the surfactant to solubilize in water or oil [30].

A classification system with corresponding applications was introduced by Griffin in 1949 and is shown in Fig. 2.3. On this scale, low values of HLB represent lipophilic surfactants that tends to be more soluble in oil and form w/o emulsions, while high values of HLB are attributed to the

hydrophilic surfactants that are more soluble in water, consequently forming o/w emulsions.

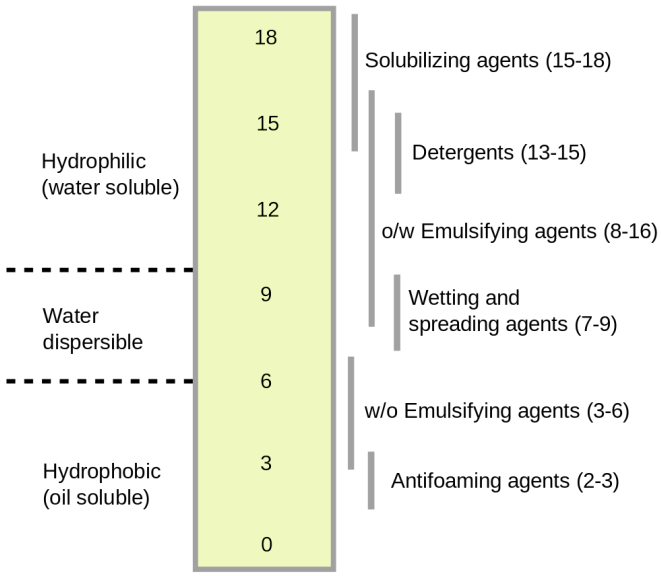

Figure 2.3: Position of the different groups of surfactants on the scale HLB.

When a surfactant is initially added to a phase it will start to adsorb at the interfaces. At low surfactant concentration, an equilibrium is established between surfactant in solution and surfactant adsorbed to the water-oil interface. The higher the concentration of surfactant in one of the phases, the more saturated the surface becomes and the more energy is required for the surfactant to adsorb to the surface. Above a certain concentration, the interface is completely saturated and the energy required for a surfactant to adsorb to the interface is so high that it becomes energetically more favorable for surfactants to associate as micelles. This concentration is called Critical Micelle Concentration (CMC) and all amount of surfactant added from this point will remain diluted in the continuous phase and will prefer to form a micelle rather than adsorbing at the interface [27, 31].

So, the CMC defines the concentration at which the surface between the fluids is completely saturated with surfactants. Above the CMC, the surfactants will spontaneously form aggregates to minimize the contact area with the continuous phase [32]. When the surfactant is added in the aqueous phase, the surface of the micelle is composed of some polar heads that isolate the non-polar linear tails inside it. Similarly, inverse spherical micelles are formed when the surfactant is diluted in an oil phase, as sketched in Fig. 2.4 [31].

The IFT decreases with the adsorption of the surfactant at the interfaces, but as the critical micelle concentration is reached, the IFT stabilizes and do not vary with further addition of surfactant, as sketched in Fig. 2.4 [31].

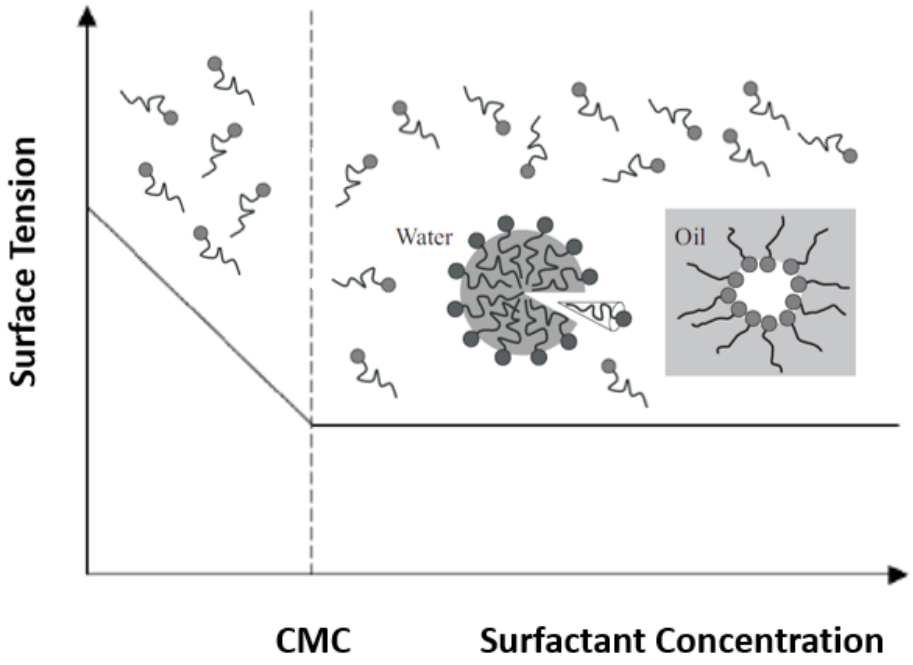

Figure 2.4: Surface tension as a function of surfactant concentration, highlighting the schematic cross-section through a spherical micelle both in water and in oil phases (adapted from [31]).

2.3 Emulsion Stability

Stability of an emulsion is an ability of the droplets to remain suspended in a continuous phase at equilibrium over time. Some aspects can directly influence the stability of an emulsion, such as: droplets size, dispersed phase concentration, viscosity of the continuous phase, interfacial properties (interfacial tension and interfacial rheology), temperature as well as the aging of the emulsion.

The processes related to the separation of phases of emulsions are illustrated in Fig. 2.5 and may be distinguished: phase separation by density difference (creaming and sedimentation), flocculation, Ostwald ripening, coalescence, and phase inversion [33, 34].

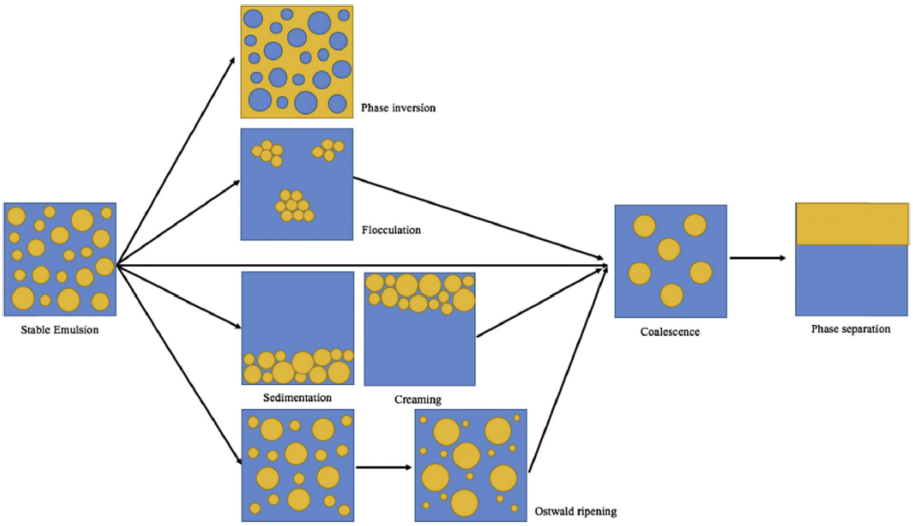

Figure 2.5: Instability mechanisms in the emulsion systems [34].

Creaming or sedimentation occurs due to the difference in density between the oil phase and the water phase. For an o/w emulsion, the drops of oil will segregate and form a cream on the top of the samples. On the other hand, for w/o emulsions, the water drops will fall forming a water free zone at the top of the sample. Basically, these processes depend on gravity forces and the difference between the density of the dispersed phase and the continuous phase. Flocculation is caused by van der Waals attraction when there is not sufficient repulsion between the drops and promotes the formation of aggregates. Coalescence is a process that consists of the fusion of two or more drops to form a single larger drop and happens by thinning and disruption of the liquid film between them [33]. It can happen naturally or it can be induced in order to break the emulsion. When induced, the process can be classified as chemical, electrical, or mechanical [35]. Finally, due to the difference of pressure between the small and large droplets Ostwald ripening may occur, at which larger droplets absorb the smaller droplets by diffusion as a consequence of the pressure difference, once the Laplace pressure is higher in smaller droplets [36].

In this work the focus is on the evaluation of the coalescence process of emulsions. So, the next section will present a brief literature review about this phenomenon.

2.3.1 Literature Review of the Coalescence Process

Although droplet coalescence is a phenomenon that has been studied for over a century [37], it is only recently that technological advances in high-speed

camera imaging have made it possible to capture details of the process that contribute to a better understanding of it.

Coalescence can be studied through two different points of view: a macroscopic analysis of the stability of the emulsions by evaluating the phase separation over a period of time [23, 38] or a microscale study of a single coalescence event between two dispersed droplets. Regarding the techniques used to study the microscale analysis, different approaches have been used in the literature to study this phenomenon; using a droplet formed at a needle tip and forced against a planar interface (that can be considered a large drop) of a bulk liquid phase [15, 39–41] or against another droplet [35, 42, 43], or by using microfluidic devices [22, 44–47] (Fig. 2.6). The deformations undergone by the interfaces during the collision are of two types: shear deformation with a change of shape for a constant area and dilatational deformation associated with changes in the interfacial area. Regardless of the approach adopted, coalescence phenomenon is extremely sensitive to phase composition and therefore it is important to run experiments with well controlled fluid composition and free of impurities [48].

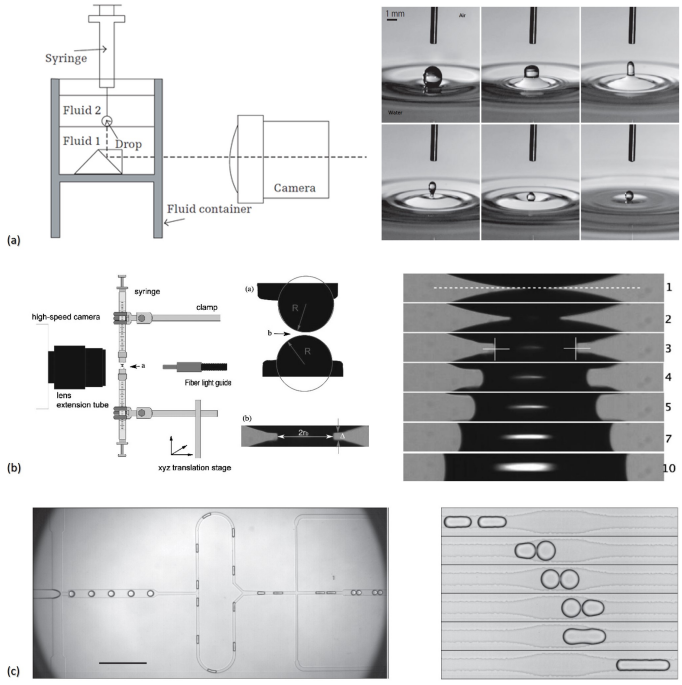

Figure 2.6: Microscale analysis of the coalescence process: (a) coalescence between a drop and a flat interface [39], (b) coalescence between two droplets of the same size [42], and (c) coalescence between two droplets using a microdevice [47].

To better understand the phenomenon of coalescence, the flow between two drops can be divided into different stages: approaching of two single drops, deformation of the approaching drops with the formation of a flat film between the droplet interfaces, and thinning of this film to a critical thickness at which the film becomes unstable, breaks, and the two drops unite to form a single larger drop. Initially (Figure 2.7(a)), there is a thinning of the film due to the action of capillary pressure acting normal to the interface. In the presence of surfactants, the flow towards the bulk phase generates a convective flow of surfactant in the sublayer (Figure 2.7(b)) which causes the surfactant concentration at the interface to be increased in the direction of this flow. There are other flows associated with the drainage process, such as droplet mass flow, film phase mass flow, interfacial diffusion flow caused by the concentration gradient at the interface, diffusive flow from an adjacent layer to the film interface, and the adsorption of this layer at the interface [35].

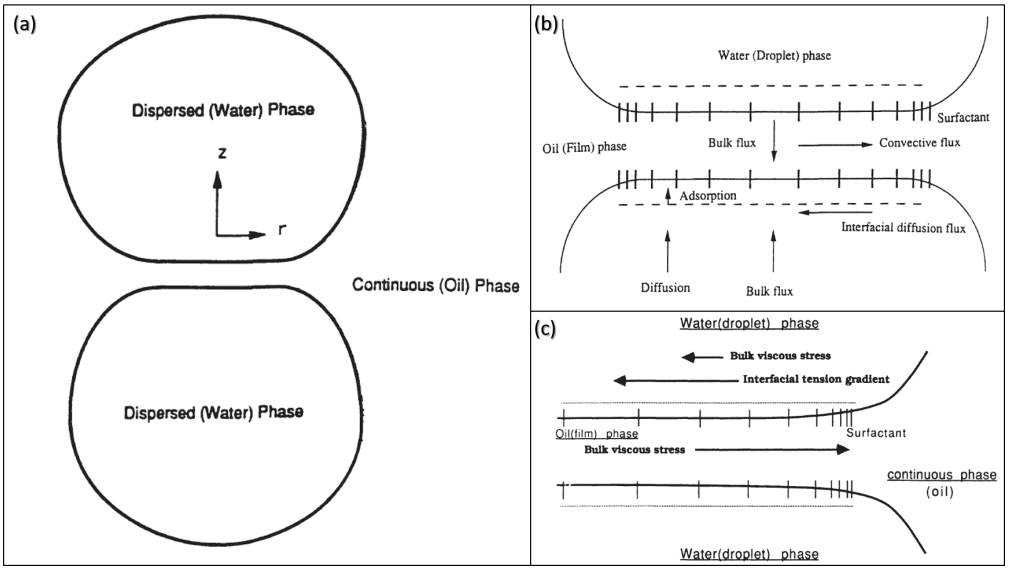

Figure 2.7: Coalescence process between drop-drop: (a) approaching of two drops and forming a film between them; (b) surfactant mass balance at the film interface; (c) balance of tangential stresses at the film interface [35]

Figure 2.7(c) illustrates the balance of tangential stresses at the film interface. As mentioned before, the drainage of the thin film causes a convective flux of surfactant, leading to a lower concentration away from the bulk, since the interfacial tension is higher at lower surfactant concentration, a surface tension gradient flow (Marangoni flow) starts driving liquid from the bulk to the thin film. Additionally, the surfactant monolayer can undergo a shear and expansion deformation that also produces interfacial stresses. The sum of

the above stresses and the tangential volume stress of the liquid in the drop must counterbalance the tangential stress of the liquid in the film, causing the interfacial flow.

The same phenomena occur during the coalescence of a drop on a fluid flat surface, as sketched in Fig. 2.8. Droplet (fluid 1), initially suspended in fluid 2, moves at terminal velocity under the action of gravity through a semi-infinite continuous phase (fluid 2) and approaches the flat surface of a semi-infinite liquid (fluid 1). When in contact with the surface, the fluid between the interfaces will be drained until the thickness is so thin that van der Waals forces cause the break of these interfaces and generate a hole in the film, starting the coalescence process. The duration of this initial process is known as the film drainage time. At this point, the measurement of another time parcel begins, which is known as coalescence time, and occurs at the beginning of the break in the thin film until the fusion between the two domains of fluid 2 is complete (in the case of complete coalescence) or until a secondary drop to be formed (partial coalescence) [39, 41, 49, 50]. The coalescence time is generally short in comparison with the drainage time.

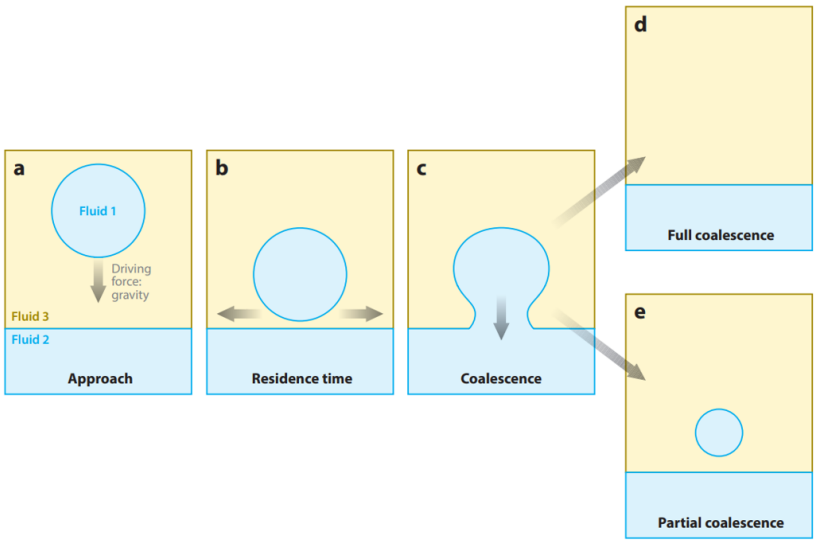

Figure 2.8: Coalescence process between a drop and a flat interface [21]

The coalescence phenomenon is impacted by several factors that directly influence the stability of the interfaces, such as: the surface tension gradients [41, 42, 51, 52]; the viscosities of the phases [22, 39, 40, 50]; the nature and the geometry of the surfactants [43, 53] including natural surfactants as the asphaltenes [15].

The effects of interfacial behavior on the drop/drop coalescence and emulsion stability is the main focus of this thesis. However, previous experimental and numerical studies on coalescence phenomenon in general is briefly summarized to provide better knowledge of the research progress. So, this review will focus on, but not limited to, the coalescence of two drops. The review is divided in two parts, one related to studies in the absence of surfactants and the other, studies considering the presence of surfactants.

2.3.1.1
Coalescence in the absence of surfactant

Aryafar and Kavehpour (2006) investigated the effect of different parameters on droplet coalescence on a flat interface (Fig. 2.9), using fluids with different viscosities that allowed exploring a range of Ohnesorge number (Oh), which represents the ratio of the viscous time scale to the inertial time scale for a flow governed by capillary forces and is a suggested parameter to determine the global behavior of coalescence. It is usually defined as $Oh = \mu/\rho R\sigma$, where μ is the viscosity of the phase with the highest viscosity in the system, ρ is the density, R is the radius of the drop, and σ is the interfacial tension. The authors observed that there is no specific viscosity relationship between the different fluids studied that describes the variation in the radius of the secondary droplet formed in relation to the wide range of analyzed Oh.

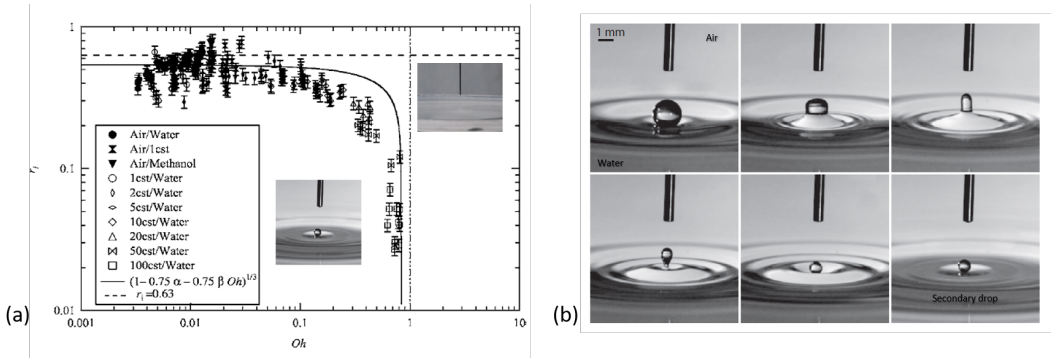

Figure 2.9: a) Droplet radius plotted as a function of Ohnesorge number for a combination of different fluids and (b) example of partial coalescence of a drop of water at the air/water interface [39].

The initial stage of coalescence is the formation of the rupture of the thin film that separates the interfaces. The rupture of this film results in the formation of a bridge. In the case of a drop and a flat interface, due to the

great curvature of the free surface of the drops in relation to the reservoirs, there is a pressure imbalance that pushes the liquid from inside the drop into the reservoir. As this process of coalescence takes place, the bridge expands [40].

Wu, Cubaud, and Ho (2004) studied this phenomenon experimentally, through the coalescence of two drops of liquid driven by surface tension, as shown in Fig. 2.10. They evaluated the initial evolution of the liquid bridge that is formed in the initial contact of two drops of liquid in the air. Their experimental results confirmed the scaling law proposed by previous studies. They found that the radius of the bridge follows a proportional relation to the square root of time ($r_b \propto t^{1/2}$) in the inertial regime, as observed previously by Duchemin et al. (2003) and in a numerical study by Thoroddsen et al. (2005) [51, 52]. In these studies, it was observed that the film opening is dominated by inertial forces instead of viscous.

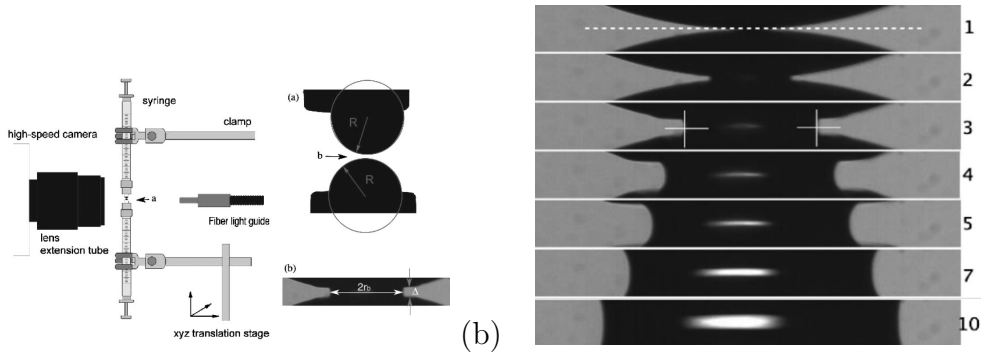

(a) (b)

Figure 2.10: (a) Experimental apparatus (b) sequence of images that show the growth of this bridge [42].

For cases in which the drop is immersed in a fluid more viscous than air, such as oil, viscous forces are expected to be as relevant as inertial forces, and thus the dependence suggested by Wu et al (2004) is no longer valid. Aryafar et al (2006) studied the temporal dependence of the growth of a bridge formed by approaching a drop to a planar surface now immersed in a fluid different from the air. In a similar way, they concluded that the radius can be defined as a function of a power relation of time, but with the proportion of $r_b \propto t^{3/2}$, during the rupture of the film. Their results are in agreement with the power-law predicted behavior for drop-drop coalescence and fully agree with numerical simulations for the variety of fluid combinations by using correct dimensionless numbers [40].

Blanchette et al. (2009) investigated the coalescence of a droplet with a liquid reservoir of a miscible but not identical fluid with a different surface

tension. They characterized the coalescence according to the ratio between the surface tension of the reservoir and the surface tension of the drop ($R_\sigma = \sigma_2/\sigma_1$) and identified three distinct patterns presented in Fig. 2.11: (a) partial coalescence favored as the surface tension of the reservoir increases, forming secondary drops; (b) full coalescence; and (c) a new type of partial coalescence with the formation of capillary waves at the interface, and vertical elongation of the droplet.

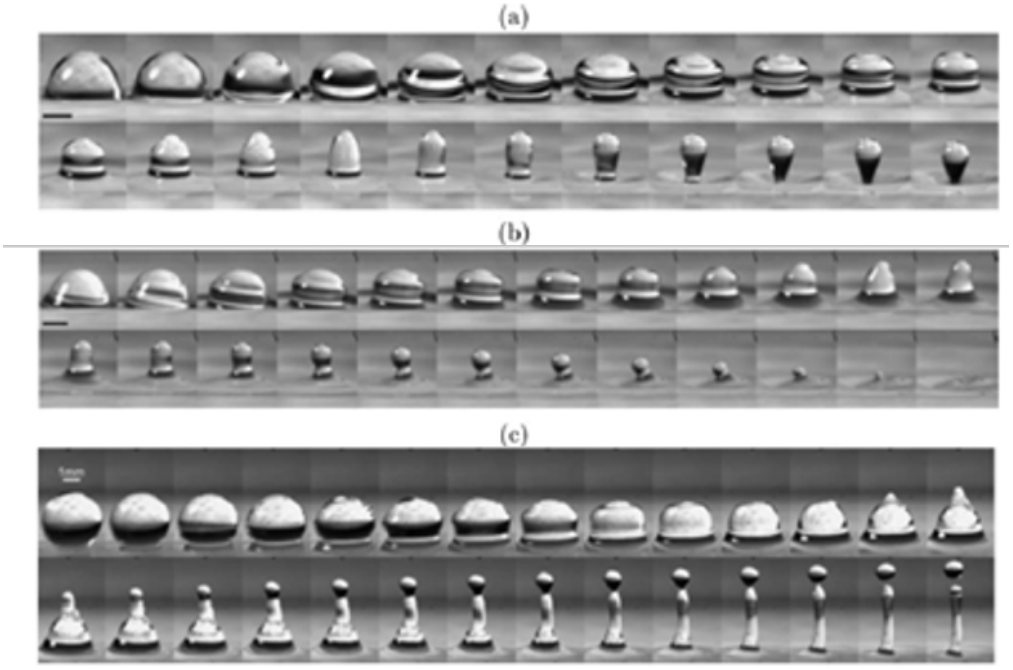

Figure 2.11: Photo sequences recording coalescence events for different fluid pairs with different ratio between surface tension: (a) $R = 1.09$; (b) $R = 0.91$ and (c) $R = 0.30$. In (a) a daughter drop was formed and downward moved. In (b) complete coalescence was observed and (c) a small daughter droplet was ejected upwards, adapted from [41].

Using micro-scale fluid methodology, Tan et al. (2004) designed and analyzed three different channel geometries to decrease the forward drop flow, as illustrated in Fig. 2.12, and promote drop to drop contact. The different geometries included a rectangular expansion, a conical expansion, and a rectified flow. In the first case, the drop decelerates, causing a continuous phase liquid discharge, which reduces the space between the drops and promotes coalescence. In the second case, the rapid decrease in droplet velocity and the draining of the continuous phase allow subsequent drops to merge. And finally, in the last case, the cross-shaped geometry allows controlling the drainage time by controlling the flow rate in the upper and lower microchannel to control the

fusion at the intersection.

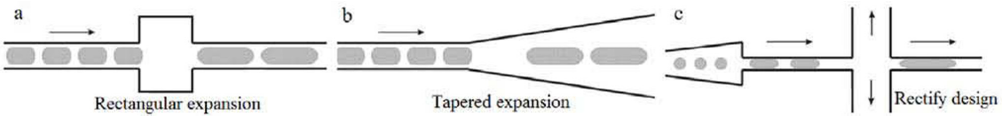

Figure 2.12: Three different channel configurations for droplet coalescence [45].

Deepening the study using the last configuration, Tan et al. (2007) built a new channel with the configuration shown in Fig. 2.13(a). This channel allowed emulsion droplets to be formed periodically, equally spaced, redistributed and to fuse consistently, as illustrated in Fig. 2.13(b). All this dynamics was obtained by controlling the relationship between the droplet transport time through the junction and the drainage time of the fluid volume that separates the droplets.

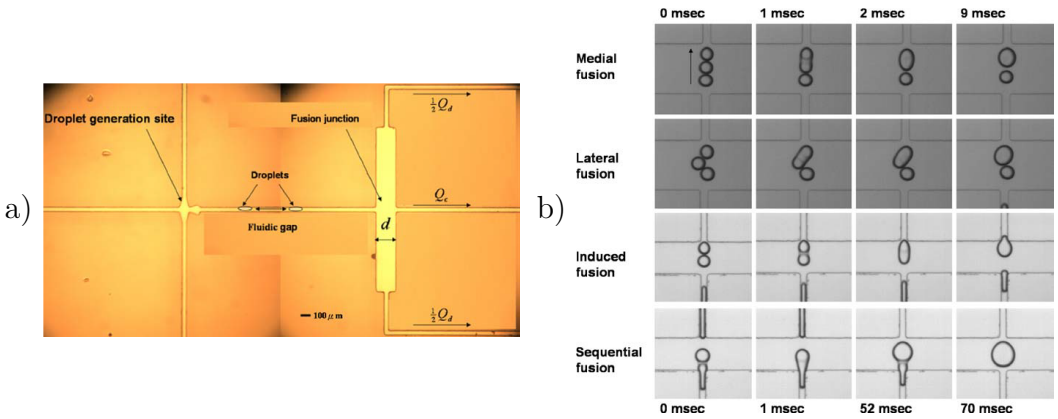

Figure 2.13: (a) Geometry of the drop melting device. On the left, the drops are generated and on the right, part of the channel that promotes their coalescence. (b) Representation of the three types of coalescence that occurs in this device [46].

As observed in these studies [45, 46], channel expansion became a general framework for droplet coalescence. However, Bremond et al. (2008), in their study, observed that the coalescence of the drops did not occur by contact as they entered the expanding channel, but occurred further on, during the separation phase, when one of the drops enters the narrow channel (Fig. 2.14).

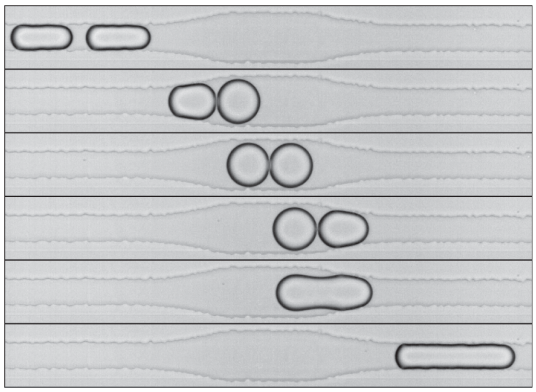

Figure 2.14: Sequence images over time showing the destabilization of a pair of drops passing through a channel with an expansion: collision, relaxation, separation and fusion [47].

2.3.1.2 Coalescence in the presence of surfactant

In the previous section, regardless of the approach used to assess coalescence, the work presented did not consider the presence of surfactants. However, already in 1992, Wasan highlighted that the film drainage rate is strongly dependent on the surfactant adsorption kinetics, its interfacial activity, solubility and interfacial rheological properties, such as interfacial tension gradient, elasticity, and interfacial viscosity. Several studies have shown that the droplet residence time becomes longer in the presence of surfactants, even in small amounts, this effect being attributed to the flow caused by the Marangoni forces that slow down the process of drainage of the thin film formed between the interfaces [35, 41, 54–58].

Dai and Leal (2008) numerically studied the influence of surfactant on the coalescence of two droplets of the same size when colliding frontally. They found an effect of equal importance to the Marangoni effect in draining the film formed between drops. As the hydrodynamic force that pushes the drops against each other is increased, the interface evolves to a configuration having pits that delay the drainage process. This behavior is shown in Fig. 2.15; when surfactant is present, Fig. 2.15(b), the interface configuration presents a strong thinning of the film near the bulk, slowing the drainage flow.

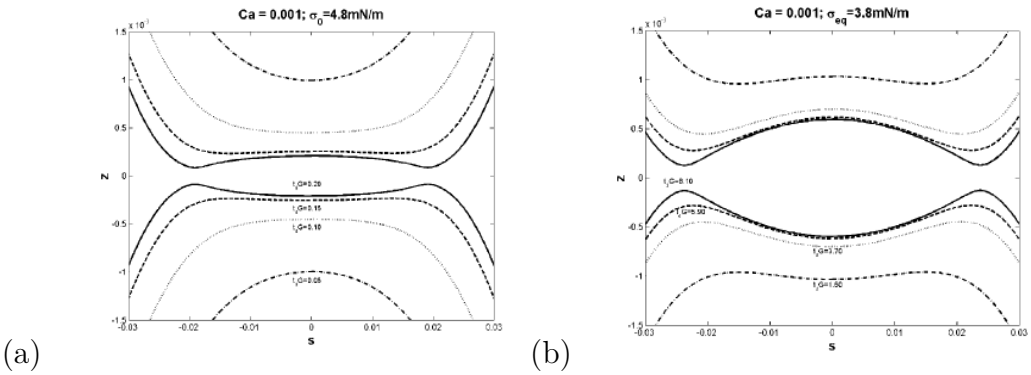

(a) (b)

Figure 2.15: Film formats computed at four different time steps during film draining to: (a) clean interface and (b) surfactant interface [55].

Also with a numerical study, Martin and Blanchette (2015) showed that the presence of surfactant can reduce the value of the critical Ohnesorge number by more than 30 % that directly affects the partial coalescence regime [59].

In 2016, Nowak et al. carried out an experimental study of the coalescence of two water drops immersed in silicone oil with different viscosities, only one of which had a surfactant in its composition, as shown in Fig. 2.16. They observed that the growth of the rupture bridge obeyed a power law with an exponent of ~ 0.5 multiplied by a factor that depends both on the surfactant concentration and on the external phase, and the growth rate of this bridge was reduced with the increase of the surfactant concentration due to lower tension at the bridge interface. They observed considerable movement of the convective mass in coalescence between a surfactant-free droplet and a droplet with surfactant, unlike when the droplets were surfactant-free or similar surfactant-laden droplets. For the coalescence of a surfactant-free droplet and a surfactant-loaded droplet, the curvature of the meniscus was different on both sides of the growing bridge due to the uneven interfacial tension of the drops.

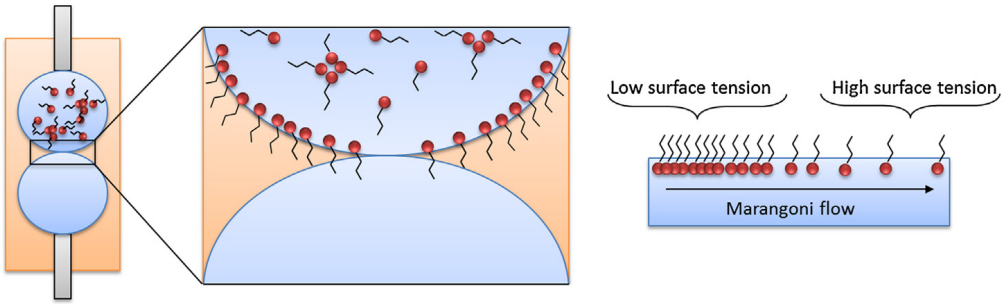

Figure 2.16: Representative scheme of the influence of Marangoni stresses on the coalescence of droplets with different compositions [43].

Araujo et al. (2017) studied coalescence in the presence of asphaltene adsorption for both w/o and o/w emulsions where the oil phase consisted of a simple mixture of asphaltenes dissolved in toluene. They evaluated the stability of the emulsions by measuring the coalescence time as a function of aging time and asphaltene concentration. They observed that o/w emulsions are less stable when compared to w/o emulsions. The difference in the coalescence dynamics of oil and water droplets was attributed to the arrangement of asphaltene molecules at the oil/water interface and the resulting interface-interface interactions, as shown in Fig. 2.17. In the case of water droplets, the aliphatic portion of the asphaltene molecules extends into the oil layer, leading to a strong hydrophobic repulsion of the tails. In the case of oil droplets, the aromatic portion of the asphaltenes is exposed to a film of draining water, producing an attractive interaction.

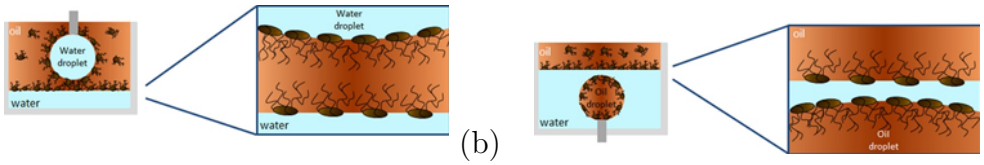

Figure 2.17: Scheme of the interaction between asphaltene molecules and interface of the (a) water and (b) oil [15].

Some studies using microfluidics allow experiments with small droplets and coalescence in flow. Lin et al (2018) used a device with a T-junction geometry to form the droplets and a wide channel where the drops slow down and touch each other (Fig. 2.18(a)). They studied emulsification and demulsification of asphaltene-stabilized w/o emulsions concluding that the presence of demulsifiers and their concentrations impact significantly on the drop coalescence rate [60]. With similar device, Dudek et al. (2019) presented a study of crude oil droplet coalescence in produced water from oil reservoir

(Fig. 2.18(b)). They show that the coalescence is typically stronger in the lower or neutral pH and with less complex water composition. Furthermore, the experiments indicated that the droplets merged more readily right after formation, whereas coalescence was impeded when they were allowed to age. In addition, it was found that larger droplets coalesced slower. They emphasized the importance of the chemical composition of the phases on the coalescence process [61]. Narayan et al. (2020), using similar microfluidic device, studied the coalescence behavior of dispersed aqueous droplets formed in a continuous phase of mineral oil with sorbitan oleate (Span 80) as a nonionic surfactant (Fig. 2.18(c)). Varying the surfactant concentration, they showed that the film drainage time increases with an increase in surfactant concentration and droplet size. Their results also reinforced the theory previously presented by others authors that the thin film's mobility is not constant during film drainage [62].

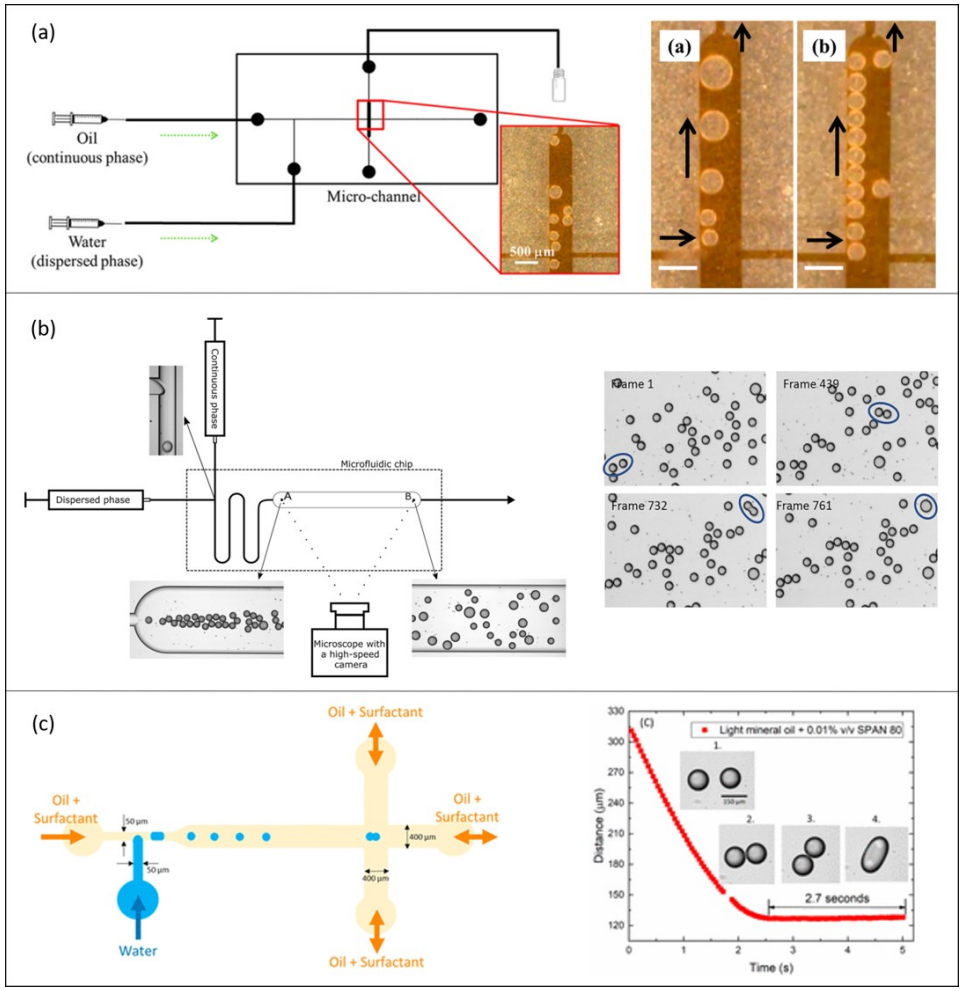

Figure 2.18: Schematic of the microfluidic device used by: (a) Li et al 2018; (b) Dudek et al 2019; and (c) Narayan et al (2020).

The coalescence studies cited above, in the presence of surfactant or not, occur in the absence of external forces and do not consider the effect of gravity. However, in many cases, additional forces are used to promote coalescence. An example of an important external force that has been frequently used is the application of an electric field [21]. Experimental studies show that, as the electric field strength increases, the residence time of coalescence decreases [63].

2.4 Interfacial Rheology

Rheology is the study of the relationship between force (stress) and deformation (strain) of materials. Two simple rheological behaviors can be highlighted, which are viscous fluids and elastic solids. A fluid at rest can not resist shearing forces, so under the action of such forces it deforms continuously. With the removal of the force, it ceases to deform, but any prior deformation remains. If this force is applied to an elastic solid, it will deform instantaneously, but the deformation will be fully recovered with the removal of the force. This happens because for solids, the resistance to a shear deformation depends on the deformation itself; that is, the shear stress is a function of the shear strain. Already for fluids, the shear stress is a function of the rate of strain. However, there are materials that have an intermediate behavior between these two, known as viscoelastic materials, because they have both viscous and elastic characteristics.

Interfacial rheology studies interfaces formed when two immiscible liquids are placed in contact. Knowledge about the mechanical response of these complex interfaces is extremely important. The study of these complex characteristics of interface is associated with the term two-dimensional or 2D rheology while the bulk properties are well-know as 3D rheology [64]. Interfacial tension (IFT) is reduced by the adsorption of surfactants at the water/oil interface, and emulsion formation is eased. The interfacial structures affect the formation and stability of emulsions. The strength of the film formed delays or inhibits the coalescence process. The interfacial properties, directly related to the characteristics of the adsorbed layers, are very important in the dynamics of coalescence [23, 24]. Interfacial dilatational rheology, which represents the response of the interfacial stress to dilatational deformations of the interface, allows the characterization of the viscoelastic properties of the adsorbed layer [65–67].

The interfacial region is able to response the perturbations on it like deformations of expansion/compression (changes in area or volume at constant

shape) or shearing (changes in shape at constant area or volume).

When a rheologically complex interface is deformed or dilated, interfacial or surface stresses can emerge [68]. So, a general expression for the interfacial stress tensor σ of a viscoelastic liquid interface can be expressed as [67]:

$$\sigma = \sigma_{\alpha\beta}(\Gamma, T)I_s + \sigma_e$$

where $\sigma_{\alpha\beta}(\Gamma, T)$, is the interfacial tension between phases α and β which depends only on the interfacial concentration Γ and temperature T, I_s is the second order surface identity tensor, and σ_e is the extra rheological stress tensor. Deviatoric and isotropic contributions compose σ_e and can be probed by distinct interfacial techniques. Shear rheology by keeping the interfacial area constant and changing its shape provides the deviatoric stresses. And, dilatational rheology by inducing changes in area without changing the interfacial shape will provide the isotropic stresses [67].

2.4.1 Shear Rheology

Interfacial shear rheology measures the response of the interface to constant area deformations by changing its shape. Shear rheometers are classified according to the direct or indirect method applied to their operation. In the direct method, the interfacial properties are obtained by measuring the force or torque applied at the interface. And in the indirect method, the interfacial properties are obtained by the analysis of velocity profiles [68, 69].

Common measurement configurations of interfacial shear rheometry are rotational and projected to be conducted on flat interfaces rather than complex curved interfaces. The main types of rheometers are: surface channel rheometer; bicone rheometer (cross section), double-wall ring geometry rheometer, and interfacial rod rheometer [68].

When sinusoidal oscillations in the linear regime (small amplitudes) is applied on the interface, the surface tension oscillates with the same frequency of the area, but with a phase shift δ [70]. A sinusoidal shear deformation γ :

$$\gamma = \gamma_0 sin(\omega t) \tag{2-1}$$

is performed at an angular frequency ω and strain amplitude γ_0, and an out-of-phase response is obtained for the stress tensor σ with a phase angle δ [71]:

$$\sigma_{\alpha\beta} = \sigma_0 sin(\omega t + \delta) \tag{2-2}$$

The storage modulus G and loss modulus G describe the elasticity and viscosity of the film, respectively, and can be expressed by:

$$G' = \frac{\tau_0}{\gamma_0} cos(\delta) \tag{2-3}$$

$$G'' = \frac{\tau_0}{\gamma_0} sin(\delta) \tag{2-4}$$

2.4.2 Dilatational Rheology

Dilational interfacial rheology presents itself as an important tool for systems that containing surfactants or, more in general, for composite interfacial layers where the interfacial tension changes due to surface relaxation processes or diffusion. Different from the interfacial shear rheology, in the expansion of interfaces (compression/expansion), the deformation is in fact the variation of interfacial tension according to the variation of its area [72].

Furthermore, dilational rheology is a unique tool to access the characteristics of the transport and the kinetic processes determinant for the adsorption reequilibration and the physicochemical properties of the involved surfactant-interface system through the close link existing between the dynamic properties of the interfacial layers and the adsorption mechanisms [72].

The resistance to the creation of gradients in surface tension can be measured using the Gibbs elasticity, written as:

$$E^* = \frac{\partial \gamma}{\partial ln A} \tag{2-5}$$

where γ is the surface stress and A is the area of the droplet. The complex viscoelastic modulus E^*, in its turn, can be expressed as the sum of a storage (elastic) E' and a loss (viscous) E'' moduli:

$$E^* = E' + iE'' \tag{2-6}$$

The elastic modulus E' may be associated with the elastic response of a structured interface or to the impact of the area change on the surface concentration of the surfactant. The loss modulus E'' may be associated to

a gradual diffusional exchange of surfactant molecules between the interface and the bulk or to microstructure deformation and friction with the subphases.

The equipment most commonly used today to measure these dilational interfacial rheological parameters is the drop tensiometer. This equipment can monitor interfacial tension in two ways: by drop profile or by capillary pressure measurements [66]. In this work the drop profile was used and will be described in the next Chapter.

Interfaces with a large elastic modulus experience large increases in energy as their area increases; therefore a droplet surrounded by an elastic film is less likely to deform and break up in a collision. Additionally, the drainage of the thin film between two adjacent drops is slowed down by the elastic surface stresses, and consequently, the coalescence process can be delayed or even prevented [22, 73, 74]. There is still much to be understood about the individual role of isotropic changes in the interfacial tension (surfactant adsorption/desorption) that lead to Marangoni stress and deviatoric interfacial stress on coalescence dynamics [75].

3
Materials and Interfacial Rheological Properties

In this chapter, the materials used in the experiments are presented. A combination of Span 80 (non-ionic surfactant) and Primol 345 (mineral oil) was used as a model oil phase, which could produce complex interfaces, as found in the real oil industry scenario, and mili-Q water as the water phase. The rheological properties of the oil-water interface was performed to evaluate how the surfactant concentration affects the mechanical behavior of these interfaces.

3.1
Materials

The water phase used was produced by the Direct-Q® Water Purification System (18.2 $M\Omega.cm$ at 25 ^oC). The oil phase selected as a model of crude oil is a mixture of a mineral oil (Primol 352) and a nonionic surfactant (Span 80). Primol 352 (Exxon Mobil) is a medicinal-grade mineral oil (66 % paraffinic, 34 % naphthenic carbon type) produced from petroleum distillation [11]. Span 80 ($C_{24}H_{44}O_6$), sorbitan monooleate, (Sigma Aldrich) is a nonionic oil soluble surfactant (Figure 3.1), with an HLB of 4.3, frequently used to make W/O emulsions. It is effective to reduce IFT and past investigations showed that it possesses interesting interfacial viscoelastic properties to prevent coalescence [76]. As the coalescence events are extremely sensitive to the composition of both the water and oil phases, to avoid uncertainties associated with the liquid compositions, we used well controlled systems.

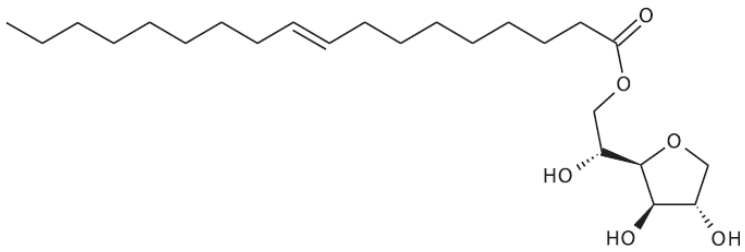

Figure 3.1: Molecule of the surfactant Span 80 [77].

Density and viscosity of these materials are presented in Table 3.1.

Properties of the water and the oil were measured at the laboratory; the density was measured using a DMA4200M densimeter (Anton Paar) and the viscosity was measured with a capillary viscometer, both at 23^oC. And the properties of the surfactant was obtained by the supplier.

Fluid	**Viscosity** (cP)	**Density** (g/cm^3)
Water	0.890	0.9982
Primol	99.22	0.8607
Span 80	1200 - 2000	0.9860

Table 3.1: Properties of fluids measured at 23 ^oC.

3.2 Interfacial Rheological Experiments

As already discussed in section 2.4, the formed interfacial structures affect the formation and stability of emulsions. So, it is important to study and understand their properties and their influence on our system. This section will be divided in a brief explanation of the principles of the pendant drop technique and a description of the experiment used in the interfacial rheological measurements.

3.2.1 Pendant Drop Technique

Axisymmetric drop shape analysis (ADSA) consists in obtaining the interfacial tension (IFT) from a drop profile with a revolution symmetry of a drop attached from a needle in a bulk phase (Fig. 3.2). The ADSA requires a non-spherical droplet because for quasi-spherical drop, interfacial forces dominate gravitational forces, a small change in the drop profile would then result in a large change in the apparent IFT. The analysis of the drop shape is based on the Young-Laplace equation that expresses the pressure difference, resulting from the surface curvature, being proportional to the average curvature:

$$\Delta P = \gamma(\frac{1}{R} + \frac{1}{R'}), \tag{3-1}$$

the coefficient of proportionality γ is the interfacial tension, R and R' are the main drop surface curvature radii, as sketched in Fig. 3.2.

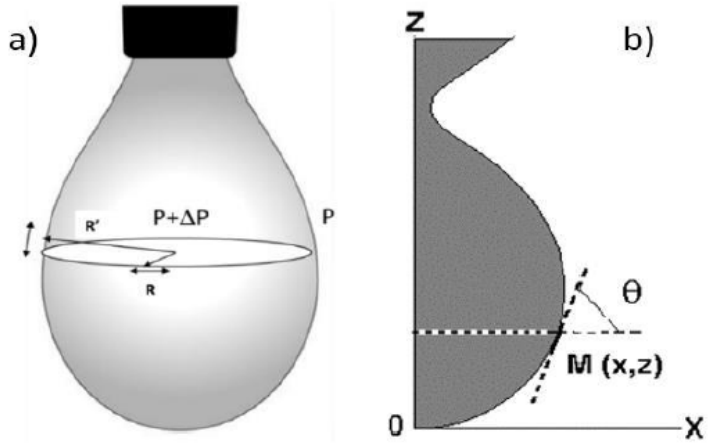

Figure 3.2: (a) Surface curvature of the droplet and (b) Coordinates of a point M of the drop surface.

The shape of a drop is characterized by the Bond number (B_o):

$$B_o = \frac{g\Delta\rho}{\gamma b^2}, \tag{3-2}$$

where $\Delta\rho$ is the density difference between the two fluids, g is the acceleration of gravity, γ is the interfacial tension, and b is the inverse of the radius of curvature at the apex. This parameter measures how close the shape is to spherical and is used to determine the accuracy of ADSA method applied to a given drop. When $Bo \to 0$, IFT dominates, and the drop does not deform, it remains spherical. Increasing the volume of the drop allows to significantly increase the Bond number and to conduct the measurement of the IFT. In general, it is considered that $Bo \approx 0.1$ is the value for which the ADSA algorithm can be applied without problems.

The dilatational rheology can be obtained by subjecting the drop to periodic expansion and compression by injecting and withdrawing liquid into and from the drop. The surface stress γ is measured during the sinusoidal oscillations of the area of the droplet A [78]. As the drop is non-spherical, the interface does not change its surface to a constant shape, so the response to interface oscillation is not truly dilatational. At low amplitude harmonic perturbations at a fixed frequency, the dilatational complex modulus (viscoelastic modulus) E^* is written as:

$$E^* = \frac{\partial\gamma}{\partial A/A} = \frac{\partial\gamma}{\partial lnA}, \tag{3-3}$$

representing the increase in surface stress as a function of surface deformation.

The complex viscoelastic modulus E^* is a complex number in which the real part E' represents the stored and recoverable energy (elastic modulus) and the imaginary part E'' corresponds to the mechanisms that dissipate mechanical energy (viscous modulus):

$$E^* = E' + iE'', \tag{3-4}$$

$$E' = |E|cos\phi, \tag{3-5}$$

$$E'' = |E|sin\phi, \tag{3-6}$$

ϕ represents the phase angle displacement between the wave curves of the physical stimulus (area A variation), and the interfacial stress response [13], as shown in Fig. 3.3.

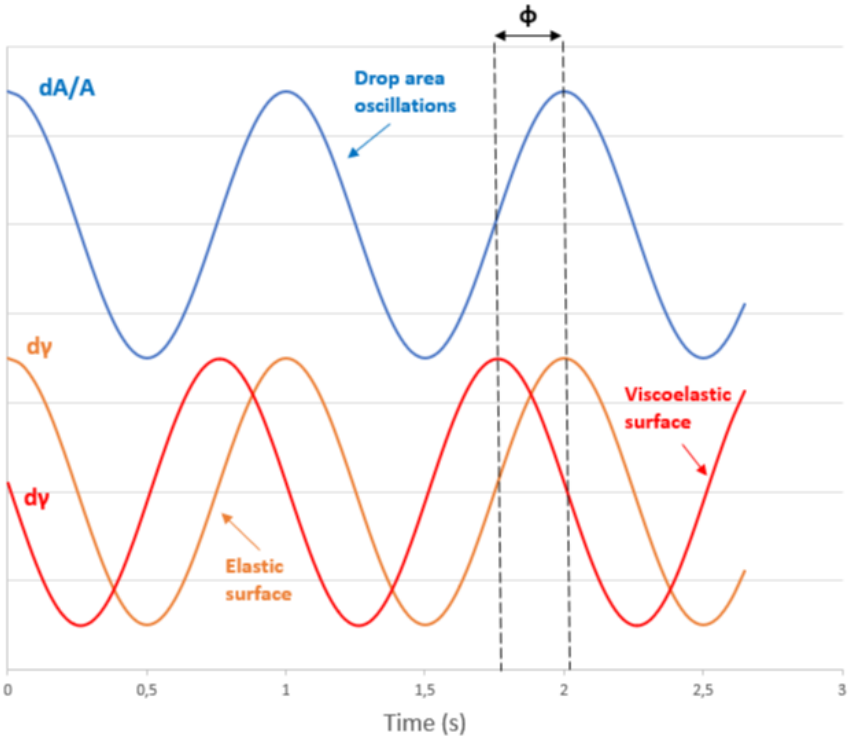

Figure 3.3: Evolution of the area and the surface tension of a drop of water undergoing a sinusoidal variation.

3.2.2 IFT measurements

The interfacial properties (interfacial tension and interfacial dilatational rheology) were measured at 23±1 ^oC with the axisymmetric drop shape method using a Tracker Teclis tensiometer (Figure 3.4), equipped with a thermostatic module to control the temperature. A droplet of milliQ water was formed at the tip of a steel needle (2 mm diameter) inside of a glass cuvette (10 mL, HELMA 700) containing the oil phase. The droplet surface area was controlled, via software, by a stepper motor attached to a glass micro syringe (100 μL) plunger. For the equilibrium interfacial tension measurements, the volume of the drop was kept constant. All the experiments were done with a Bond number (B_o) above 0.1.

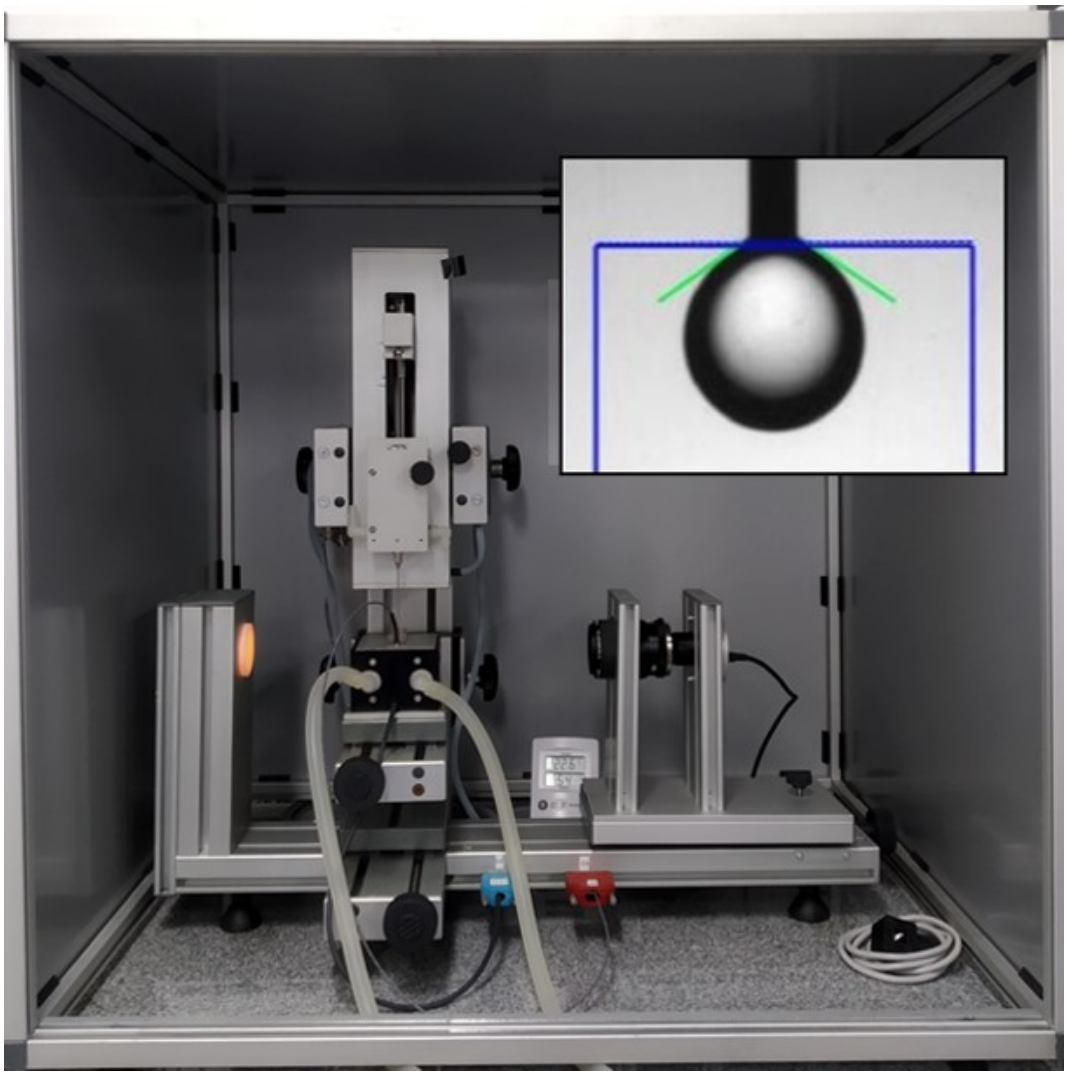

Figure 3.4: Tracker Teclis tensiometer.

The interfacial rheological tests were conducted at fixed low frequency

(0.05 Hz) and low amplitude (10 %) sinusoidal oscillation. The viscoelasticity of the Span 80 adsorbed layers at the water/oil interface was measured during the adsorption kinetics. A fresh drop was formed and the interfacial stress was measured as a function of time, while the oscillation was imposed to its surface area. Figure 3.5 shows the results for the 1.5 $\%wt.$ concentration of surfactant in the oil phase. Three measurements were made for each condition (Figure 3.6).

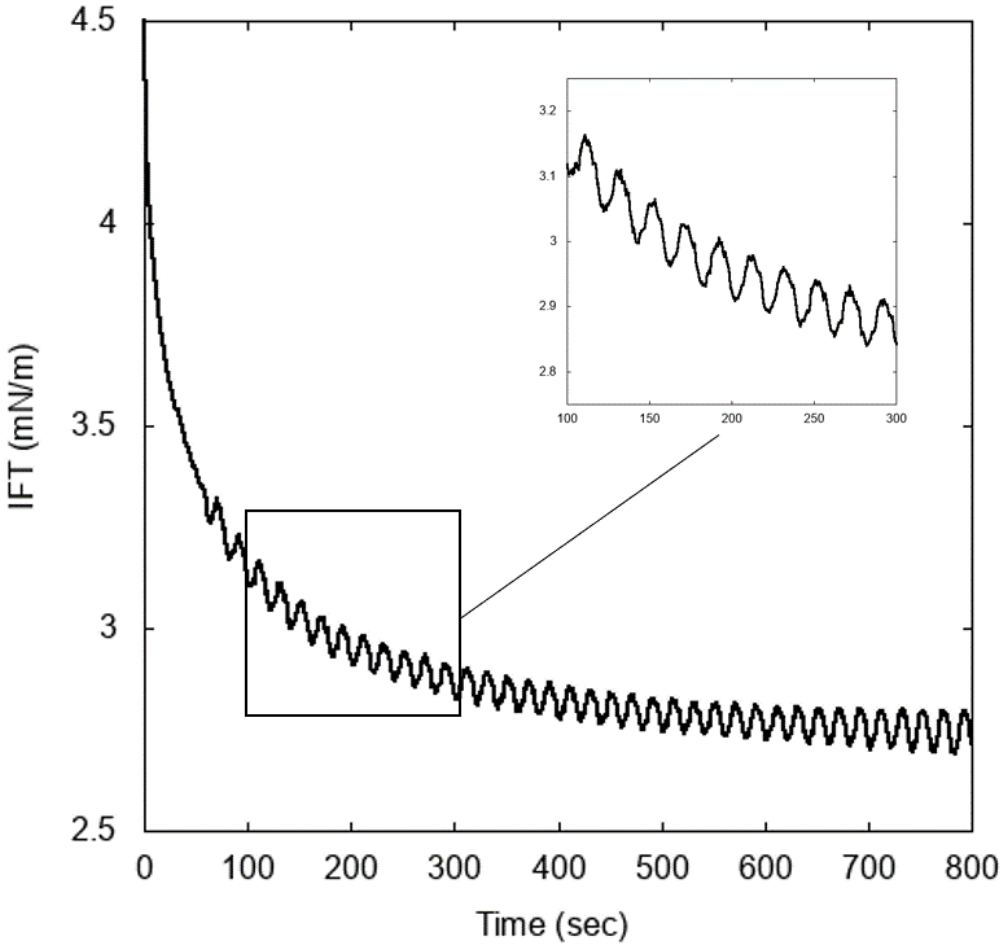

Figure 3.5: Dynamic interfacial tension for 1.5 %wt. of Span 80, during the oscillation of the drop volume at frequency of 0.05 Hz. (IFT: interfacial tension)

The density of each phase are used as input parameter in the measurement of the interfacial rheology by the pendant drop method, the results are presented in Table 3.2.

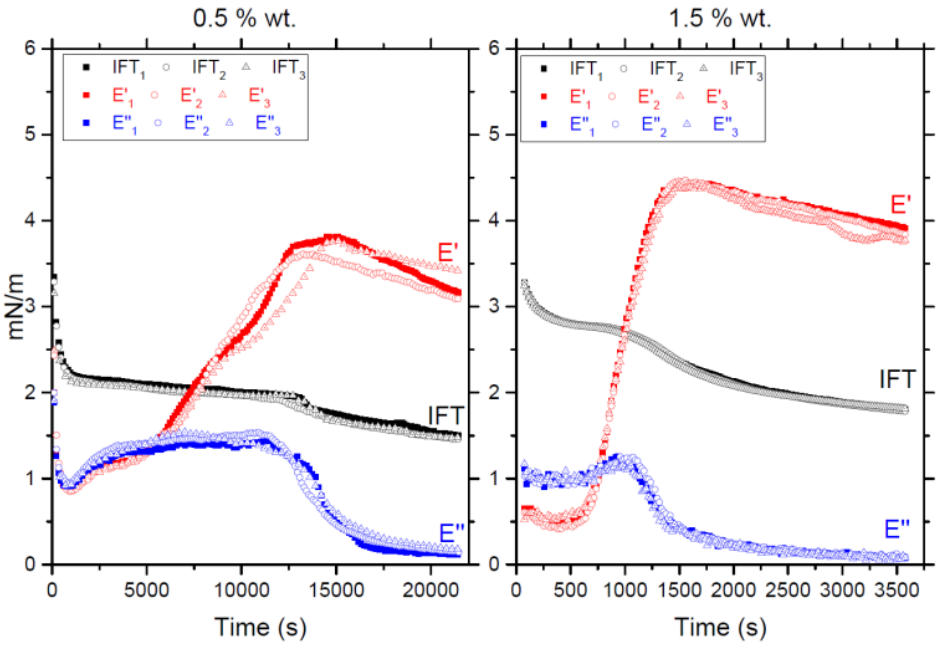

Figure 3.6: Example of repeatability of interfacial rheological tests conducted at 0.05 Hz and 10% amplitude for 0.5 and 1.5 %wt. Span 80 (E': elastic modulus, E": viscous modulus).

Fluid	**Density** (g/cm^3)
Primol + 0.5 %wt. Span 80	0.8621
Primol + 1.0 %wt. Span 80	0.8627
Primol + 1.5 %wt. Span 80	0.8632
Primol + 2.0 %wt. Span 80	0.8637

Table 3.2: Density of fluids measured at 23 ^oC.

3.3 Results of the Interfacial Rheological Characterization

Before reporting and discussing the measurements of interfacial properties, we first show that when the surfactant concentration is high enough, a solid-like film is formed at the interface after some time (Fig. 3.7).

Drops of water in contact with Primol at different Span 80 concentrations were evaluated to observe the evolution of the behavior of the water/oil interface along the time. The best way to prove the appearance of a structure at the interface is to reduce the volume of the drop to show the presence of wrinkle, as shown in Fig. 3.7. Images of the water drop suspended in the needle is presented at different times and surfactant concentrations. The last image

of each row, which corresponds to a different surfactant concentration, was obtained after the drop volume was purposely reduced. In the absence of Span 80, first row of the figure, the drop keeps its almost spherical shape as the volume is reduced. At high enough surfactant concentration, the presence of a solid-like film is clearly observed as the volume of the drop is reduced. Wrinkles, characteristic of a solid film under compression, appear as the volume of the drops is reduced, confirming that Span 80 allows to obtain a film-like structure at the interface.

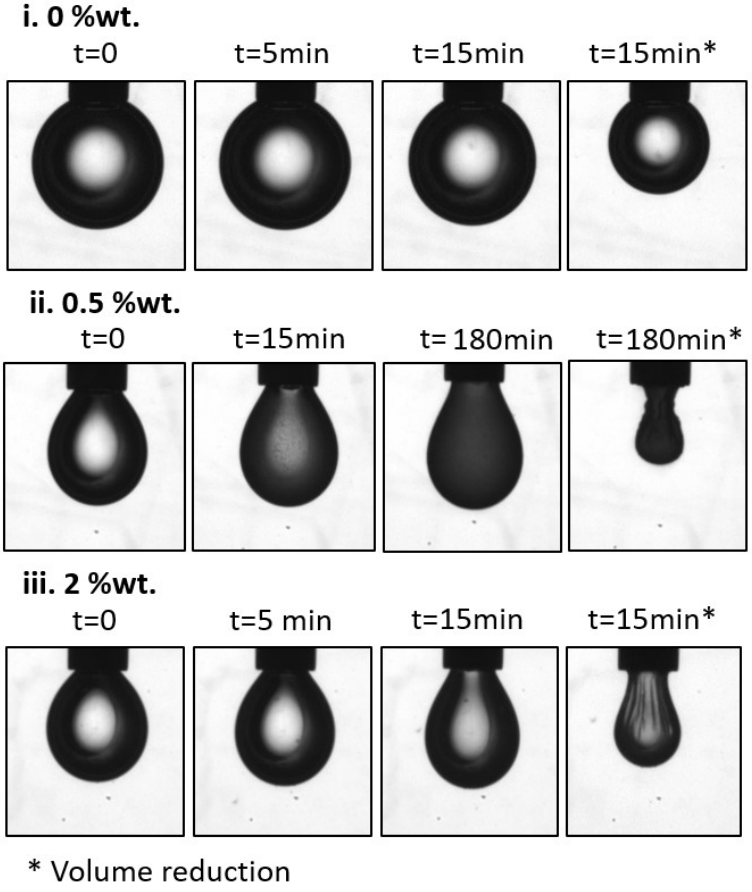

Figure 3.7: Droplet interface aging for different surfactant concentrations showing the formation of the solid-like interface.

3.3.1 Interfacial tension

Firstly, it was obtained the CMC. Figure 3.8 presents the evolution of oil/water interfacial tension with time for different concentrations of Span 80 in Primol 352. Figure 3.9 presents the interfacial tension at the end of the experiment as a function of Span 80 concentration. The apparent CMC of the Span 80 in Primol 352 in contact with the water phase was estimated from

data of Fig. 3.9 to be equal to 0.05 $\%wt.$ which is consistent with literature [22, 23, 79]. The time evolution presented in Fig. 3.8 is strongly dependent on the surfactant concentration. For concentrations lower and close to the CMC (Fig. 3.8a), the interfacial tension rapidly falls within a few seconds and then slowly approaches its equilibrium value. The rate of decrease rises with surfactant concentration. Indeed, when a fresh interface is created, there will be a diffusion of surfactant from the bulk to the sub-surface, which can be considered as an imaginary plane, a few molecular diameters below the interface. In this case, once in the subsurface, the surfactant directly adsorbs at the interface. In this model, the entire process is only controlled by surfactant diffusion and the timescale of adsorption from the subsurface to the interface is very fast. Benmekhbi et al. [11] confirmed that at low concentrations (below CMC), the adsorption of Span 80 is purely diffusion-controlled with negligible barrier to adsorption. They also showed that the naphthenes present in Primol 352 can intercalate between the surfactant molecules at the interface, increasing the hindrance and therefore altering the interaction between surface active species.

The long time data below the CMC are well fitted by the Ward and Tordai model (Fig. 3.8.a) for the diffusion controlled adsorption of nonionic surfactants:

$$\gamma(t \to \infty) \approx \gamma_{eq} + \frac{RT}{c}\Gamma_{\infty}^{2}\sqrt{\frac{\pi}{4Dt}}$$

where γ_{eq} is the interfacial tension at the equilibrium, Γ_{∞} is the maximum surface concentration, T the temperature, R the universal gas constant, and c is the bulk concentration. For the long-time data, the Gibbs equation to determine the surface coverage is only applicable close to equilibrium conditions [80].

A closer look in Fig. 3.8.a reveals that the interfacial tension has not reached a steady state and the system is not yet truly at equilibrium, but still slowly varying with time, even after two hours. The equilibrium times of the Span 80/Primol 352 systems are also much higher than those already published for different oils [23]. This phenomenon is even observed at 0 $\%wt.$, where there is still a slow drop in the IFT - meaning there are some interfacial processes going on with other components from the oil beyond Span 80. As the rapid early decay of IFT for the Span 80 system is not completely captured by pendant drop tensiometry, it is unfortunately not possible to use the short time approximation to model the diffusion process.

Therefore, using Gibbs equation and data presented in Fig. 3.9 will not lead to accurate estimation of Γ_{∞}. As an alternative, we estimate the equilibrium IFT γ_{eq} from the Ward and Tordai model fit. Table 3.3 compares

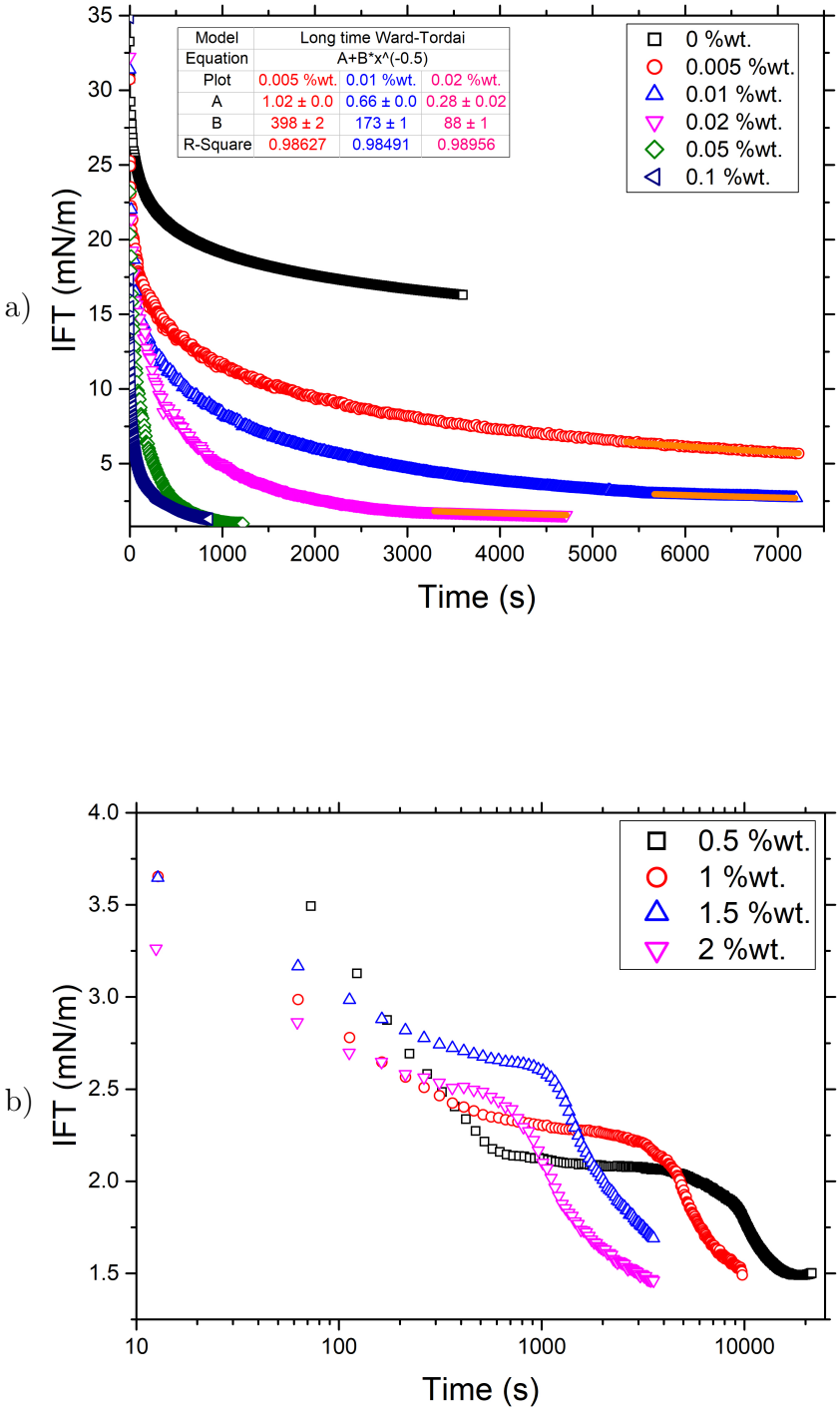

Figure 3.8: Dynamic interfacial tension as a function of Span 80 concentration: a) low surfactant concentrations (b) high surfactant concentration.

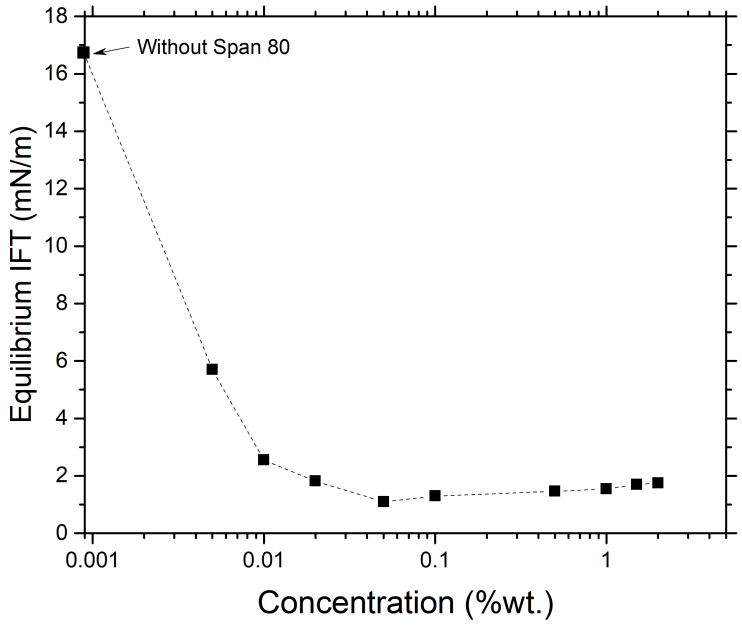

Figure 3.9: Equilibrium interfacial tension as a function of Span 80 concentration (dash black lines simply guide the eye).

	γ_{eq} (mN/m)	
Concentration	Data	Model
0.005 $\%wt.$	5.7 ± 0.1	1.02 ± 0.09
0.01 $\%wt.$	2.5 ± 0.1	0.66 ± 0.05
0.02 $\%wt.$	1.8 ± 0.1	0.28 ± 0.02

Table 3.3: γ_{eq} for concentrations below the CMC determined from long time experimental data and from Ward and Tordai fit.

the equilibrium IFT from the experiments, which have not reached equilibrium, and those estimated by fitting the long-time data to the Ward and Todai model. As expected, the values estimated by the curve fit were lower and equilibrium would be reached at much longer time. However, it becomes almost impossible to measure the IFT for such low values because the drop ends up detaching from the needle before equilibrium is reached.

We used the fitted γ_{eq} at concentrations equals to 0.005, 0.01, and 0.02 $\%wt.$ and Gibbs equation to estimate the maximum surface concentration $\Gamma_\infty \approx 1\times\ 10^{-6}\ mol/m^2$, which is close to values previously determined in the literature for Span 80 with different oils (alkanes, parraffins) [23, 79]. Using the Ward and Todai model with the estimated value of Γ_∞, we estimate the diffusion coefficient to be $D \approx 5\times10^{-15}\ m^2/s$, lower than the values of diffusion coefficient for nonionic surfactants [11, 81]. This difference arises from the influence of the compounds of Primol 352 as it has already been observed in Fig. 3.8.a with a delay to reach an equilibrium IFT, even without surfactant.

For concentrations greater than 10 times the CMC (Fig. 3.8b), the diffusion of the surfactant to the interface is initially very fast, as the first interfacial tension value measured is already very low (between 3 and 4 mN/m). The interfacial tension decreases until reaching a first equilibrium plateau, and then a second decrease is observed until a new, lower equilibrium value is reached. This second drop occurs earlier as the surfactant concentration increases. This behavior may correspond to the mixed kinetic-diffusion model which assumes that the surfactant diffuses from the bulk to the subsurface, but the rate-controlling process is the transfer of these molecules to the interface. Once the surfactant has diffused to the subsurface, there may be an adsorption barrier present preventing their adsorption. This barrier may be due to increased surface pressure, or attributed to less 'vacant sites' available for adsorption. There may also be steric restraints on the molecule in the proximity of the interface. This will cause the molecule to back diffuse into the bulk rather than adsorbing, thereby increasing the timescale of the dynamic interfacial tension decay. An important point that needs to be taken into account is that, as shown in Fig.3.7, at high surfactant concentrations, a skin-like film is formed with aging. The mechanisms by which interfacial tension is lowered when macroscopic skin is formed are not yet well understood; it may not come from phenomena at the molecular scale, but rather from a macroscopic interface which no longer suits the Laplacian conditions of the drop shape [82]. Santini et al. (2007) observed a similar behavior with 3.5 $\%wt.$ Span 80 in a paraffin oil [23]. The y reported transient behavior of the interfacial tension value also presented two plateau regions, with a second sharp decrease at about 500 s.

3.3.2 Interfacial Dilatational Rheology

From now on, we focus on the characterization of the interface for the higher surfactant concentrations (0.5 to 2 $\%wt.$) at which the solid-like structure behavior is observed. We measure the time evolution of the interfacial tension, the dilatational storage and loss moduli of the interface as a function of surfactant concentration; the results are presented in Fig. 3.10. Three time regimes of change in the elastic modulus are delimited by dotted lines: (I) initial plateau, (II) increased elasticity, and (III) loss of elasticity.

At short times (I), the elastic and the viscous moduli are almost equal. At this point, the values of the moduli are close and also lower than the interfacial tension which suggests that the interfacial stress is close to isotropic. This initial plateau is attributed to the adsorption of surfactant monomers

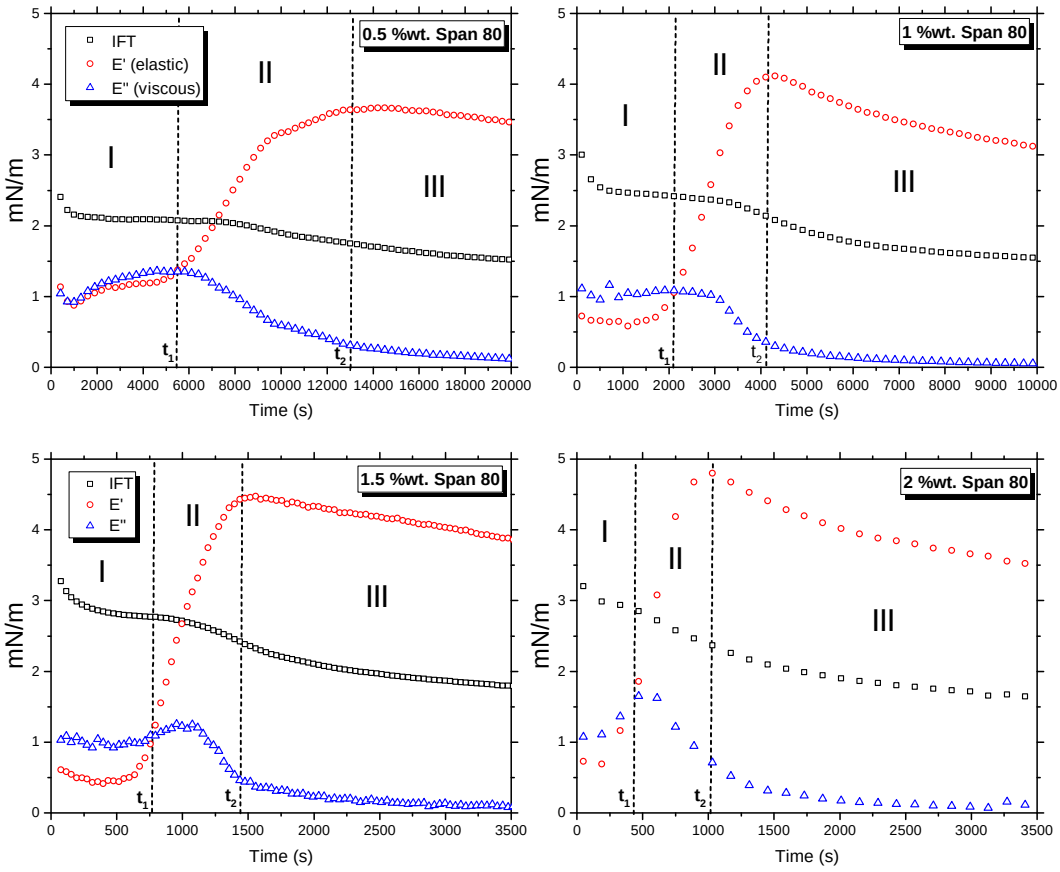

Figure 3.10: Interfacial tension and interfacial dilatational moduli E' and E" (10 % volume amplitude and 0.05 Hz frequency) for different Span 80 concentrations over the CMC.

or inverse micelles, or both at the interface as it corresponds to the first equilibrium of IFT [76]. After a certain level of interface aging, the elastic modulus increases and becomes higher than the viscous modulus (II). The time (t_1) at which this occurs depends on the bulk surfactant concentration (Table 3.4) and can be related to the dynamic rate of adsorption of the surfactant to the interface. For the 0.5 $\%wt.$ surfactant concentration, the elastic modulus becomes higher than the viscous modulus at approximately $5,500$ s, whereas this value was close to 400 s for the 2 $\%wt.$. The increase in elastic modulus also corresponds to the second drop in IFT. The structural change at the interface could be due to molecular interactions or rearrangements [76]. Moreover, the interactions between the hydrophobic tails of the Span 80 and the satured hydrocarbons of Primol 352 also play an important role on the interfacial surfactant organization and the viscoelastic properties [11, 23, 76, 83].

As aging progresses, the elastic modulus rises until reaching a maximum value and then slightly falls (III). The time (t_2) taken to reach this maximum decreases with the surfactant concentration (Table 3.4). Conversely, the viscous

modulus decreases reaching a value close to zero at long time. The formation of a solid-like interface is well identified by the increase in the elastic modulus. We can also notice that the maximum value of the elastic modulus increases with the concentration of Span 80, varying from 3.66 to 4.80 mN/m while the value of equilibrium interfacial tension is unchanged. These data indicate that an excess of Span 80 may be favorable in preventing coalescence as the film strength increases with the concentration of the surfactant.

	t_1 (s)	t_2 (s)
0.5 $\%wt.$	5,500 ± 300	12,500 ± 100
1 $\%wt.$	2,100 ± 200	4,000 ± 100
1.5 $\%wt.$	775 ± 50	1,500 ± 50
2 $\%wt.$	410 ± 50	1,100 ± 100

Table 3.4: Characteristic times t_1 and t_2 of changes in modulus of elasticity as a function of Span 80 concentration.

The low values, about several mN/m, measured for the elastic modulus at Span 80 concentrations higher than the CMC are in accordance with the literature [23, 84]. The evolution of the interfacial tension is consistent with the dilatational moduli, both evolve over very long periods of time which clearly indicates the development of the interfacial structure. However, the late-time decrease in the elastic modulus is unexpected, because skin formation is normally associated with a slow continued increase in the storage modulus [82, 85]. Similar behaviors have been reported for proteins [86, 87] and for Span 80 [23] but without further explanations. As we observed previously in Fig.3.7, this behavior is accompanied by the appearance of a skin at the interface leading to non-homogeneous deformations of the drop (wrinkles and local deformations) during the oscillations. The characterization of the dilational viscoelastic properties is dependent on the correct evaluation of the interfacial stress during the oscillations [75, 88]. In addition, the values of the modulus may also depend on the oscillation frequency as the response could be nonlinear due to the extremely long time scale of the adsorption. To check if the elastic modulus drop is the result of a measurement artifact, we increased the oscillation frequency and observed that the drop in elastic modulus increases with the oscillation frequencies (Fig. 3.11). Therefore, the data of the elastic modulus measured after the maximum cannot be interpreted.

Additional tests were carried out to verify whether the oscillations of the drop affect the viscoelastic properties of the interface, as it may hinder

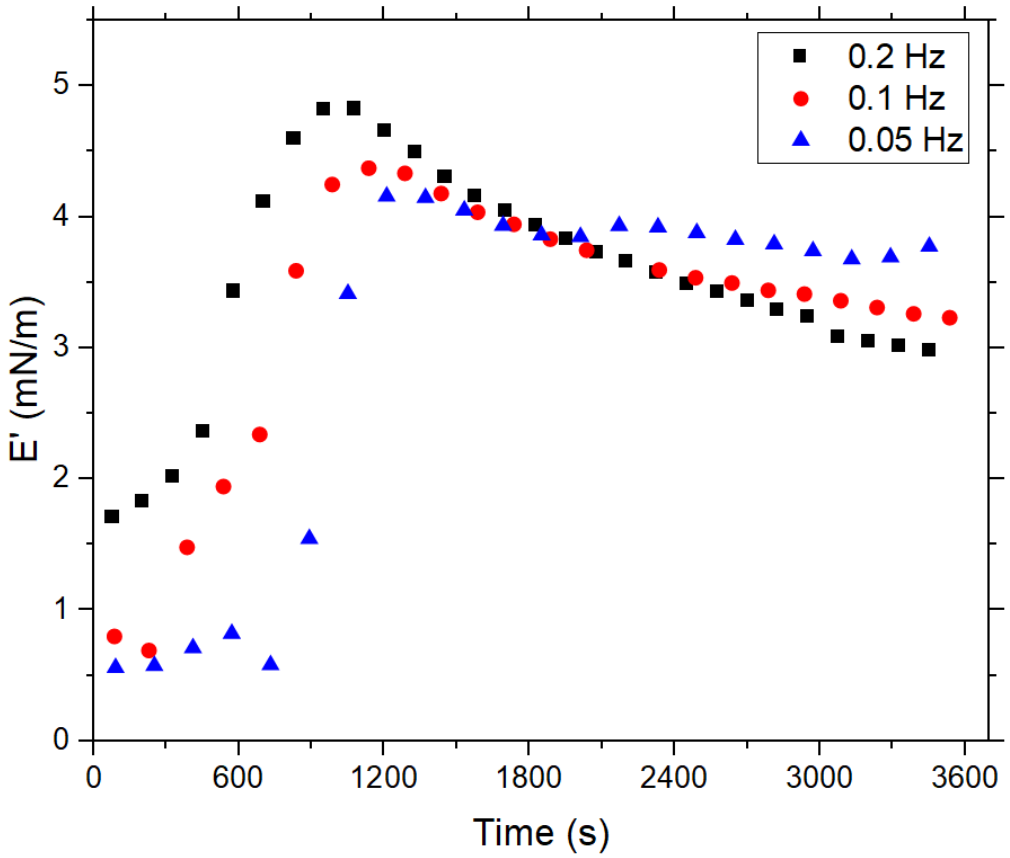

Figure 3.11: Influence of oscillation frequencies on elastic modulus for 2 wt%. Span 80.

surface structuring. The oscillatory interface characterization experiments were carried out by varying the start of the drop oscillation from 0 to 20 minutes after the drop formation for the 2 $\%wt$. Span 80. Figure 3.12 shows that the start time of the oscillation does not affect the interfacial properties as the interfacial tension, storage and loss moduli measured in experiments with different oscillation starting time are identical. At the amplitude and frequency used in the interface characterization experiments, the interfacial behavior does not depend on the history of interface deformation.

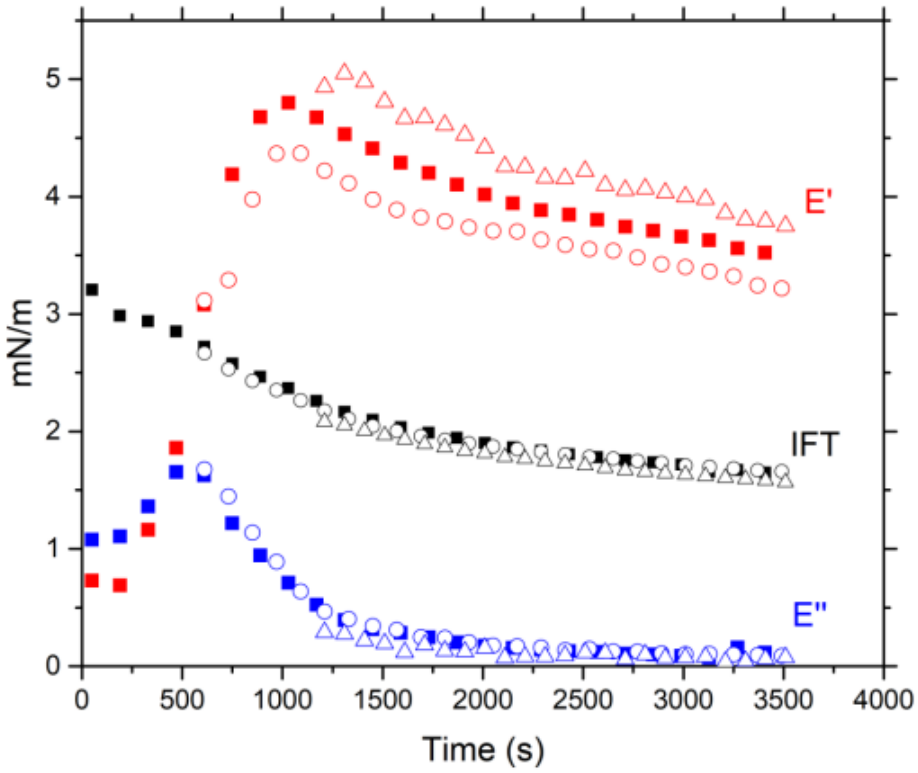

Figure 3.12: Influence of aging time on the interfacial properties of 2 %wt. Span 80. Oscillations of the interface are started after 0 min (squares), 10 min (circles), and 20 min (triangles) of aging.

3.4 Brief conclusions

The time evolution of the IFT and the dilatational storage and loss moduli of the interface as a function of surfactant concentration were measured using the oscillatory pendant drop technique. The apparent CMC of the Span 80 in Primol 352 in contact with the water phase was estimated to be equal to 0.05 %wt. IFT presented a strong dependence on the surfactant concentration. Concentrations lower and close to the CMC, the IFT rapidly falls and approaches its equilibrium value. Whereas, concentrations above the CMC presented very fast diffusion of the surfactant to the interface, decreasing the IFT until a first equilibrium plateau. After that, a second decrease in the IFT is observed could correspond with the moment of the solid-like film formation at the interface. The formation of this film can both affect the accuracy of the measurement of the interfacial tension using the axisymmetric

drop shape analysis and the mechanical response of the interface to oscillations, once the drop could lose its Laplacian shape.

The elastic and viscous moduli showed a correlation with surfactant concentration and interface aging time. Three time regimes were identified during the time evolution: (I) initial plateau, (II) increased elasticity, and (III) loss of elasticity. The initial plateau represents the regime in which the elastic and viscous moduli are almost equal and lower than the IFT. In this sequence, the elastic modulus increases and becomes greater than the IFT, while the viscous modulus decreases, representing the second regime. Lastly, after reaching a maximum value, there is a decrease in the elastic modulus at the same time that the viscous modulus tends to zero.

A solid-like interface is formed when the elastic modulus rises, and the increase in elastic modulus occurs with the second drop in IFT. Molecular interactions or rearrangements could be responsible for the structural change at the interface. Furthermore, the interactions between the hydrophobic tails of the Span 80 and the satured hydrocarbons of Primol also play an important role in the interfacial surfactant organization and the viscoelastic properties.

4
Relationship between interfacial properties and drop coalescence

This chapter presents the relationship between the coalescence and the behavior of oil-water interfaces discussed in the previous chapter. Firstly, the coalescence between two isolated water droplets immersed in the oil phase was studied as a function of surfactant concentration and the aging time of the drops. Then, a briefly study about the stability of emulsions were conducted and we linked it with the behavior observed previously for two water droplets.

4.1
Experimental Procedure

4.1.1
Coalescence between two drops

The coalescence process of two large water drops immersed in the oil phase was investigated using the setup presented in Fig. 4.1, which was based on the setup proposed by Bochner et al. [15]. Figure 4.2 presents the experimental on the lab. The setup consists of:

A - pressure transducer (Wika, 0.1 bar) to measure the pressure in the tube that connects the needle to the syringe;

B - syringe pump (model Pump 11 Elite from Harvard Apparatus) used to form and control the volume of each drop, a linear stage to vertically move the bottom drop towards the top drop;

C - glass cuvette (25 mL, HELMA 700) equipped with a 3D printed base with holes to lodge the bottom drop in place, filled with the oil phase; inside which a needle is used to form the water drops;

D - high speed visualization system, composed by a high speed camera (model Fastcam Mini UX100, Photron) and a light system;

E - lift to move the drops against each other;

F - computer to record the events and the pressure data.

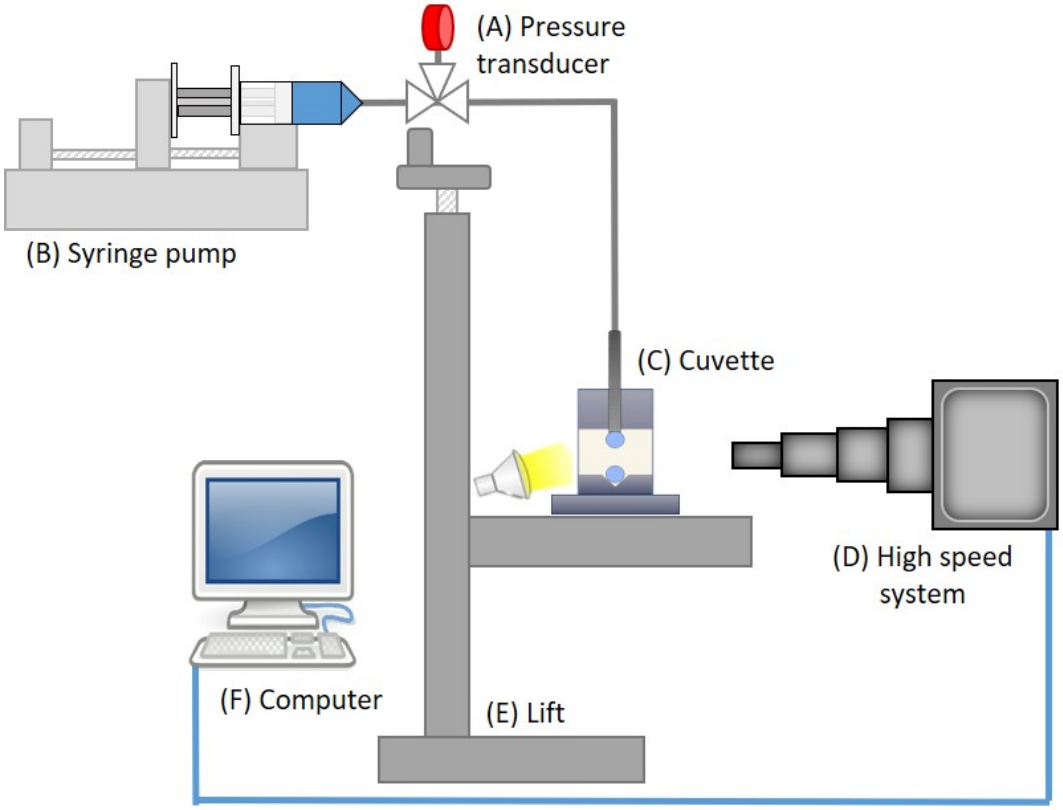

Figure 4.1: Scheme for the experimental setup for the coalescence study.

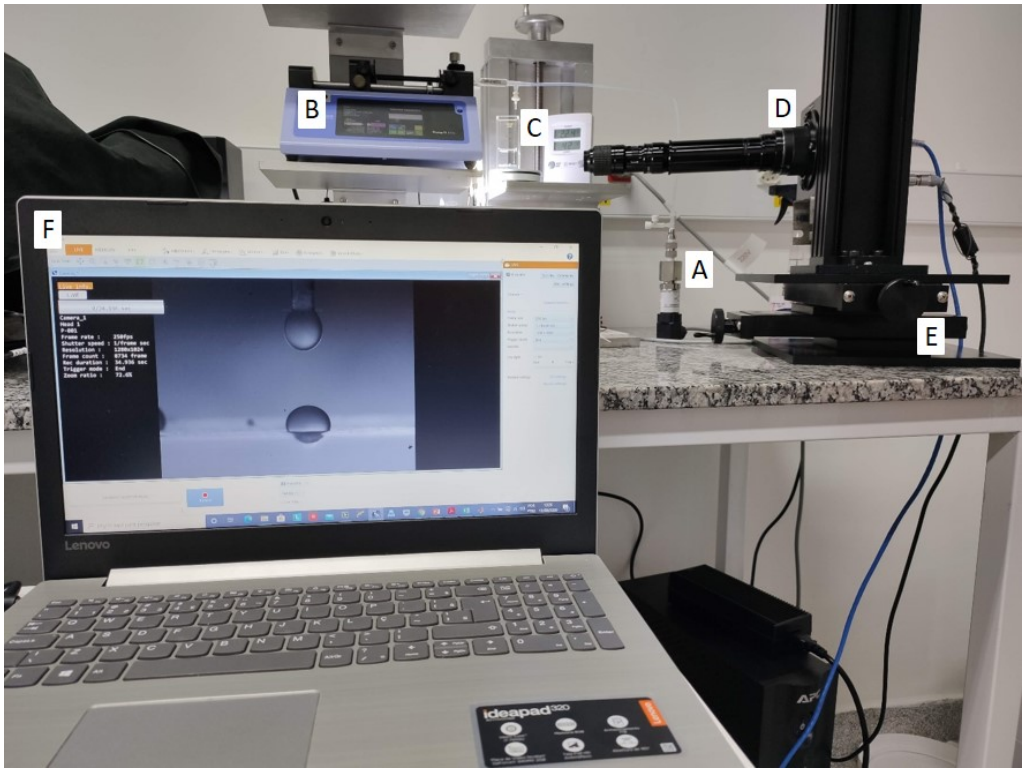

Figure 4.2: Experimental set-up of the droplet coalescence, including: (A) pressure transducer, (B) syringe pump, (C) cuvette, (D) high speed system, (E) lift, and (F) computer.

As it was crucial to avoid lateral slippage of the drop and to promote alignment of the two drops a 3D printed base was inserted into the cuvette, as shown in Fig. 4.3. Another important gain with this device is that it allows to run more than one experiment before changing the oil phase and cleaning all the devices without compromising the results, thus optimizing the time.

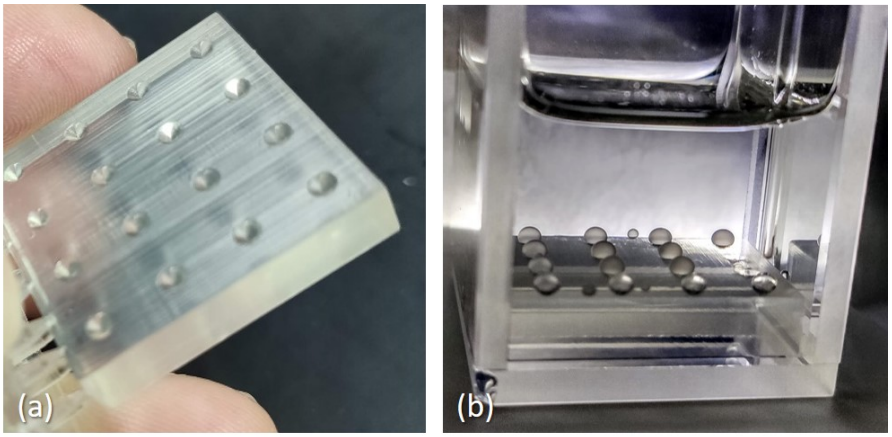

Figure 4.3: (a) 3D printed base and (b) example of the experiments with this base inserted into the cuvette.

After filling the cuvette with the oil phase, each series of coalescence time determination consisted of the following steps, illustrated in Fig. 4.4:

1. forming the first droplet and placing it at the bottom of the cuvette, as shown in Fig.4.4a-c;

2. releasing the droplet from the needle by moving down the lift manually, as shown in Fig.4.4d;

3. forming the second droplet at the tip of the needle and wait for the set interface aging time (Fig.4.4e-f);

4. moving the droplets close to each other until contact (Fig.4.4g);

5. wait for the coalescence to occur, as shown in Fig.4.4h-l.

The pressure in the needle is used to track all the different steps and precisely determine the instant at which coalescence occurs (Fig.4.6). The signal is treated and converted using a National Instruments Data Acquisition (DAQ) board (cDQA-9171 chassis, NI 9203).

The pressure response in the transducer refers to the sum of the hydrostatic pressure (P_h) and the Laplace pressure (P_L). This response will vary a few times during the experiment as exemplified in Fig 4.5.

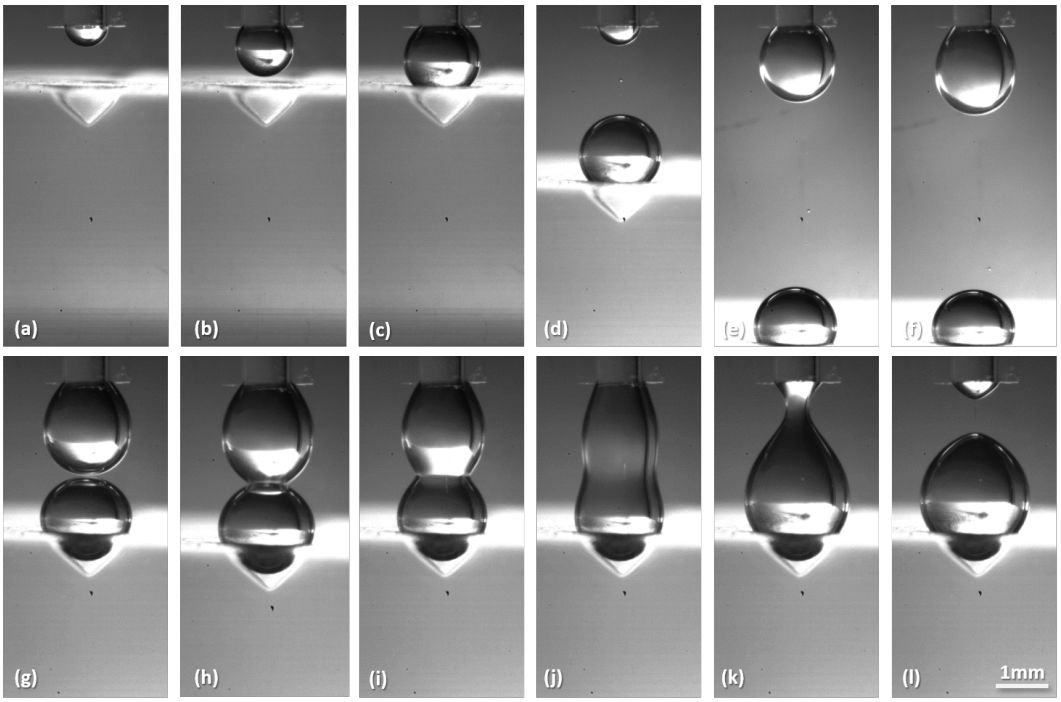

Figure 4.4: Sequence of images representing the process: starting with the drops formation (a-f), then they are let in rest to aging the interface (f), after that they are put in contact (g), and finally when the oil film between them is drainage occurs the rupture of the interfaces and the drops coalescence (h-l).

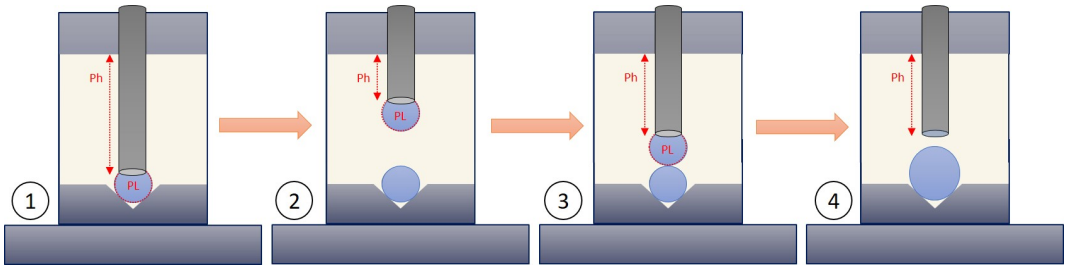

Figure 4.5: Diagram representing the steps of the coalescence process: (1) formation of the first droplet; (2) formation of the second droplet and aging time of the interfaces; (3) approximation of the drops and oil film drainage time between them and (4) droplet coalescence.

The transient evolution of the pressure is divided in 5 different regions:

– Region 1 corresponds to the water drop formation steps. Each pressure peak in this region represents the time at which each drop was formed.

- Region 2 corresponds to the aging time of the interfaces. As the drops remain at rest, the pressure remains almost constant while the surfactant adsorbs onto the water-oil interface. The small reduction in the pressure value is probably caused by the reduction in the interfacial tension which affect the Laplace pressure.
- Region 3 corresponds to approximation of the droplets. As the stage rises and brings the bottom drop closer to the drop attached to the needle, the pressure increases, as the height of the oil column above the needle increases. This change in pressure is associated with the motion of the drops.
- Region 4 corresponds to the drainage time, moment after the interfaces of the two drops come into close contact.
- Region 5 corresponds to the moment that the coalescence occurs, i.e. the thin oil film between the drops is drained. The pressure signal is marked by a sudden increase.

An important information is that the total interface aging time is the sum of the time intervals of Regions 2 and 3.

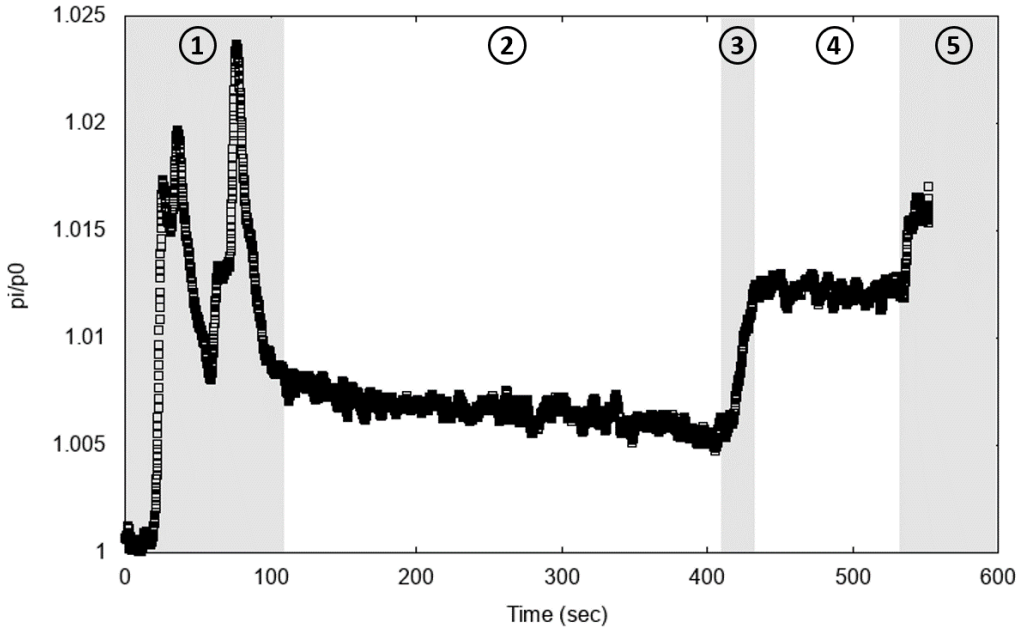

Figure 4.6: Pressure data representing all the steps since the droplets formation until the coalescence process: (1) water drop formation, (2) aging time, (3) contact of the 2 drops, (4) drainage phase, (5) coalescence.

4.1.2 Emulsion stability

A brief study about the stability of emulsions produced with the phases used in the coalescence experiments were performed. Water-in-oil emulsions containing 30 $\%vol.$ water with different Span 80 concentrations in Primol 352.

The emulsions were prepared by a two-step method. First, a premix was obtained by the slow addition of the water phase into the oil under constant stirring with a magnetic bar at 500 rpm. Then, this coarse emulsion was stirred by a T25 Ultra-Turrax (IKA) at 13,500 rpm for 5 min. Hereafter, 20 mL emulsion was placed in a vial for further turbidity scanning with a Turbiscan LAB (Formulaction Inc., France), Fig. 4.7(a).

The Turbiscan is an equipment that uses static multiple light scattering (SMLS) as an optical method to directly characterize concentrated emulsions in their native state. It consists of sending photons (near infrared light source) into the sample (Fig. 4.7(b)). These photons, after being scattered many times by the particles in the dispersion, emerge from the sample and are detected by two synchronous detectors: Backscattering (BS) for opaque and concentrated samples, Transmission (T) for turbid and transparent samples.

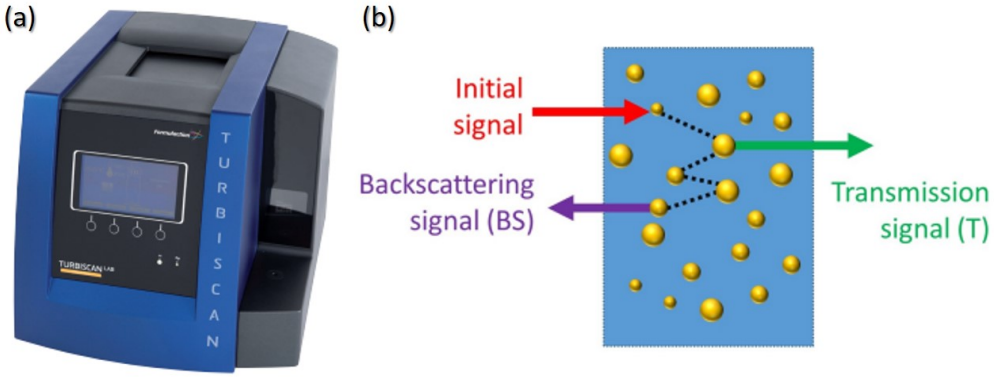

Figure 4.7: (a) Turbiscan LAB and (b) representation of the photos entering in the sample showing the difference between BS and T signal for a dispersion, adapted from [89].

The time evolution of the dispersion is evaluated measuring in scanning mode. So, the optical reading head scans the length of the sample, capturing T and BS data along the sample. Therewith, it can be plotted two curves pro-

viding the transmitted and backscattered light flux in % relative to standards as a function of the sample height. Examples of backscattered light flux curves are presented in Fig. 4.8.

The profile at t_0 is selected as a reference and subtracted to all other profiles to obtain ΔBS and ΔT in order to better analyze the variations of the profiles. At a given time t the expressions are

$$\Delta BS(t) = BS(t) - BS(t_0), \tag{4-1}$$

$$\Delta T(t) = T(t) - T(t_0) \tag{4-2}$$

When the system undergoes several instabilities simultaneously (migration and particle size increase) becoming difficult to set the threshold for phase thickness calculations it is better to use the calculation of ΔBS.

Figure 4.8 presents the cases of the emulsions destabilization and their respective BS profile, listed below:

- Creaming occurs when the density of the dispersed phase is lower than the continuous phase, consequently the dispersed phase concentration at the top increases and at the bottom decreases. On the top, the BS flux will increase and at the bottom of the sample will decrease in function of the reorganization of the dispersed phase within the sample.
- For sedimentation, the dispersed phase concentration in the top will decrease, resulting in a decrease of the BS flux while at the bottom occurs an increase of the concentration of the dispersed phase increasing the BS flux.
- Flocculation and coalescence promote an increase in the dispersed phase size and a decrease of the BS over the total height of the sample.

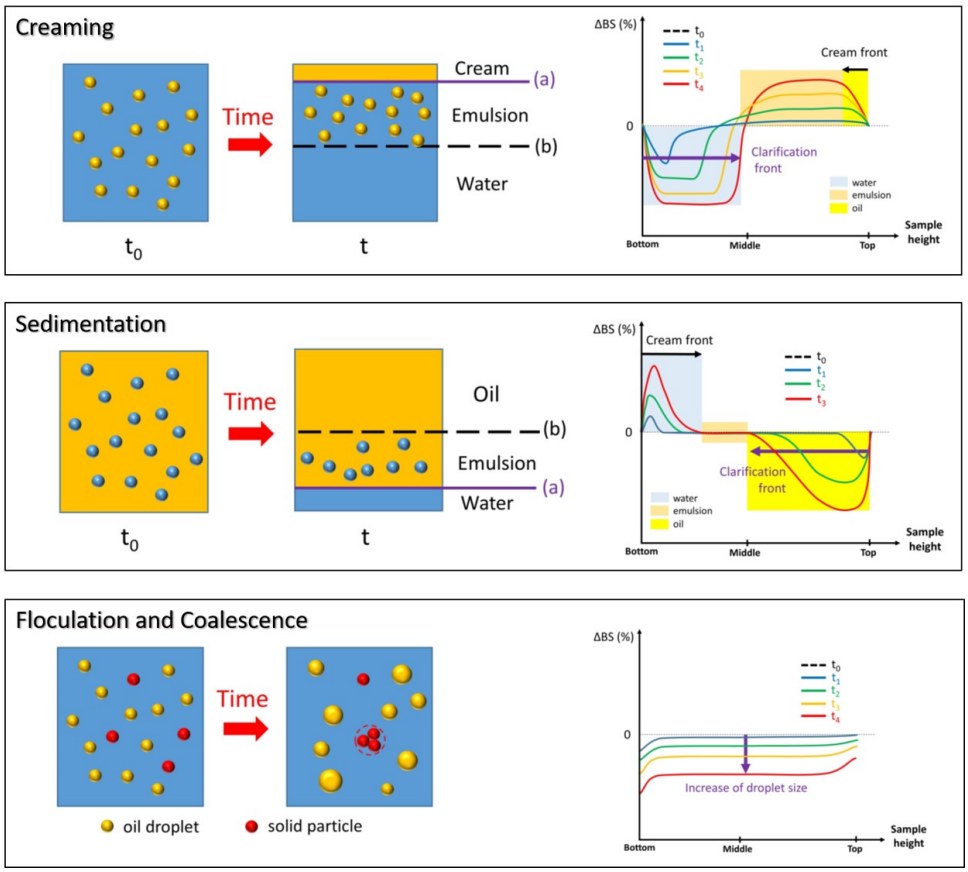

Figure 4.8: Representation of the phenomenon and the backscattering profile (ΔBS) corresponding, adapted from [89].

Both backscattering and transmission signals are function of the photon mean free path, as represented in Fig. 4.9. They are directly dependent on the particle mean diameter d and their volume fraction Φ and can be calculated as

$$T = T(t_0).exp(-\frac{2r_i}{l}), \tag{4-3}$$

$$l = \frac{2d}{3\Phi Q_s}, \tag{4-4}$$

$$BS = \frac{1}{\sqrt{l^*}}, \tag{4-5}$$

$$l^* = \frac{2d}{3\Phi(1-g)Q_s}, \tag{4-6}$$

where l represents the mean distance traveled by photons before undergoing a diffusion phenomenon in Transmission flux; l^* the distance above which the photon loses the initial direction of the incident beam, or from another point of view, it corresponds to the distance of penetration of the photon in the

dispersion in Backscattering flux; Q_s and g are parameters given by the Mie theory.

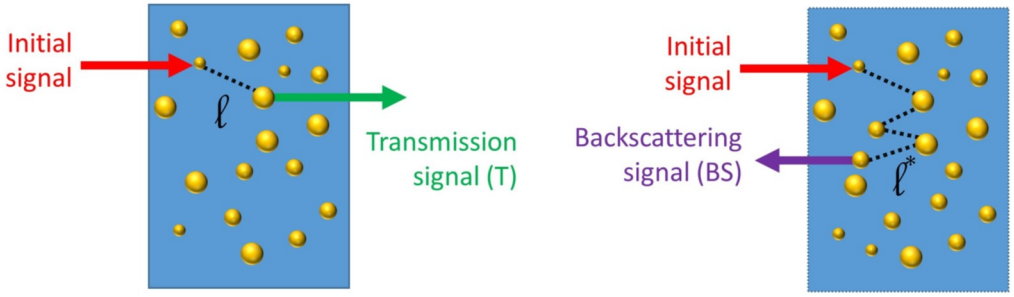

Figure 4.9: Representation of mean free path l and l^*.

So, although this equipment does not provide a droplet size distribution, it is possible to obtain an average droplet size when the volume fraction and the refractive index of the 2 phases is known. The signal used for the calculation depends on its response strength, which is related to the characteristics of the sample, and the equipment decides between T and BS which one will be used.

Emulsions were scanned at 25 $°C$ with an 880 nm near-infrared light-emitting diode (LED) source. At least 2 independent emulsion samples were prepared to check for reproductibility.

4.2 Results and Discussion

The formation of the film, presented at the Chapter 3, has a dramatic impact on the coalescence dynamics, as we discuss along this section. For example, in Fig. 4.10 is represented the attempt to force the coalescence of two old droplets pushing one drop against another (a) without success. In the sequence, they were separated (b-h) without compromising their interfacial structure. This test was performed using the surfactant concentration of 2 $\%wt.$, same from the case (iii) presented at the Fig. 3.7. We can see that the structure at the droplet interface prevents the coalescence of them.

4.2.1 Coalescence of two drops

Coalescence process of two drops involves four consecutive stages: deformation of contacting drops and formation of a thin film, drainage of the film,

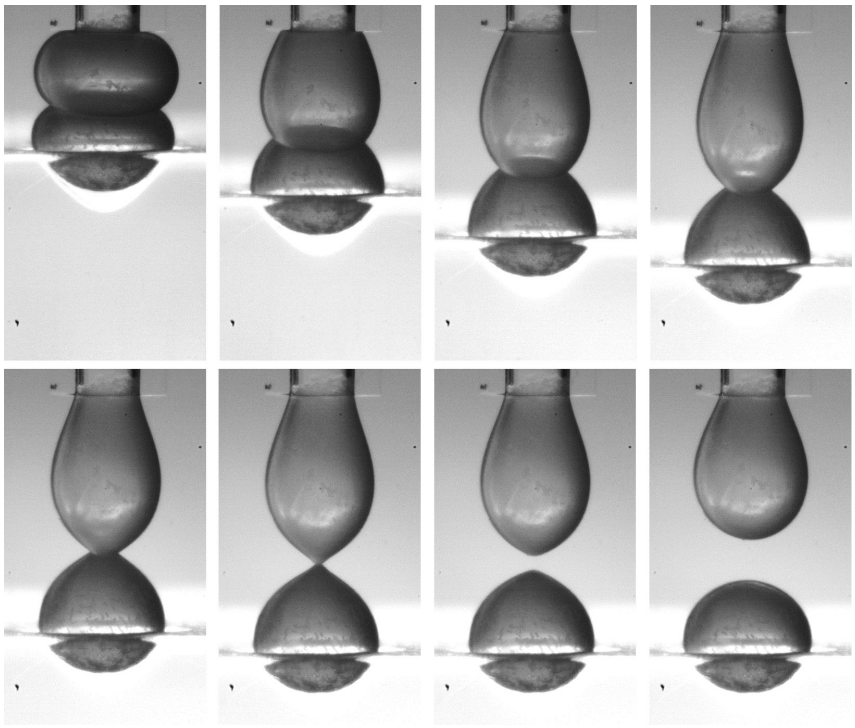

Figure 4.10: Separation of two water droplets that have not coalesced over time.

rupture of the film, and merging of the drops. The drop coalescence experiments consisted of measuring the time required for drop coalescence, called drainage time or drop rest time, after they are pushed against each other. The approach causes liquid to drain out of the trapped thin oil film to the bulk as it can be seen between frames (g) and (h) in Fig. 4.4. In the absence of interfacial material, when the thin film reaches a thickness of about 100 nm, van der Waals forces become significant and cause the film rupture [90]. On the contrary, the presence of Span 80 surfactant molecules at the oil/water interfaces hampered the creation of a hole in the oil film due to the strong steric frustration of the Span 80 hydrophobic tails.

Figure 4.11 presents the drainage time as a function of interface aging time for large water drops (2 μL) at different surfactant concentrations. Lines drawn on this figure simply guide the eye. The aging time corresponds to the time before the two drops come into contact. The time referring to the experiment without surfactant is not presented in the plot, since the coalescence occurs almost instantly, taking only a few milliseconds. The results are an average of at least six experiments with the respective values of standard deviation. We waited for 60 minutes after the contact between the drops to consider that coalescence did not occur.

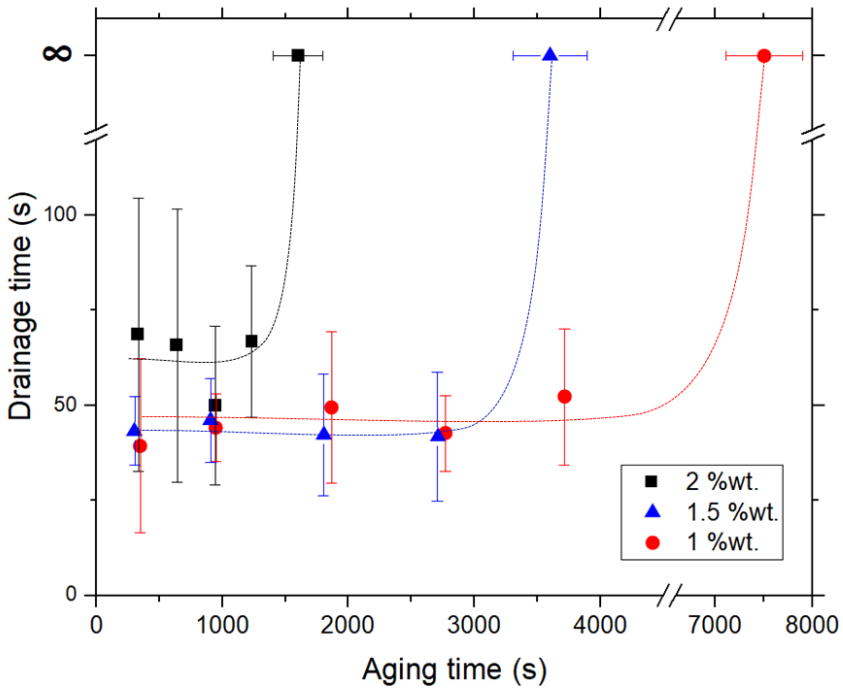

Figure 4.11: Drainage time for the Span 80 concentrations analyzed (lines simply guide the eye).

For Span 80 concentrations over the CMC, there is always a critical aging time above which coalescence was not observed (t_c, critical non-coalescence time), corresponding to the infinite ordinate points on the plot of Fig. 4.11. This critical time falls as the surfactant concentration rises, it is approximately 125 minutes for the 1 $\%wt.$ system and 25 minutes for the 2 $\%wt.$ system. We did not plot the data of 0.5 $\%wt.$ because it is complicated to determine the critical non-coalescence time when the aging time range increases dramatically, however we measured that there is no more coalescence after 240 minutes while there is still coalescence at 60 minutes. For time below t_c, the drainage time is virtually independent of the aging time and weakly dependent of the surfactant concentration. For short aging time, the drainage time for the 2 $\%wt.$ system is slightly higher than the values for the lower concentration systems.

Many parameters as the drop size, surfactant concentration, and viscosity of the oil phase can affect the stability of water drops delaying or preventing the rupture of the water-oil-water film [84]. Although the lifetime of large drops is normally shorter due to the faster thinning of the oil films, Politova et al. [84] confirmed that the stability of large water drops increases dramatically when a concentration of Span 80 above the CMC is used. In the same way, Politova et al. [83] studied the water-oil-water liquid film stability containing Span 80 and they concluded that at 1 $\%wt.$ surfactant concentration the film life-time increases further, due to the longer life-time of the blackfilms with thickness

$<10\ nm$. Several workers [77, 83] proposed that the stability of these thin films is mainly ensured by the steric stabilization of the surfactant tails, adsorbed on the two film surfaces. Others [91, 92] suggested that this exceptional stability in the presence of surfactants arises due to the Marangoni back flow of the fluid into the film, which reduces the net drainage velocity. However, Gosh and Juvekar [93] suggested that the only effect of the Marangoni stress is to suppress the circulation of the fluid inside the drop and thereby increase the interfacial rigidity of the drop. Santini et al. [23] linked this stability to an increase of the inverse micelle concentration which acts as a barrier for drop coalescence even if the dilatational elasticity of the adsorbed layer is very low. To our knowledge, the precise mechanism explaining this phenomenon is not yet clearly identified.

As non-coalescence can be related to formation of solid-like film at the interface, we analyzed the evolution of the profile of the surface of the drops after contact. The formation of the structured film at the interface is clearly observed in Fig. 4.12.1, which presents images of both drops during the entire duration of the experiment for a surfactant concentration of 2 $\%wt.$. The first frame (a) shows the state of the drops after 30 minutes of aging time. After 60 minutes of aging, the bottom drop is moved until coming into close contact with the top drop; this is the start of the drainage process (b). After more than 120 minutes, no coalescence was observed (c). The solid-like film is evidenced by the opaque appearance of the interface. In order to verify the existence of a structured film at the interface, the volume of the top drop was slowly increased. The interfacial structure breakup is clearly observed (d-f). Similar behavior has been reported on other studies using Span 80 [77, 94] and also in some cases using asphaltenes, in which they attributed a thickening of surface layers to the asphaltenes adsorption in the form of aggregates [13, 95, 96]. Even when coalescence occurs, as the interface ages, it is possible to observe the formation of a structured skin at the interface, as shown for 1 $\%wt.$ of Span 80 in Fig. 4.12.2. The first frame was obtained at the beginning of the experiment. It is worth noting the difference in opacity between the two first frames, indicating a change on the interface state.

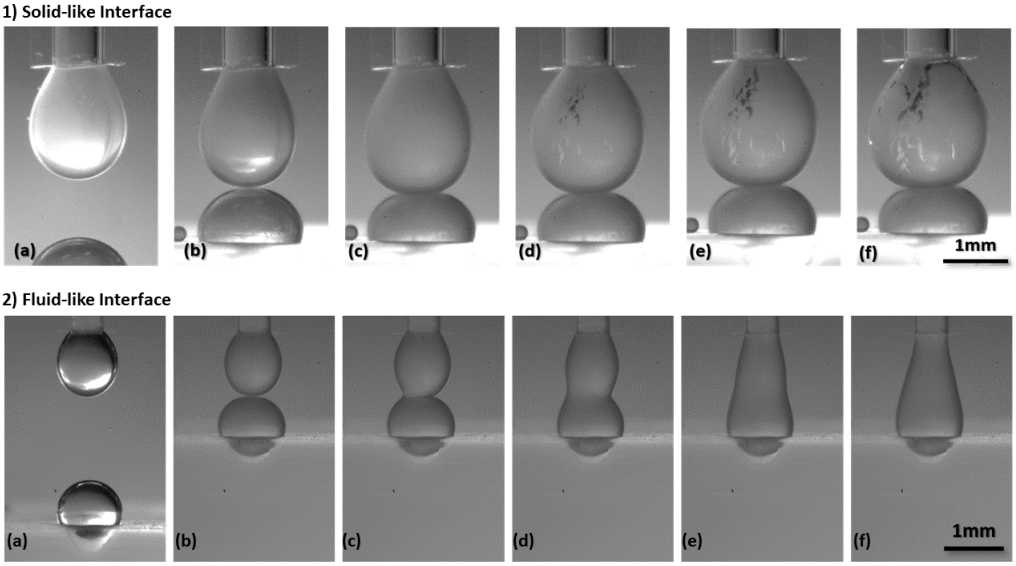

Figure 4.12: Frame sequences of coalescence experiment for 1) 2 $\%wt$. Span 80: (a) drops aging, (b) no coalescence after contact and (c-f) volume increase evidencing a solid-like "skin" without coalescence; and for 2) 1 $\%wt$. Span 80: (a) drops formation, (b) drops approximation after one hour of drops aging and, (c-f) coalescence phenomenon evidencing a fluid-like film.

In general, drop coalescence tests focus on the comparison between the drainage time and the adsorption time of the surfactants. If the drainage time is longer than the adsorption time, it allows the formation of a dense adsorption layer on the film surfaces, able to stabilize the drops by steric repulsion [77, 83] or even by low electrostatic repulsion [97–99]. In our study, we wait before approaching the drops, this duration which corresponds to the aging time of the oil/water interface is always sufficiently large for the adsorption of surfactants at the interface to reach its first equilibrium state (Fig.3.10). To get a better understanding of the phenomenon occurring with the aging, we plotted in Fig. 4.13 the critical non-coalescence time (t_c) obtained from Fig.4.11 and the characteristic times (t_1, t_2) obtained from dilatational elastic moduli (Fig.3.10) as a function of the surfactant bulk concentration. Lines drawn on this figure simply guide the eye. It can be easily noticed that $t_c > t_1$, i.e. coalescence always occurs during the initial plateau regime of the elastic modulus (I) where the interface is considered fluid-like with a low interfacial elasticity. Moreover, t_c is always higher than the time t_2 to reach the maximum of the elastic modulus (Fig.3.10 and Fig.3.11) which means that non-coalescence phenomenon requires more aging time than the time determined by interfacial dilatational rheology. This observation confirms that the elastic modulus should continued to increase as the interface strengthens. Unfortunately, we

cannot access the values of the elastic modulus corresponding to the critical non-coalescence time t_c.

It can be concluded that the drainage time is no longer the determining parameter to study coalescence as soon as a strong enough interfacial solid-like film has formed at the interface. The interfacial properties seem to play a more important role in the non coalescence phenomenon than the properties of the oily thin film between the drops. Moreover, it is more judicious to study the coalescence by comparing the aging times with the characteristic times obtained by the viscoelastic characterization of the interface rather than with the equilibrium times of the interfacial tension.

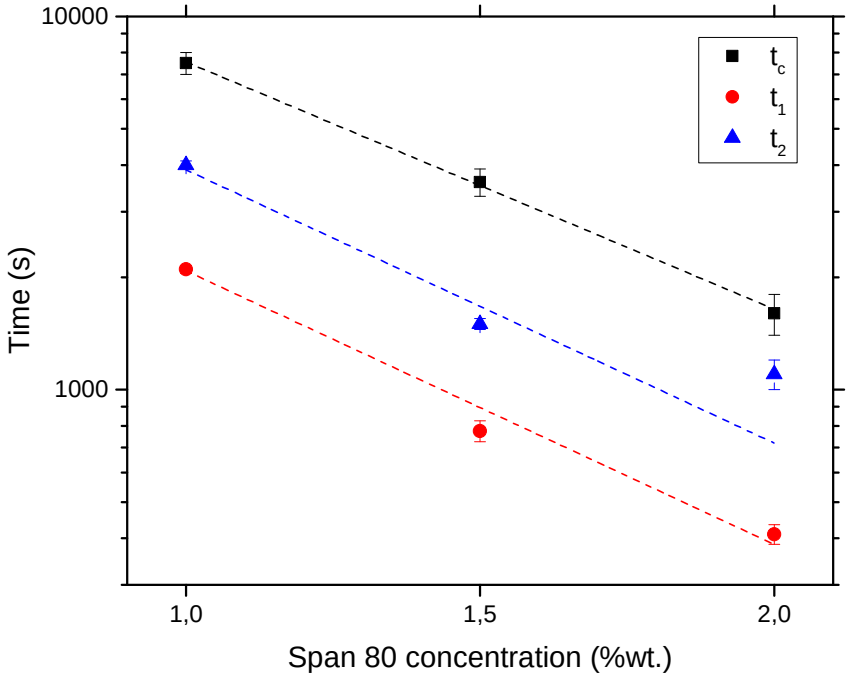

Figure 4.13: Comparison between t_1, t_2, and the critical non-coalescence time t_c.

Politova et al. [84] showed that the stability to coalescence depends on the initial size of the drop. At Span 80 concentrations above the CMC, the stability of the water drops in hexadecane or in Isopar V solutions passes through a minimum: the large and the small drops are very stable, whereas the drops with intermediate radius about 200 μm are unstable. In our study, the drops have a radius about 1 mm, so the relationships between t_c, t_1, and t_2 will be different for medium drops about 200 μm but may be equivalent for smaller drops less than 50 μm.

4.2.2
Stability of emulsions

Water-in-oil emulsions were prepared, as described in section 4.1.2, to relate the interfacial film properties to the stability of batch emulsions for Span 80 concentrations below and above the CMC. The turbidity profiles of the emulsions were measured over time (Fig. 4.14) which makes it possible to study the stability of the emulsions and to identify whether they are subject to coalescence. The signal used to measure turbidity changes depending on the state of the emulsion. Blue corresponds to the signal measured in transmission (T) for the transparent areas of the samples while orange corresponds to the backscattering (BS) for the opaque areas of the samples. The appearance of a blue zone at the bottom of the samples is characteristic of coalescence of the water drops forming a zone of free water. When the orange zone becomes increasingly clear, this reflects the sedimentation of the decrease of the volume fraction of water drops, leading to the appearance of an oil phase with very small amount of dispersed water drops. A strong orange color is characteristic of water drops dispersed in oil, the darker the orange color and the more concentrated the emulsion. As it can be seen in Fig. 4.14, emulsions prepared at concentrations below CMC (<0.05 $\%wt.$) are not stable in comparison to emulsions prepared above the CMC. A blue front quickly appears for 0 and 0.01 $\%wt.$ emulsions, and the times $t_{1/2}$ needed to separate half of the emulsified water is short, i.e. approximately 3 to 5 minutes. For the emulsion at CMC, the phase separation is much slower, $t_{1/2}$ is greater than 1 day and the amount of free water is half that measured for concentrations below the CMC. For Span 80 concentrations greater than CMC, there is no free water in the bottom of the vial, in fact the water drops settle due to gravity but there is no coalescence. We centrifuged (15 min at 6,000 rpm) the samples to try to break the emulsion but the water drops did not coalesce and the emulsion remained stable. A picture of the emulsions taken one day after emulsification (Fig. 4.15) confirmed the observations obtained from the study of turbidity. There is a clear separation of water and oil for 0 and 0.01 $\%wt.$ emulsions whereas there is no free water in the emulsions made above CMC.

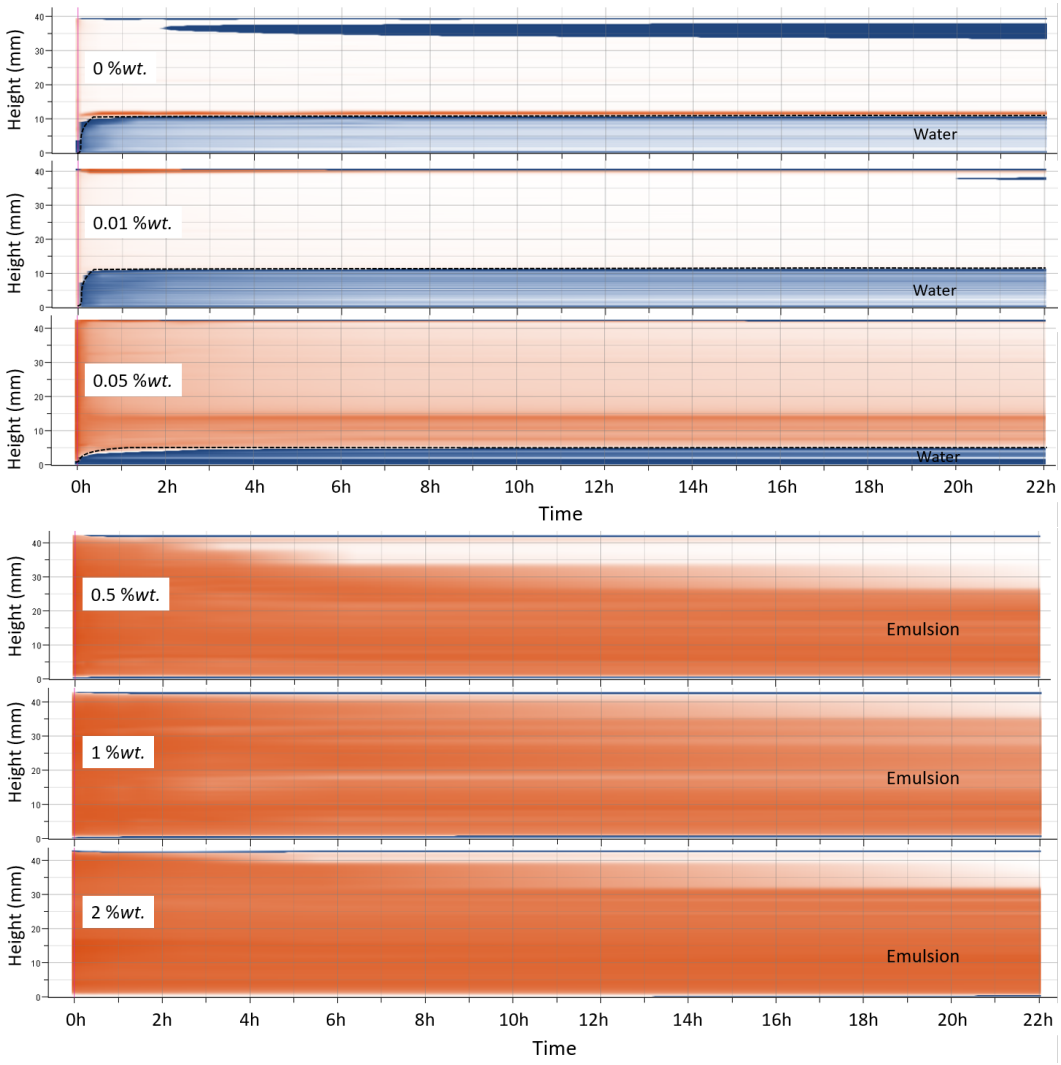

Figure 4.14: Turbidity over time for different Span 80 concentrations. Blue refers to the signal measured in transmission (T) for the transparent areas and orange to the backscattering (BS) for the opaque areas.

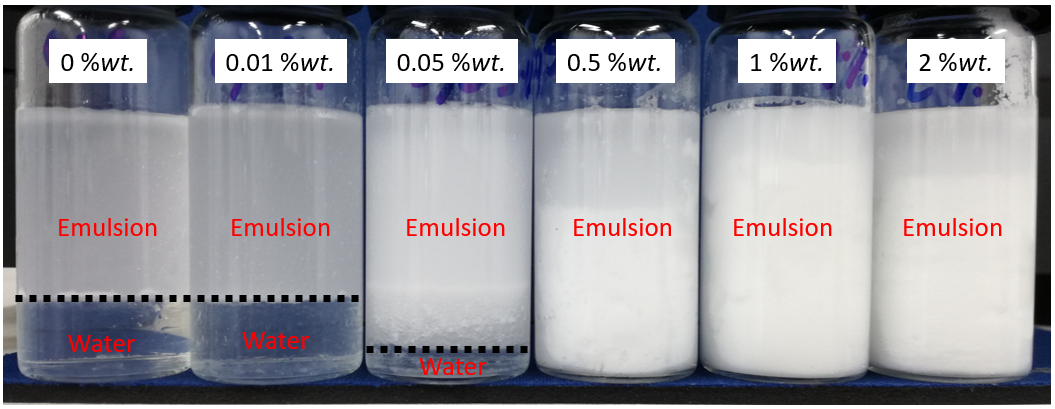

Figure 4.15: 1 day picture of 30/70 water-in-oil emulsions at different Span 80 concentrations.

The average water droplet size of the emulsion was also measured by SMLS (Fig. 4.16). While the size increases very quickly for emulsions with low concentrations of Span 80, it is the opposite trend for concentrations above the CMC, the higher the concentration of Span 80 and the less the size of the drops increases over time. Above the CMC, the initial water drop size is about 14 μm. After 1 day, the average size of water drops of the 2 $\%wt.$ emulsion is about 16 μm whereas it is about 24 μm for the 0.5 $\%wt.$. The presence of an elastic interfacial film which will form more rapidly at 2 $\%wt.$ than at 0.5 $\%wt.$ hinders the coalescence and therefore the increase in size of the water drops.

The study of the stability of the water-in-oil batch emulsions confirmed the behavior observed previously for a single drop. As soon as the Span 80 concentration is much greater than the CMC, the phenomenon of coalescence is more or less quickly stopped, which results in the stability of the emulsion over very long times. In addition, the study of drops of millimeter size is representative of what occurs on the scale of an emulsion composed of micrometric drops.

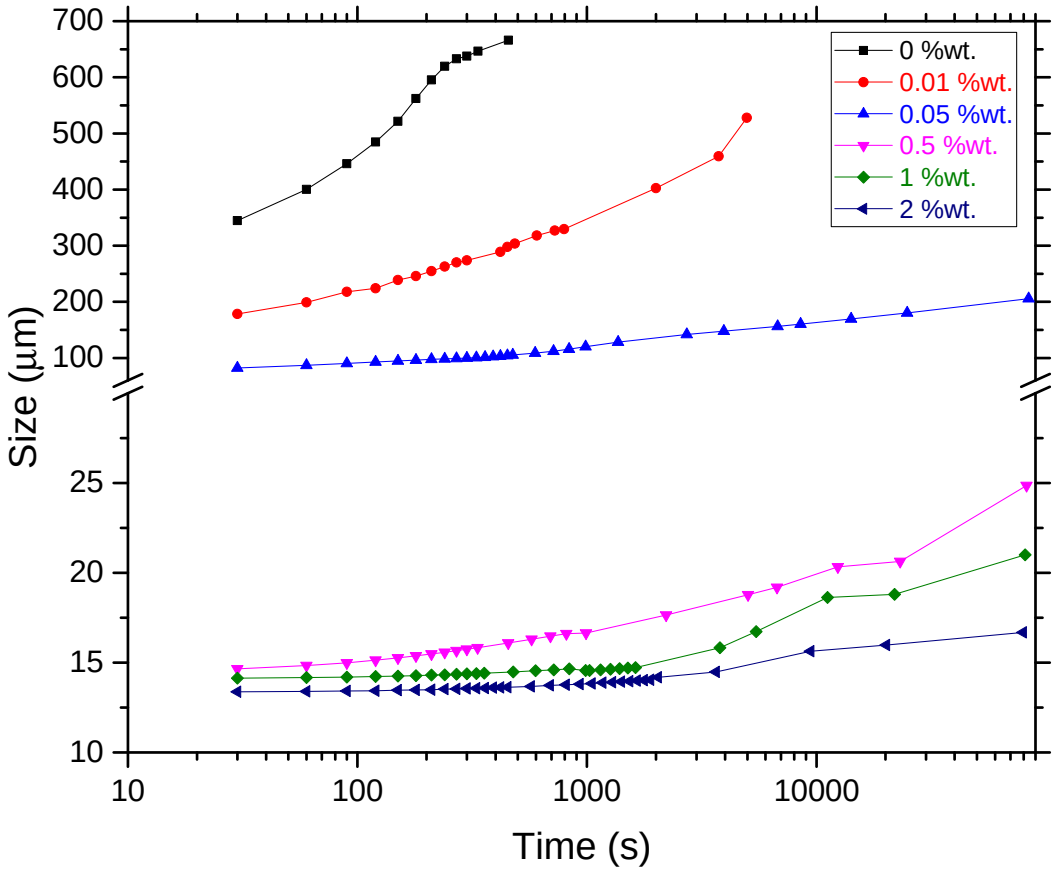

Figure 4.16: Average size of water drops over time for different Span 80 concentration.

4.3 Brief conclusions

In this chapter, different Span 80 surfactant concentrations were tested to understand and evaluate the coalescence process between water droplets. The various results obtained made it possible to link the aging time of the interface and the drainage time of the film between the drops. We observed that the drainage time seems not to be related with the aging time when the coalescence process occurred. For the cases that coalescence did not happen, a formation of a solid-like structure with strong elastic properties was observed on the drop surfaces, this phenomenon results from the strong interaction between the surfactants at the interface.

The elastic and viscous moduli, which present significant changes with surfactant concentration and interface aging, showing that the surface viscoelasticity plays an important role in the coalescence process. The coalescence was prevented when the elastic modulus predominated over the viscous modulus and the latter tends to zero. Increasing the surfactant concentration

reduces the time required for the formation of the solid-like interfacial film which prevents coalescence. These results reinforce what some authors highlighted, the properties of the adsorbed layers protect the oil-water surfaces, controlling the emulsion behavior [9].

For high surfactant concentration systems (above the CMC), non-coalescence was observed if the aging time is longer than the time at which the storage modulus starts to predominate over the loss modulus. Likewise it is quite possible that a more rigid film will eventually form at lower concentrations, below the CMC, if sufficient time (days) is allowed for the structure to change at the interface.

We showed that the coalescence process can be better understood by comparing directly the aging times of the interface with the characteristic times obtained by the viscoelastic characterization of the interface rather than with the equilibrium times of the interfacial tension.

5
Structure of the film formed at the oil-water interface

In the previous chapter, it was shown that the coalescence process is directly influenced by the structure formed at the drop interface due to the adsorption of the surfactant. Since one of the goals of this thesis was to find a way to facilitate phase separation, it was necessary to take a closer look at the water/oil interface structure. For this study, we performed microscopic analysis of the aging drop interface for different surfactant concentrations.

5.1
Observation of the structure formed at the interface of water drops

The presence of a structure at the interface that influences coalescence has been demonstrated previously (Fig. 5.1). However, due to technical limitations and due to the size of the analyzed drops (about 1500 μm in diameter) it was not possible to detail the morphology of the structure.

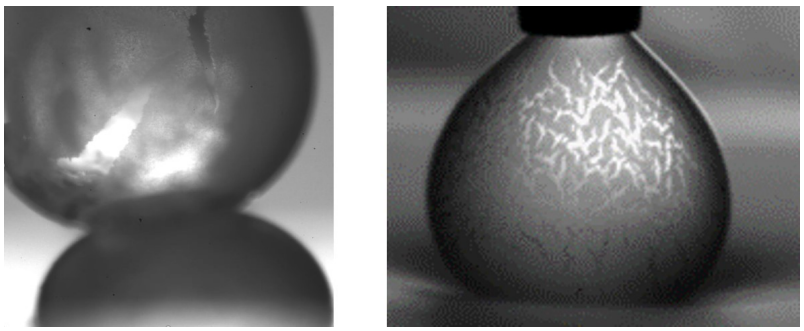

Figure 5.1: Evidence of a skin on the experiments performed during the evaluation of the coalescence of the droplets.

Thus, a single water drop was produced using a microfluid device and the aging of the interface was monitored in a microscope during a day. It has been observed that with time, this drop is progressively covered with many smaller droplets. As it is a process without any addition of fluid and extra energy over time, it can be concluded that what is happening is a spontaneous emulsification at the oil-water interface with the formation of microdroplets of water (Fig. 5.2). This phenomenon has already been reported in previous works [100–104].

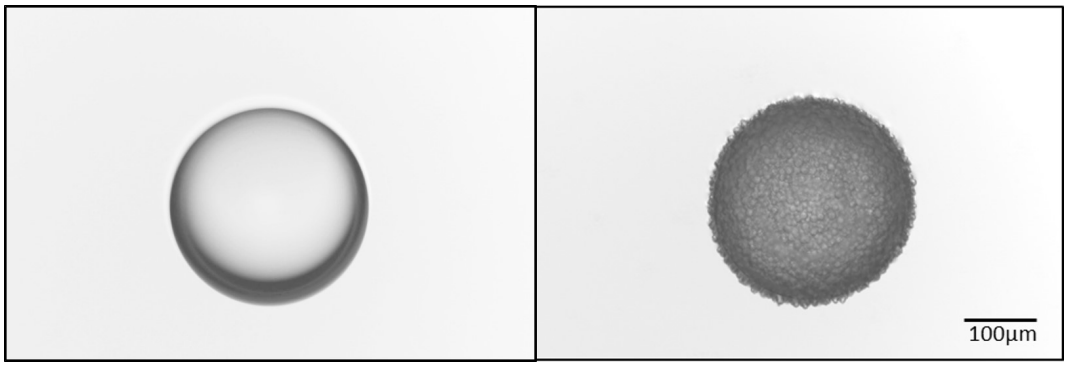

Figure 5.2: Preliminary result showing the emergence of smaller droplets at the interface of the water drop along the time (0.25%wt. of surfactant concentration). The left image shows a drop at the begin of experiment and the right image shows the drop after one day of aging.

5.2 Spontaneous emulsification

Typically, a high energy input is used to induce emulsion formation. However, there is a special case in which they form spontaneously. This work-free emulsification processing is called spontaneous emulsificiation (SE). Also known as self emulsification, this easy and reproducible way to generate submicrometer droplets without energy input [105] has been widely investigated due to its intrinsic basic interest and extensive use in numerous applications, such as improved detergents, pesticides, food production, drug delivery systems, nanoparticles, lubricant oils [106]. Nevertheless, the spontaneous creation of oil and water droplets is detrimental to oil/water separation processes in the oil industry [104].

Spontaneous emulsions represent thermodynamically stable configurations in which the total system free energy is at a minimum [105, 107]. There are two main mechanisms that can explain what happens at liquid/liquid interfaces when SE takes place: mechanical breakup and chemical instability. Interfacial turbulence or interfacial bending can cause the mechanical breakup of the interface [105]. Whereas, diffusion and stranding result from chemical instability of the interface [108]. Low surfactant concentrations are sufficient to cause SE when mechanical breakup is the driving phenomenon. Differently when the predominant phenomenon is the chemical instability, high surfactant concentrations are required. Actually, the swelling of inverted micelles due to osmotic pressure drives the SE in the last case [109].

Interfacial turbulence is generated by a mechanical instability of the

interface induced by unsteady motions, developed when two liquid phases are put in contact. A nonuniform distribution of surfactant at the liquid-liquid interface can generate localized interfacial tension gradients that induce strong Marangoni stresses, lead to violent interfacial motions [105]. Other mechanical mechanisms that induce SE is the interfacial bending. In this mechanisms the interfacial free energy coming from bending stresses (associated with changes in the mean curvature) balances the energy cost from increasing the interfacial area [110].

Spontaneous emulsification can also occur when the diffusion of the solvent into an immiscible phase generates regions of local supersaturation, which can nucleate and develop into droplets [111]. This mechanism is a chemical phenomenon and is, therefore, independent of the magnitude of the interfacial tension [105]; however, it requires the presence of a solute in one of the phases, which can be surface active or not [110].

Thus, the SE process can be influenced by different variables, such as surfactant structure, concentration and initial location, oil phase composition, addition of co-surfactant and non-aqueous solvent, as well as salinity and temperature [106].

The literature reports a few works in which the authors evaluate the influence of Span 80 in SE. González and Arauz (2007) investigated two-dimensional spherical crystalline colloidal structures formed at the oil-water interface, as result of spontaneous emulsification and colloidal self-assembly (Fig. 5.3). They showed that smaller water droplets of uniform size are spontaneously produced at the spherical interface of a water droplet introduced in oil containing Span 80. In the beginning of the process, the small droplets are of submicrometer size, forming ordered structures, then they grow uniformly with time until reaching a size of a few micrometers, maintaining the crystalline structure. Santana et al (2012), on the other hand, evaluated SE through a planar interface in order to minimize the effects of the interface's curvature on the rate of surface enlargement, using the same system of fluids studied by [101], water/dodecane-Span 80 (Fig. 5.3). They established an equation that allow to calculate the rate of interfacial area production by means of droplets growth for the fluid system.

Schmitt et al. (2017) conducted an experimental investigation of kinetics of SE with a water pendant drop in a paraffin oil solution loaded with Span 80 (Fig. 5.4). They showed a darkening of the drops due to interface modification under different surfactant concentration and that SE for low concentrations is slow producing micrometer-sized droplets, whereas for large concentrations is fast and forming bush-like microstructures at the interface.

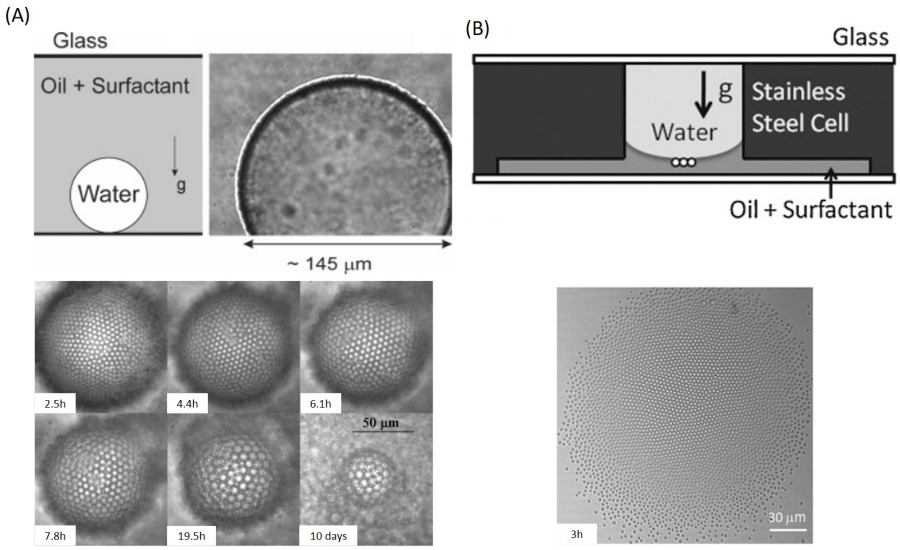

Figure 5.3: (A) Schematic transversal view of the sample cell, top view image of the initial stage of the process and time evolution of the spontaneous crystalline structure formed on the spherical interface, adapted from [101]. (B) Schematic representation of the transversal view of the sample cell and an optical microscope image of the structure at the water–oil interface, adapted from [103].

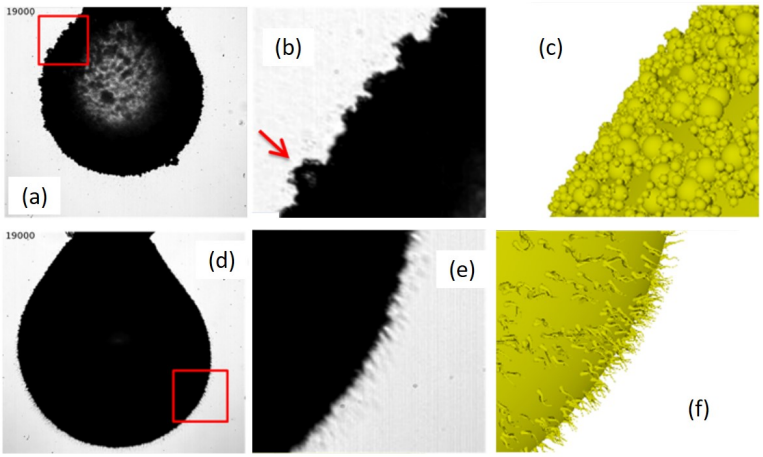

Figure 5.4: (a-c) images representing the results from the SE for low surfactant concentrations: shape of the water droplet at time $t = 19000s$, enlargement of the interface, and quantitative view of the interface structure, respectively. (d-f) the same sequence of images for the large concentrations of surfactant. Adapted by [102].

5.3 Experimental Procedure

In order to observe and evaluate the structure formed at the interface of the water droplet when in contact with the oil phase, single drops were formed and visualized at different surfactant concentration (0.25; 0.50; 2.00 $\%wt.$ of Span 80), all above the CMC (0.05 $\%wt.$). A coaxial flow (co-flow) microfluidic device (Fig. 5.5) was used to produce the droplets.

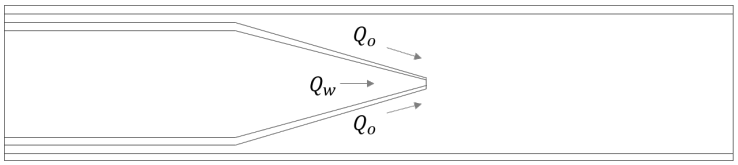

Figure 5.5: Schematic drawing of co-flow microfluidic device used to produce the droplets.

This device is composed of a cylindrical glass-capillar (World Precision Instruments Inc., USA) inserted into a square capillary (Atlantic International Technology Inc., USA), as presented in Fig. 5.5. The square capillary has an inner dimension of 1.05 mm and the cylindrical glass-capillar has inner and outer diameters of 0.58 mm and 1 mm, respectively. However, the glass-capillar was tapered with a micropipette puller (model P-1000, Sutter Instrument Co., USA) to obtain a final inner diameter of 50 μm. This system is fixed in a glass microscope slide. This device is an adaptation of the used by Michelon et al. [112].

To ensure that the two capillaries have a coaxial alignment, capillaries should be chosen such that the outer diameter of the circular capillary is the same as the inner dimensions of the square capillary [113]. The dispersed phase (water) flows through the injection capillary (cylindrical glass-capillar) while the continuous phase (oil) flows in the inner square tube. Both fluids flow in the same direction, resulting in a coaxial flow.

It was evaluated droplets with three different diameters, around 200, 400, and 600 μm. The size was controlled by changing the flow rate of the phases, where Q_o is for oil rate and Q_w is for water rate, as represented in Table 5.1.

Drop formation was monitored from the microfluidic device placed above a Carl Zeiss inverted optical microscope, model Axiovert 40MAT, as shown Fig. 5.6(a). Figure 5.6(b) presents a snapshot of the drop formation process. Drops were collected in a microscope slide with a single concave depression cavity (figure 5.7).

	0.25%wt.		0.50%wt.		2.0%wt.	
D (μm)	Q_o	Q_w	Q_o	Q_w	Q_o	Q_w
200	10	0.8	10	0.6	5.0	0.5
400	5.0	2.5	5.0	1.0	1.0	1.0
600	0.8	1.0	0.5	3.0	0.1	2.0

Table 5.1: Formation flow rates for each drop size desired and surfactant concentration, Q_o (ml/h) and Q_w ($\mu l/min$).

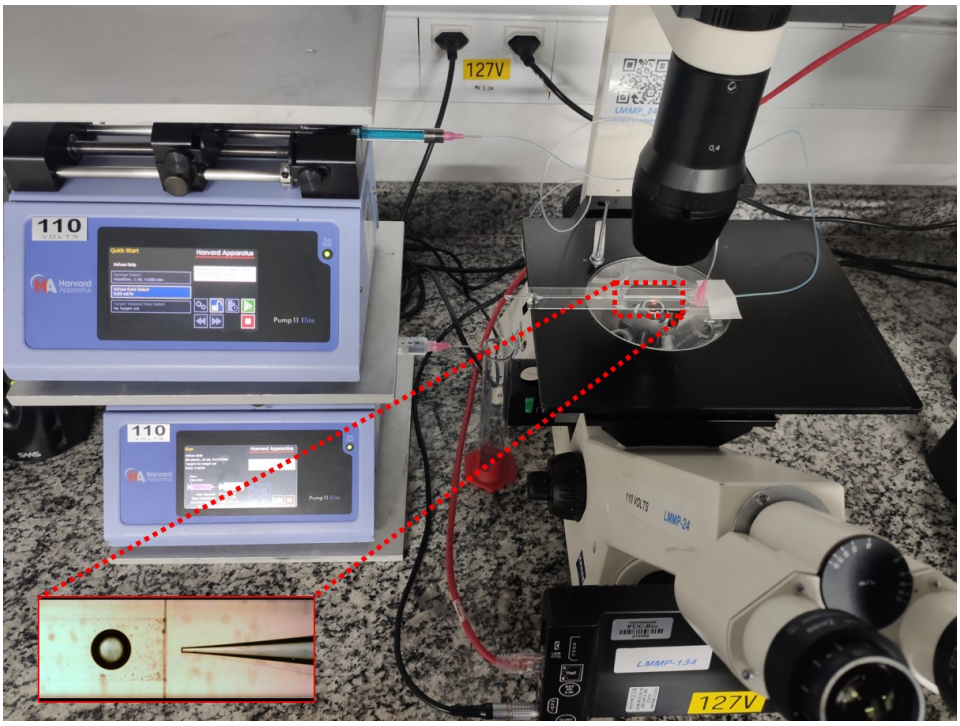

Figure 5.6: Experimental set-up for producing the droplets to evaluate the structure formed at the surface.

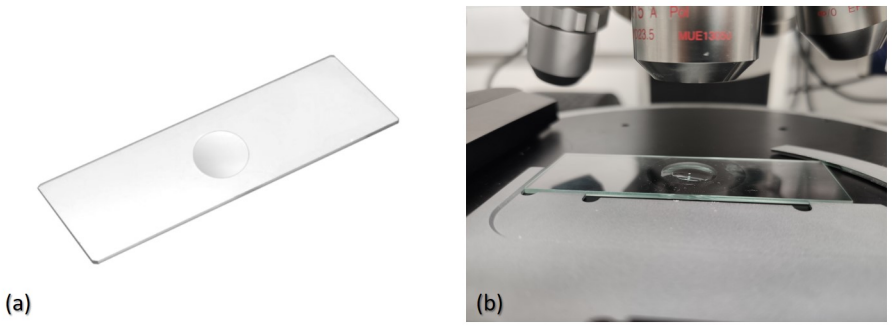

Figure 5.7: (a) microscope slide with a single depression cavity and (b) monitoring of the changes at the surface in a single water droplet.

The interface structure behavior of water drops was evaluated in a Nikon polarized microscope, model Eclipse LV100N pol. Images of the drop were taken at different time intervals. Due to the spherical shape of the drop, images in different focal planes were taken and subsequently joined to reconstruct a three-dimensional image, as represented in Fig. 5.8.

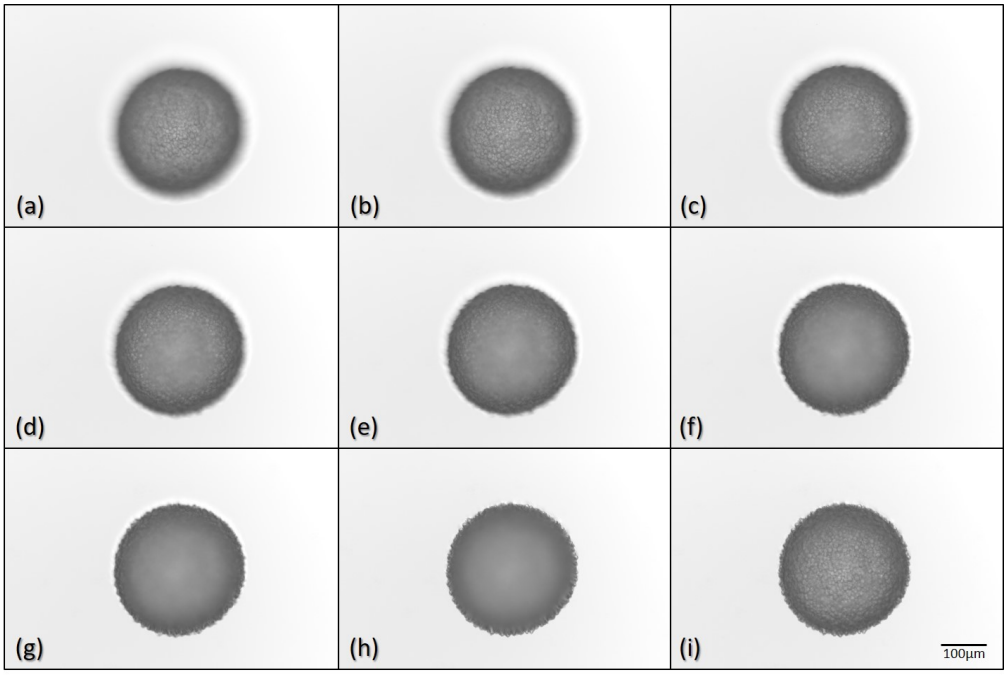

Figure 5.8: (a-h) Images from different focal planes used to reconstruct a 3D image of the droplet and (i) final image.

5.4 Results

The evidence of SE is assessed by means of optical microscopy as described above. Figures 5.9-5.11 show the time evolution of self emulsification for water drops immersed in an oil solution with different surfactant concentrations, 0.25, 0.50, and 2.0 %wt. (5, 10 and 40 times CMC) respectively. In all figures, the first image that represents the water drop at the beginning of the experiment always shows a clean interface of the drop. With time, smaller spherical drops appear, covering the spherical surface of the large water drop. After one day, regardless of the concentration of surfactants, the small droplets cover the entire surface of the large drop. However, it can be noticed that the drop interface took longer to be covered for the lowest concentration (5 times higher than CMC). After three hours of aging, the drop interface still has clean regions without microdroplets.

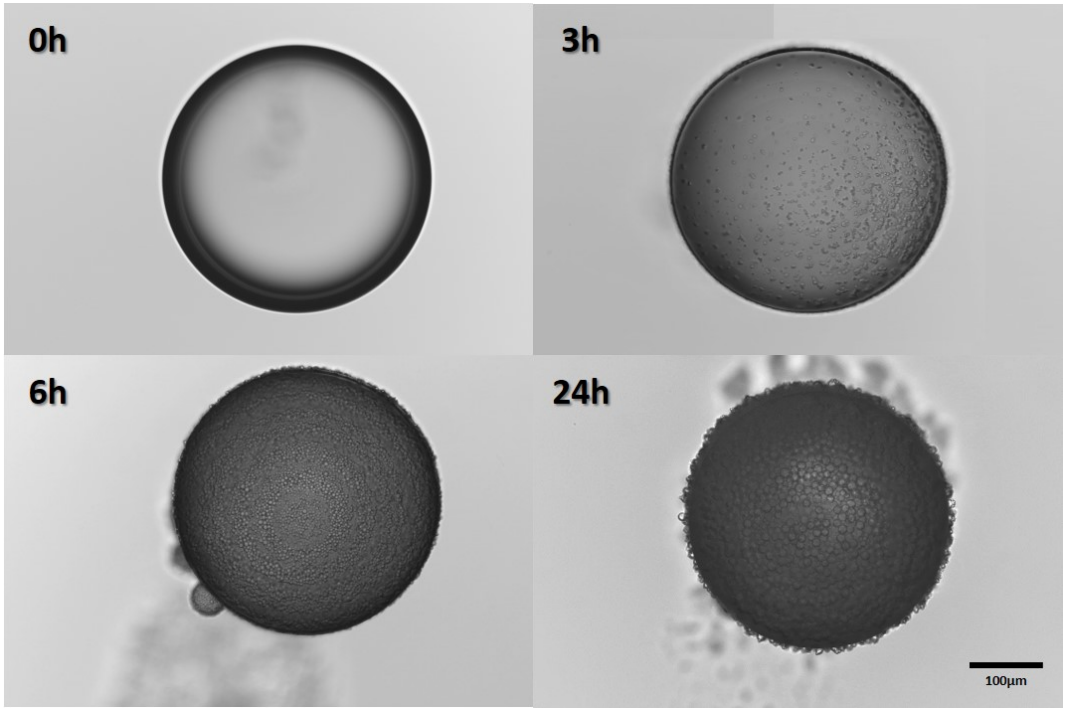

Figure 5.9: Time evolution of the SE presented at the interface of the water droplet immersed in a oil solution with 0.25%wt. of Span 80.

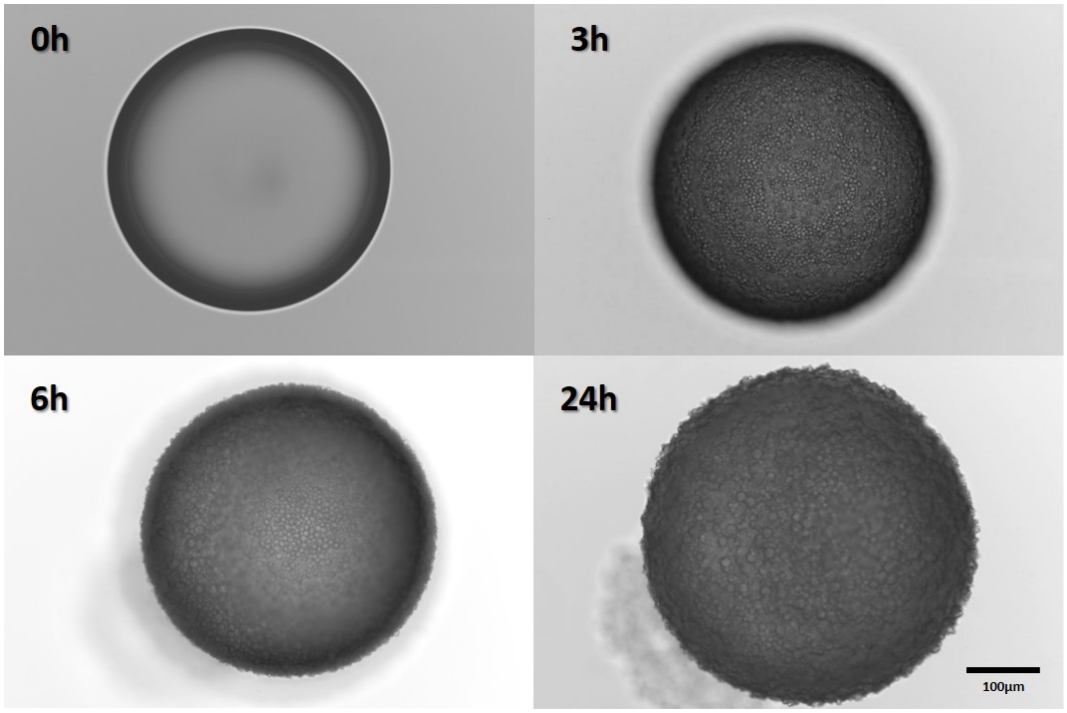

Figure 5.10: Time evolution of the SE presented at the interface of the water droplet immersed in a oil solution with 0.50%wt. of Span 80.

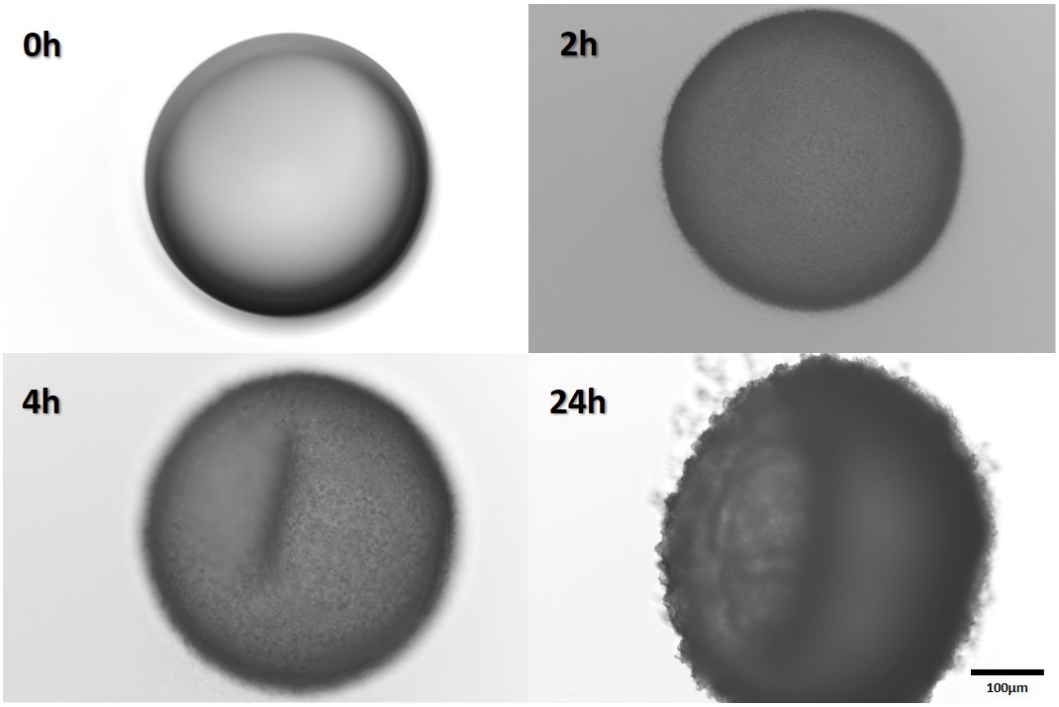

Figure 5.11: Time evolution of the SE presented at the interface of the water droplet immersed in a oil solution with 2.0%wt. of Span 80.

The rate of self emulsification increases with surfactant concentration. This behavior reinforces the theory that the amount of surfactant determines the kinetics of the process and other specific features [101]. The size of the droplets emerging at the interface of the main drop increases with time. After the interface becomes saturated with the small droplets, it can be noted a shadow region around the original drop that represents the migration of a large number of emerging droplets to the bulk of the oil phase. Figure 5.12 shows those detached droplets for different surfactant concentration. For the highest concentration (2 %wt.) the drop interface buckles losing lose their spherical shape after some time. At high surfactant concentration, the rate of self emulsification is high such that the interface becomes saturated by the small drops relatively quickly, forming a solid-like structure at the interfaces. As new small droplets are formed beyond this point and the volume of the large drop falls, a compressive stress acts along the interface, leading to the observed buckling. This behavior was observed for drops with different diameter, as shown in Fig. 5.13.

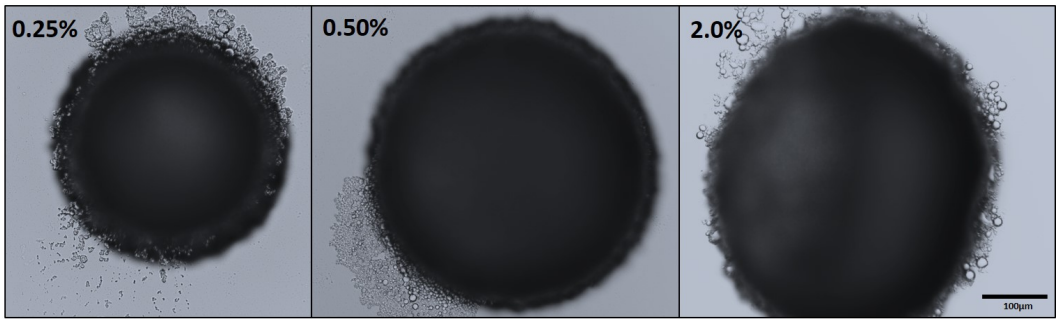

Figure 5.12: Optical microscope image of the droplets detached from the original drop for all surfactant concentration studied, 24 h after sample preparation.

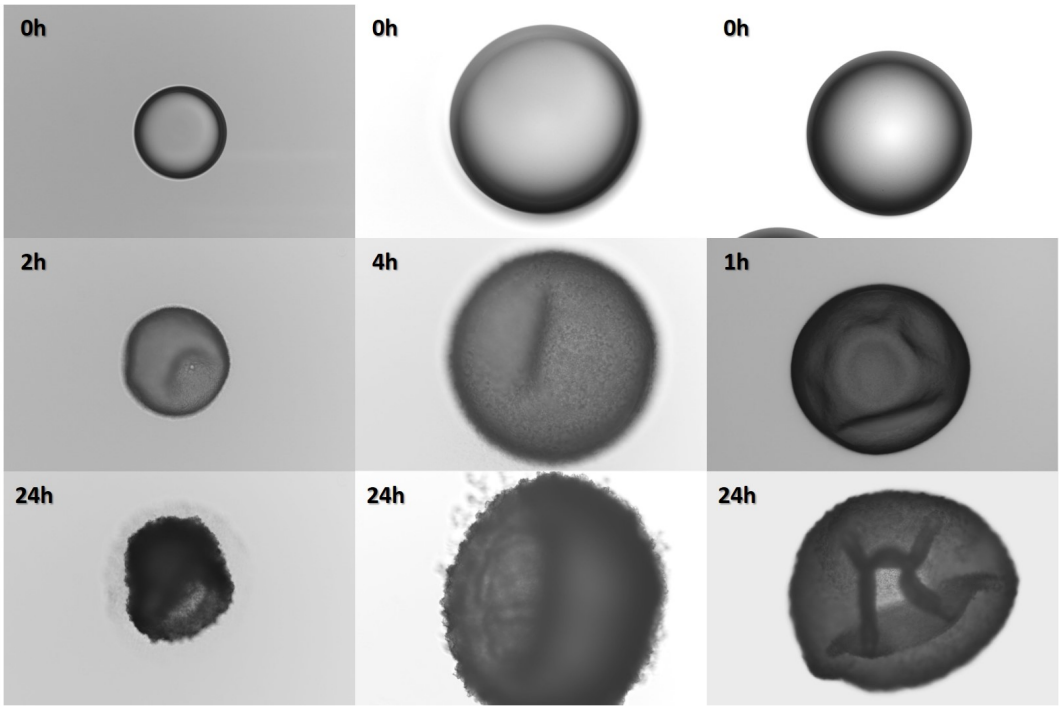

Figure 5.13: Time evolution of the SE presented at the interface of the water droplet immersed in a oil solution with 2.0%wt. of Span 80 varying the drop size. From the left for the right, the initial droplet size is 193, 394 and 650μm.

The analysis presented up to now was focused on the interface aging of single drops. However, by analyzing a group of drops, we can note the same phenomena. Figure 5.14 shows an emulsion of monodisperse water drops of 400 μm in an oil phase with a surfactant concentration equal to 0.5%wt. Initially, we observe that the drops are separated and the interface is clean. As time evolves, the drops move and touch each other and self emulsification leads to

the formation of an interface structure. Even with the contact of neighboring drops, coalescence is not observed. Figure 5.15 shows in detail the contact region of two drops. The formed interface structure hinders coalescence, as already discussed in Chapter 4.

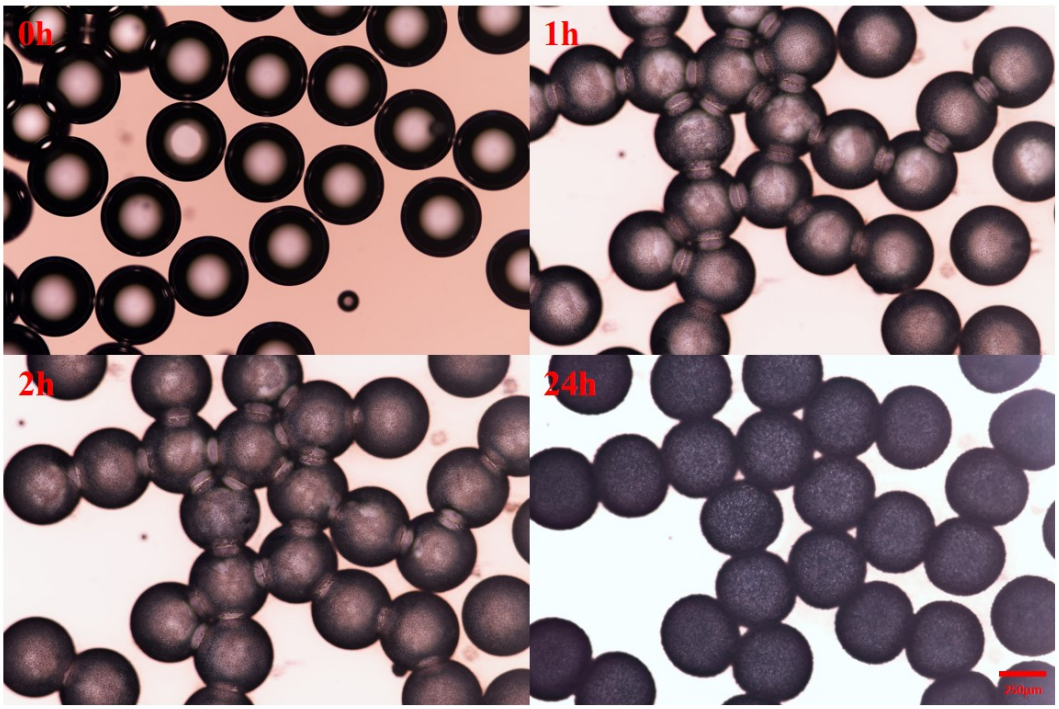

Figure 5.14: Time evolution of the SE presented at the interface of an emulsion with monodisperse water droplets of size around 400 μm, immersed in an oil phase of surfactant concentration equal 0.5 $\%wt$.

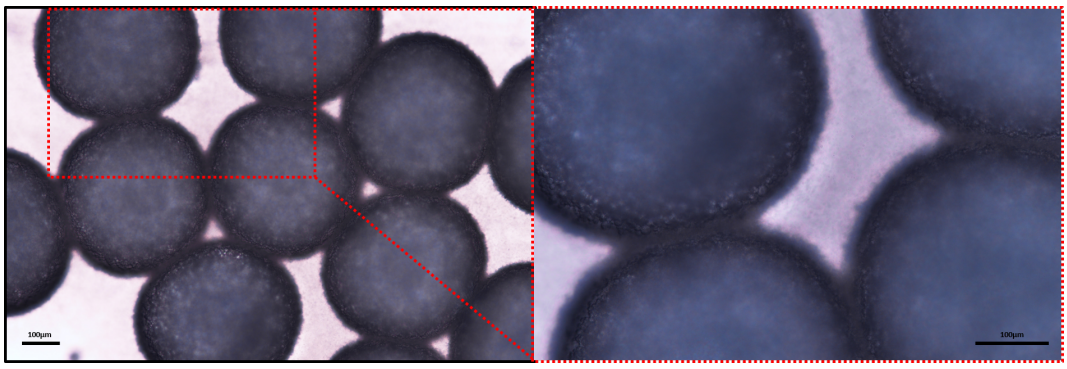

Figure 5.15: Drops from a monodispersed emulsion with water drops of size around 400 μm, immersed in an oil phase of surfactant concentration equal 0.5 $\%wt$.

González and Arauz (2007) observed similar behavior in their studies. They used pure deionized water and dodecane containing Span 80. They assumed that the formation of water droplets at the oil-water interface is a result of a sequence of physical processes starting with the self-assembly of surfactant molecules in a thick (multilayer) film around the initial water drop (Fig. 5.16(a)). Driven by chemical potential gradients, the film swells at the layer of lower interfacial tension. Liquid bridges are formed by the water accumulated in the surfactant layers, supported by a balance between wetting and surface tension (Fig. 5.16(b)) and continued to form until they undergo an instability transition, driven by capillary forces, similar to the Plateau-Rayleigh instability, breaking off in small droplets to reduce internal energy (Fig. 5.16(c)). Regarding the growth of the small water droplets at the interface, they affirmed that it is not due to either coalescence or Oswald-Ripening, but it should occur at the expense of the large drop, once they observed a decrease of its diameter. The film of surfactants provides the required connection between the large water drop and the small water droplets at the interface, which acts as a permeable membrane.

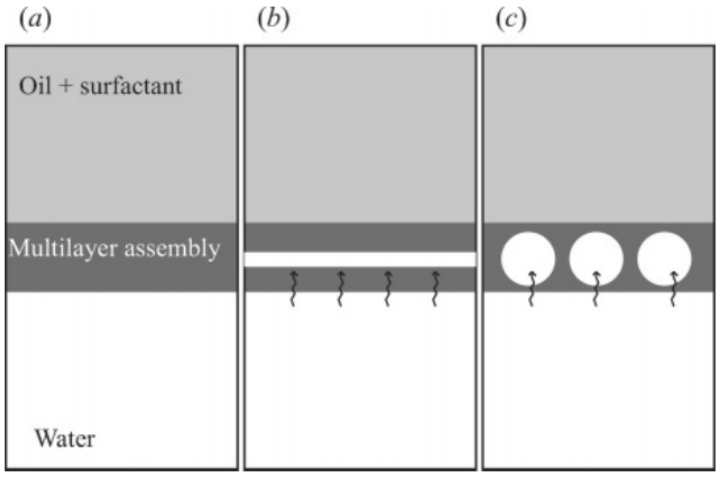

Figure 5.16: A simplified schematic of the process proposed by [101]. (a) a multilayer of surfactant forms at the oil-water interface at the beginning of the process. (b) The film of surfactant swells and forms liquid bridges. (c) Those bridges undergoes an instability transition and breaks off in small water droplets, reducing the internal energy.

5.5 Brief conclusions

This chapter presented the investigation of the morphology and the phenomena that lead to the interfacial structure formed at the oil-water

interfaces. The interface aging of a water drop was evaluated along 24 hours. During this time, small droplets appeared along the interface of the large drop. As the experiment occurred without any external energy input, we can conclude that these water droplets are the result of spontaneous emulsification at the oil-water interface. Nevertheless, the kinetics of appearance of these small droplets on the interface depends on the surfactants concentration, which can go from a few minutes to a few hours. Our first observations in Chapter 4 suggested the formation of a solid-like film at the interface while the observation on this chapter showed the emerging of small droplets at the interface, that somehow interact with each other forming a network that maintains the stability of the interface of the larger drop.

Although the self emulsification process and the resulting interfacial structure formed are directly related to the system analyzed (mineral oil Primol 352 and Span 80), similar phenomena has been observed with other systems, including different crude oils containing natural surfactants [100, 104].

6
Destabilization of water-oil emulsion breaking the interfacial structure

The previous chapters showed that a solid-like film is formed along the water-oil interface and that the interface hinders coalescence, leading to very stable emulsions. In this chapter, we propose and test a procedure to break the interfacial structure to favor coalescence between the water drops. We use the flow through a constricted microchannel to deform the drop, increasing its interfacial area, and create a strong shear stress to disturb the drop interface. We test if flowing drops through the capillary leads to drop coalescence.

6.1
Experimental Procedures

A way to destabilize emulsions removing the barrier created by the formation of a structure at the interface of the drops by the droplets from the spontaneous emulsification was evaluated. The production of the emulsions was performed using a coaxial flow microfluidic device similar to the used in the Chapter 5. After forming a drop, 3 different scenarios were explored, as sketched in Fig. 6.1:

1. Case 1: production and collection of the drops with small aging time.
2. Case 2: drops were produced and collect with time interval of at least one hour, allowing the formation of the interfacial solid-like structure.
3. Case 3: following Case 2, before collection, the drops flow through a constricted capillary, in order to perturb the interfacial structure.

Part A of this device is composed of capillaries arranged to form a flow focusing geometry for the production of the drops. Its output was connected to lines of different lengths according to the desired interfacial aging time. Part B is composed of a constricted glass capillary with a ratio of channel diameter to constriction diameter of $D_0/D_c = 580/180 \approx 3.2$. This ratio was chosen such that the drop extension was not large enough to cause a drop breakup but able to increase the interfacial area and create a shear stress near the interface.

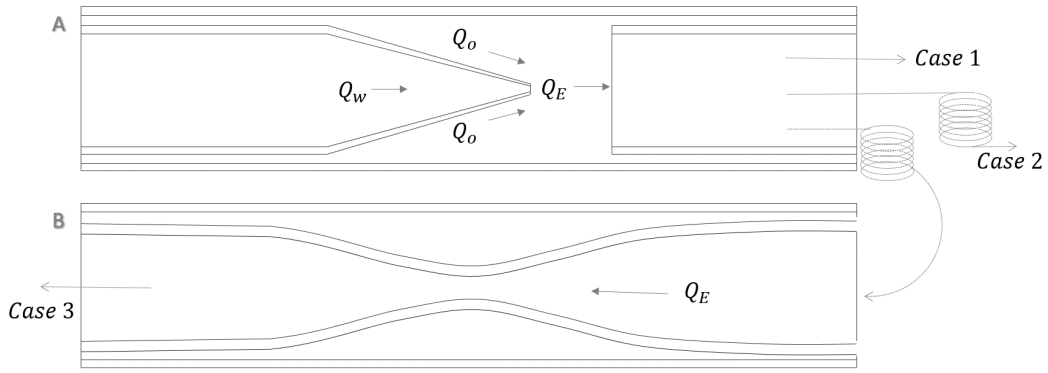

Figure 6.1: Scheme of the coaxial flow microfluidic device connected to the capillary with constriction. In this scheme is represented the cases enumerated in the text: case 1 - collection right after the production; case 2 - collection after the emulsions passing through a long line to allow the aging of the droplets; and case 3 - collection after the drops of the second case passing through the capillary with constriction.

Figure 6.2 presents the experimental apparatus used. It consisted of syringe pumps (model Pump 11 Elite from Harvard Apparatus) to inject the phases at constant flow rate; a Carl Zeiss inverted optical microscope (model Axiovert 40MAT) equipped with a high speed camera (model Fastec Imaging IL5H) to record real time images of drops passing through the constriction; a microfluidic device described in Fig. 6.1; a long line (Scientific Commodities, Inc.) through which drops flow during the aging of the interfaces when necessary; and a small vial to collect the emulsions. The line is a polyethylene micro tubing with inner diameter of 863.6 μm connected to the capillaries. The emulsion destabilization was evaluated by observing if there was a free water phase at the bottom of the vial. The water phase was dyed with blue color using a water-based dye (0.6 %vol.) to improve visualization of the phases during the visualization experiments.

Different combinations of oil and water flow rates have been used for the preparation of emulsions. Table 6.1 presents these combinations and the size of the drops obtained for each condition.

According these flow rates there is a specific residence time for each one of the cases presented in Fig. 6.1. For Case A, the drops remain a short time in the line before being collected, around 1 minute, which corresponds to the case without interface aging of the drops. For Case B, the residence time was increased by using a long line (9 meters) to allow the interface

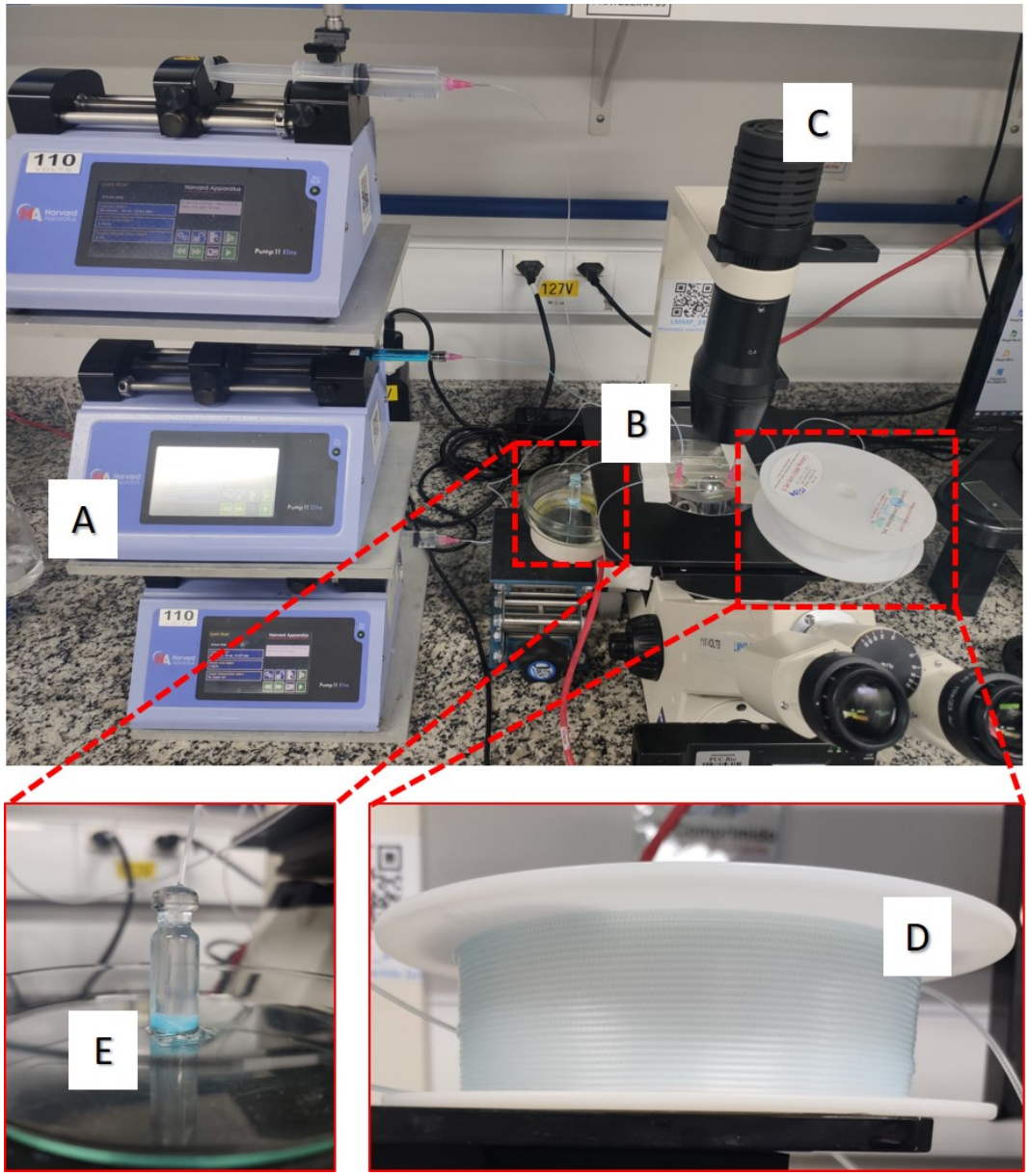

Figure 6.2: Experimental set-up for the production and collection of the emulsions to evaluate their stability, including: (A) syringe pumps, (B) the coaxial flow microfluidic device, (C) an inverted optical microscope, (D) lines for collection and (E) a vial for collection of the emulsions produced.

Φ(%wt.)	$Q_o(ml/h)$	$Q_w(ml/h)$	$D_{mean}(\mu m)$
0.25	3.3	0.2	450
0.50	5	0.5	450
2.0	2.5	1.0	350

Table 6.1: Formation flow rates for each surfactant concentration of emulsions analyzed and mean diameter obtained for each condition.

	Residence time (min)		
Φ(%wt.)	Case 1	Case 2	Case 3
0.25	0.8	90	90/0.8
0.50	0.8	60	60/0.8
2.0	1.3	-	1.3/1.3

Table 6.2: Residence time for each case analyzed.

aging. With a surfactant concentration of 0.25%$wt.$ the flow rates have been chosen so that the drops remain in the line for 90 minutes, and for surfactant concentration of 0.50%$wt.$, this time was 60 minutes. Case C corresponds to case B where the drops pass through a constriction after the aging time and then are collected and brought into contact. However, for the highest surfactant concentration (2.0 %wt.), case B was not tested, as shown in the results. For this concentration, the drops from case A pass through the constriction. Thus, the residence time of the drops before constriction is short.

6.2 Results and Discussion

6.2.1 Behavior of a single drop passing through a constriction

The first part of the results presents the behavior of drops when passing through the constriction. Figures 6.3-6.5 show snapshots of the flow of a drop suspended in an oil phase with surfactant concentration of 0.50 %$wt.$ with different aging times (0, 1, and 2 hours, respectively). Experiments were repeated at least 3 times for each aging time and the observed behavior was the same.

Comparing the first frame of these figures, we observe the effect of interface aging. For the case without interface aging (Fig. 6.3), the drop is clean and clear, while for the other two cases the interface is opaque. As mentioned earlier, the degree of darkening of the drop is related to aging time, which explains why the 2-hour aged drop (Fig. 6.5) is darker than the 1-hour aged drop (Fig. 6.4). Moreover, the drop with 1 hour of interface aging has a cracked look in the interface. This is due to the higher concentration of microdroplets

accumulated at the interface during the spontaneous emulsification process.

Figure 6.3 presents the visualization of the drop without interface aging. Drop elongates as it flows through the throat and regains its shape without losing mass. The flow of the drop with one hour of interface aging is presented in Fig. 6.4. The elongation of the drop as it flows through the constriction increases the surface area, disrupting the interface structure. Moreover, the flow leads to a strong shear stress along the interface. These two phenomena contribute to more the small drops formed during the interface aging step from the interface towards the back of the large drop. Downstream of the throat, the drop interface is clean (it is clear in the images) and cloud of small drop is observed on its trailing edge. The apparent size of the drop falls, as the mass associated with the small drops was removed from the interface. This behavior was also observed for the case in which the drops were left at rest for two hours (Fig. 6.5), providing the same conclusions. The only difference observed is the amount of mass the drop loses, because as time increases, more droplets are formed due by the spontaneous emulsification at the interface.

Figure 6.6 shows an image of the capillary downstream of the throat. The image shows a clean interface drop and a large number of small drops that were removed from the interface of previous flowing drops.

In the previous chapter was presented the evolution of the spontaneous emulsification along a day for the drops. Although the analysis of the next session was not carried out for this time, we present here an example of cleaning the interface for drops with this aging time (Fig. 6.7). Two examples are shown, on the left when a single drop passes through the constriction and on the right when two drops arrive together at the constriction. In this case we can see that the drops are close but not connected, because when they pass through the constriction they separate. It is possible to see that the number of the small droplets around the large drop increases significantly compared to the others aging time analyzed. Consequently the volume of the initial drop has decreased considerable.

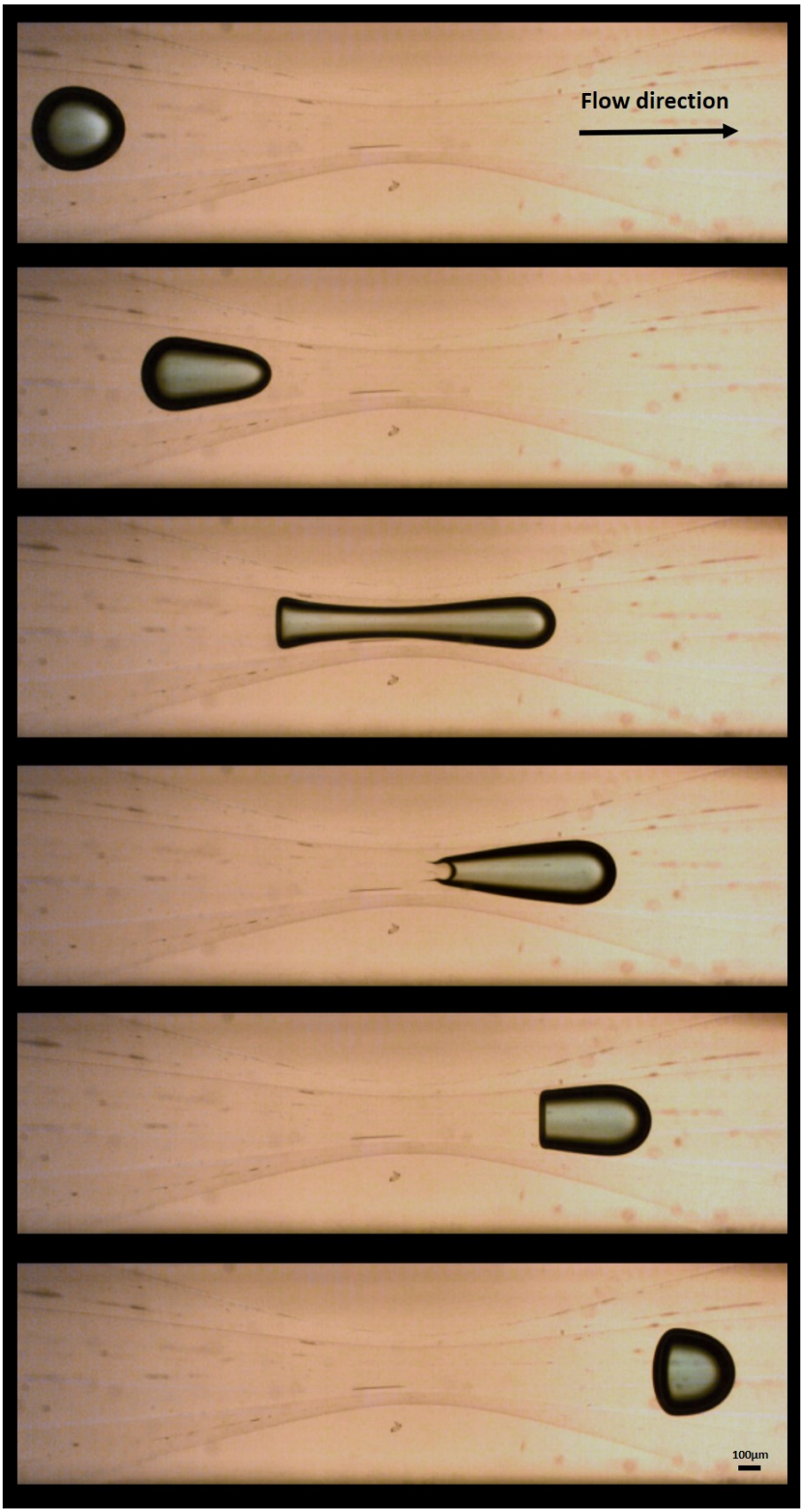

Figure 6.3: Evolution of the drop position and behavior as it flows through the constriction. Surfactant concentration of 0.5%wt. and drop without aging of the interface.

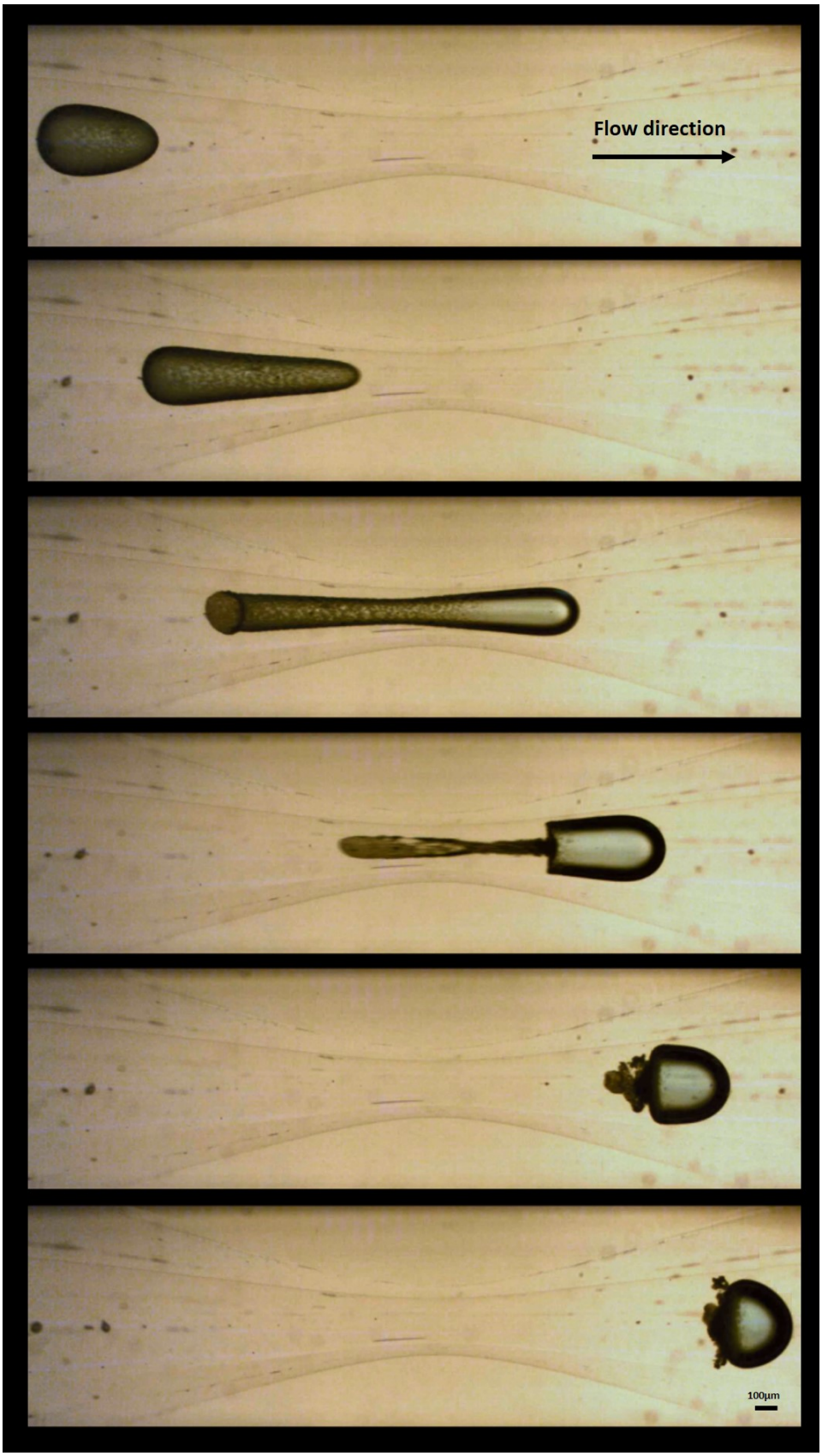

Figure 6.4: Evolution of the drop position and behavior as it flows through the constriction. Surfactant concentration of 0.5%wt. and drop with one hour aging of the interface.

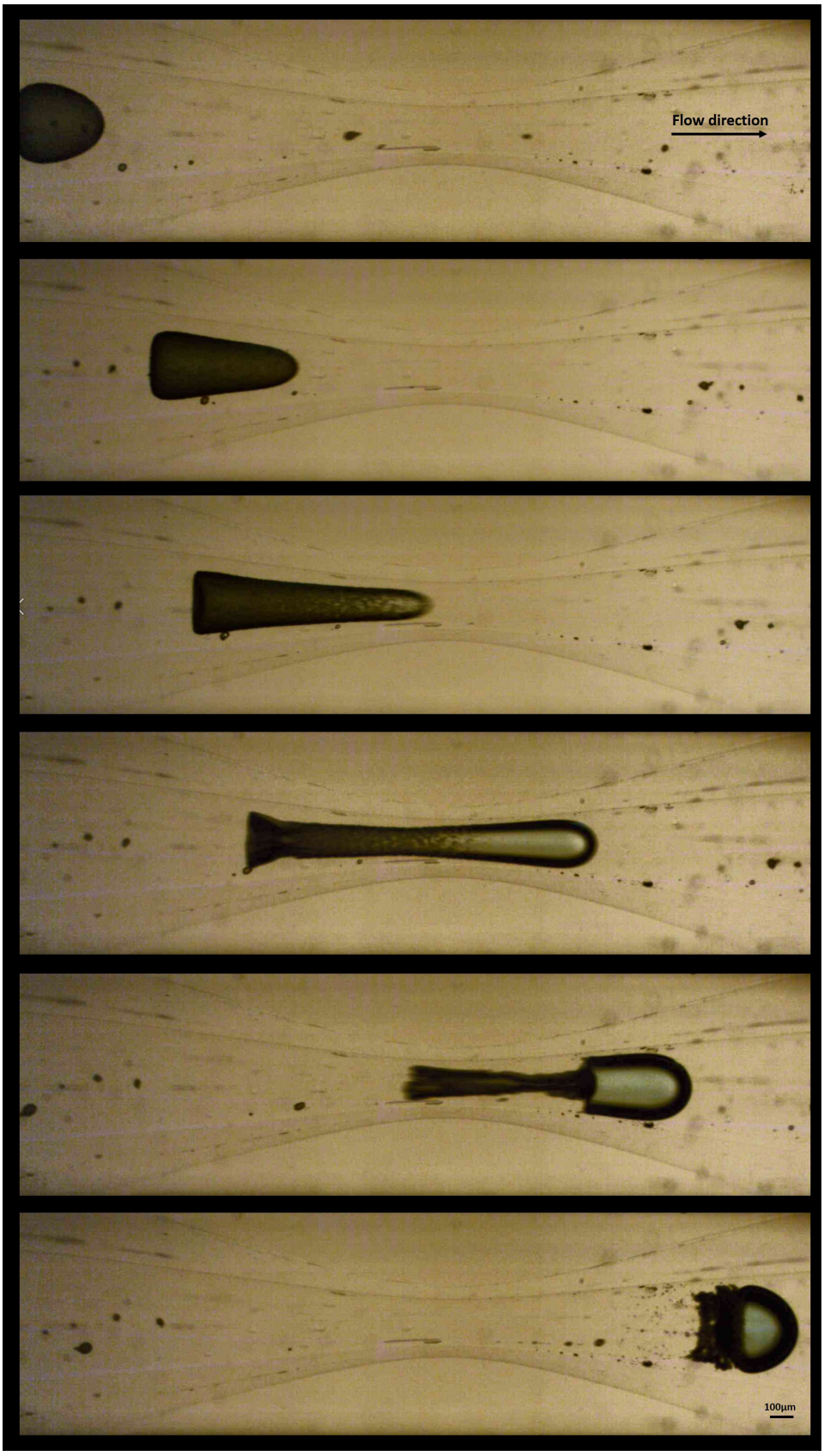

Figure 6.5: Evolution of the drop position and behavior as it flows through the constriction. Surfactant concentration of $0.5\%wt.$ and drop with two hour aging of the interface.

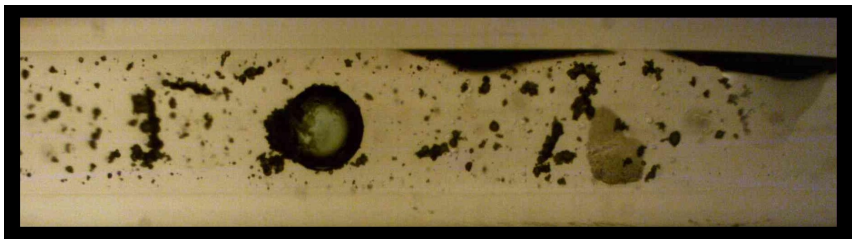

Figure 6.6: Drop position at capillary downstream showing its interface clean. Surfactant concentration of 0.5%wt..

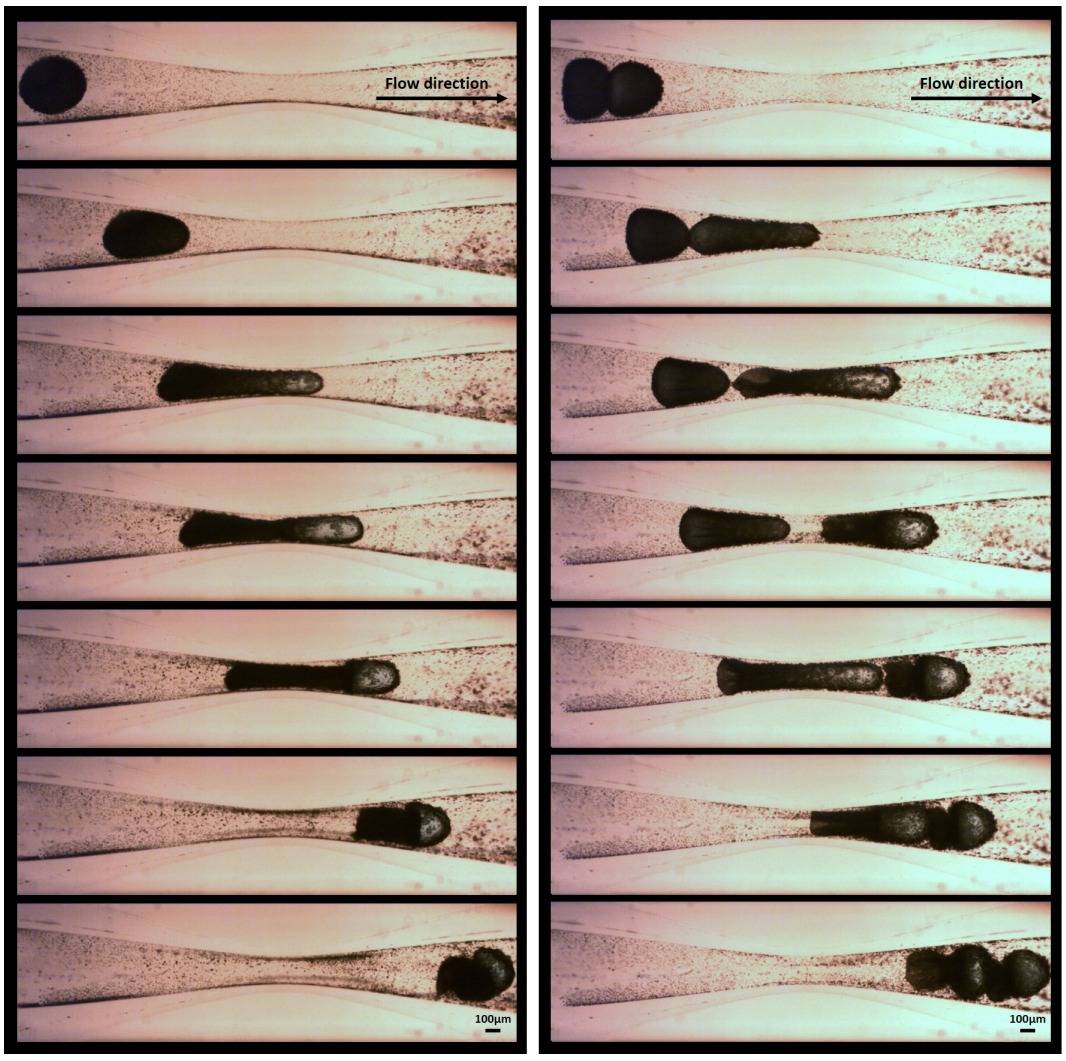

Figure 6.7: Evolution of the drop position and behavior as it flows through the constriction. Surfactant concentration of 0.5%wt. and drop with 24 hours aging of the interface. The image from the left shows one drop passing through the constriction while the image from the right shows two drops that arrive together but are not connected.

6.2.2
Evaluation of interface cleanliness for produced emulsions

Once we observed the possibility of promoting the cleaning of the interface by passing the drop through a constriction, we tested if this phenomena could be used to destabilize a w/o emulsion. We produced monodispersed emulsions with drop diameter between 350 and 450 μm with different surfactant concentration. We analyzed the stability of the produced emulsions at different interface aging time and passing or not the drops through a constricted capillary before collecting them in a vial. All experiments presented in this section were repeated 3 times and showed the same behavior.

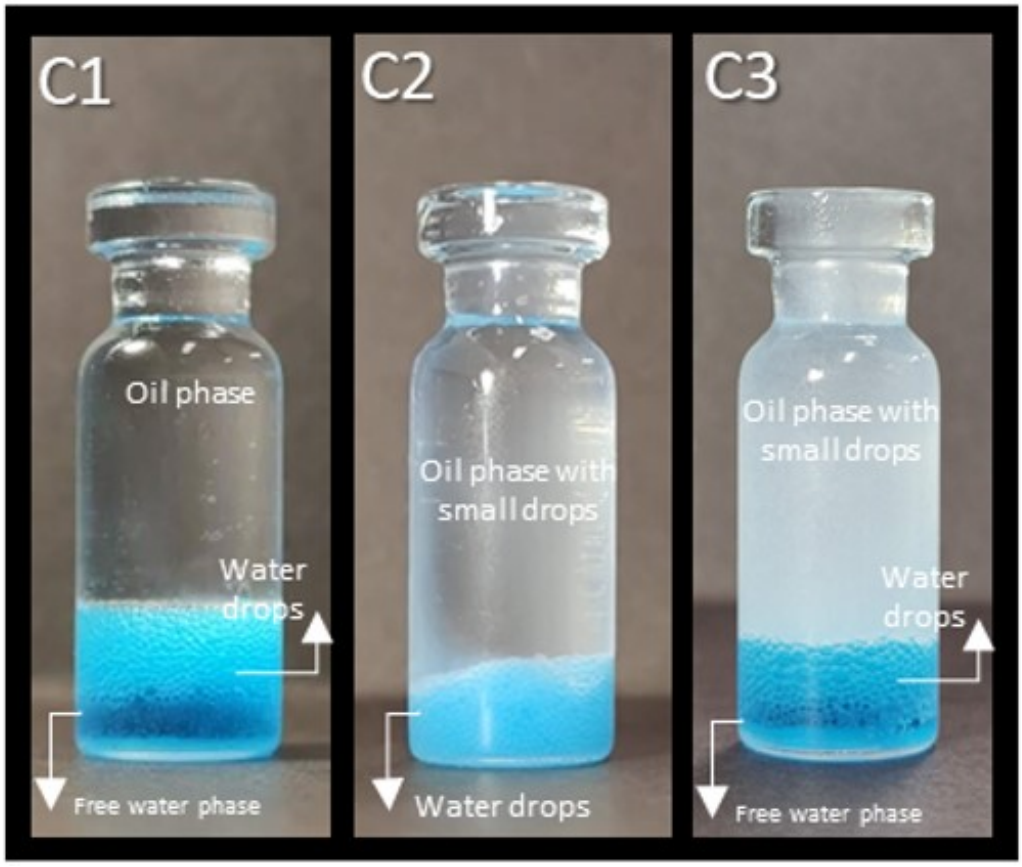

Figure 6.8: Emulsions produced with surfactant concentration of 0.5%wt.. (C1) represents the collection of the drops right after the production. (C2) represents the condition of drop interface aging of one hour. And (C3) is a continuation of case 2, but drops pass through by a constriction before being collected.

Images of the emulsions produced with the surfactant concentration of 0.5 %wt. and evaluated using the three cases presented in the methodology are shown in Fig 6.8. Case 1 represents the emulsion with drops produced and collected shortly thereafter. On the bottom part of the vial there is a layer

of water that is the result of coalescence of the drops. Above this free water layer there is a w/o emulsion, both segregated of the oil phase. To allow the aging of the interface before the contact between the drops and thus avoid coalescence, the drops were produced and collected only 1 hour later (Case 2). This was possible by the addition of a meter-long collection hose, as shown in the experimental session. Drops remain stable over time once there is no appearance of a layer of water at the bottom of the vial. Above this w/o emulsion layer there is also a stable w/o emulsion but with micro water drops. In Case 3, the drops traveled in the line, allowing the aging of the interface, but before being collected, they passed through a constriction that allowed the removal of the small droplets that formed spontaneously, as seen in the previous section. Once the interface is clean again, after being collected, it is possible to observe the formation of a free water phase on the bottom of the vial, which characterizes coalescence. It is noted that in Case 3 the oil layer above the emulsion is whitish. This is due to the small droplets that have detached from the interface of the larger drops and that, due to their size, remain suspended in the oil phase.

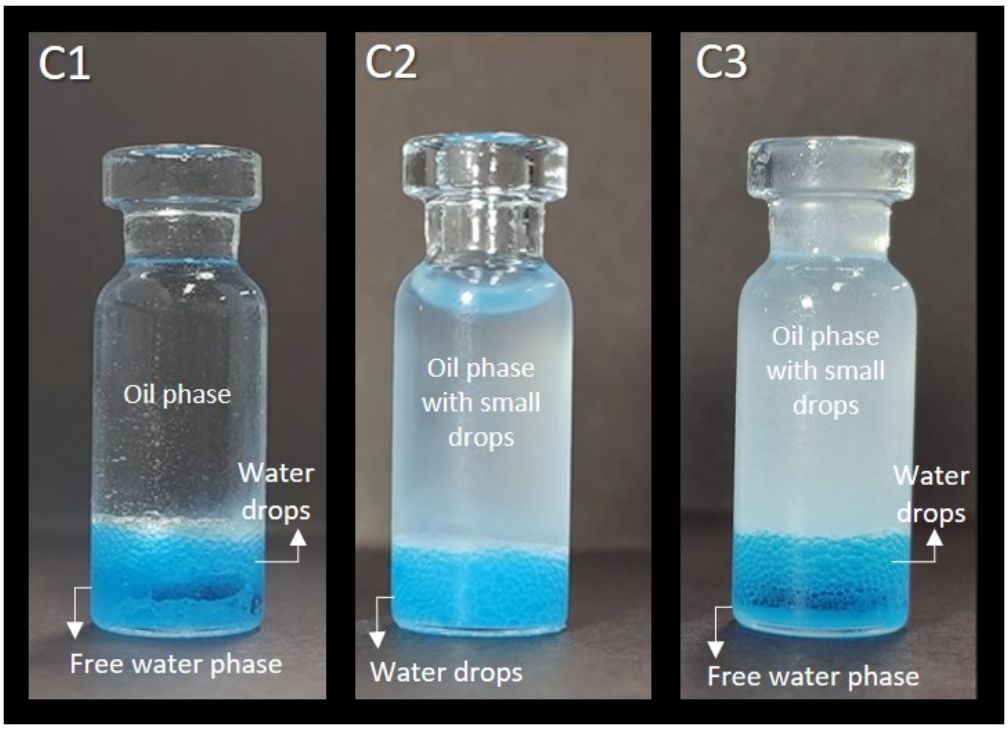

Figure 6.9: Emulsions produced with surfactant concentration of 0.25%wt.. Case 1 represents the collection of the drops right after the production. Case 2 represents the condition of drop interface aging of one hour. And Case 3 is a continuation of case 2, but drops pass through by a constriction before being collected.

Figure 6.9 presents the results for tests performed with a surfactant concentration of 0.25 $\%wt.$. The results for this concentration are similar with results obtained for the concentration of 0.5 $\%wt.$. The only difference observed was in the speed of destabilization of the samples. The emulsions produced with the smallest surfactant concentration destabilized faster than the emulsions produced with 0.5 $\%wt.$ of surfactant concentration, as expected. Again, the interface structure was removed by flowing the drops through the constricted capillary leading to destabilization of the emulsion and the appearance of a water free phase.

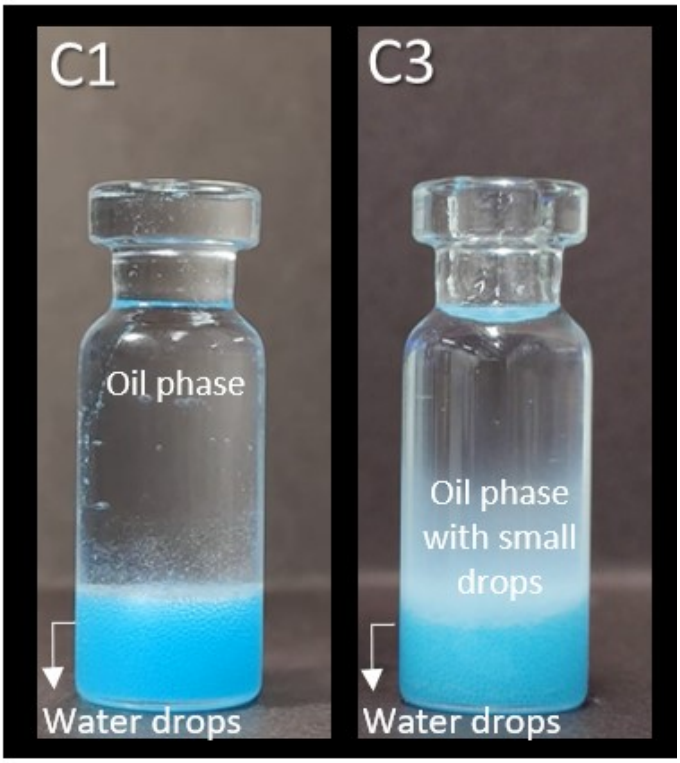

Figure 6.10: Emulsions produced with surfactant concentration of 2.0 $\%wt.$. C1 represents the collection of the drops right after the production. And in the C3 the drops passed through by a constriction before being collected.

Finally, the highest concentration was evaluated (2.0 $\%wt.$ = 40 times CMC). As observed in the previous chapters, at this concentration, interfacial phenomena occur faster than at other concentrations due to the great availability of surfactant to act at the interfaces. Case 1 in Fig. 6.10 shows the drops produced and collected with short aging time. For this case the drops remained stable for more than 1 day. Due to the high stability of the system, case 2 was not evaluated. Case 3 was evaluated but for the drops with short aging time. We observed that, even going through the constriction the drops did not coa-

lesce when collected. Although, one observes a whitish region above the water drops on the bottom. It corresponds in this case to the small drops removed from the large drop during the passage through the constriction. We believe that the spontaneous emulsification happens so fast that probably droplets with nano size growing up at the interface are enough to hindering the coalescence. A suggestion would be to vary the size and assess whether the stability is related to this parameter, once there are studies at the literature that found a strong dependence on the drop stability with its size [84, 114].

6.3 Brief conclusions

The objective of this chapter was to propose a new method to destabilize an water-in-oil emulsion by disrupting the interface structure that is formed along the water-oil interface, which hinders coalescence and leads to very stable emulsions. Three different concentrations were tested, all above the CMC (5, 10, and 40 times). The results showed that for the two lowest concentrations, emulsions with less than 1 minute of aging time showed instability, with phase separation being observed already after collection time. Differently when the drops of these emulsions had time to age (1 hour at least). In these cases, the emulsions showed stability after production and for days afterwards. As a way to promote phase separation, for these emulsions with longer aging time, the drops were subjected to pass through a constriction, which allowed a cleaning of the interfaces and, consequently, a rapid phases separation after production. Emulsions produced with the highest concentration evaluated (40 times of the CMC) were stable with short aging time before the contact between the drops. Although these drops were subjected to passage through the constriction, the residence time before collection was enough to stabilize this new drop interface formed, consequently the emulsions were stable.

7
Final remarks and suggestions for future work

The effect of interfacial structuring and the corresponding rheological behavior on the stability of emulsions was investigated. A model system was used to mimic water-in-crude oil emulsions formed by an oil phase composed by a mineral oil with a nonionic surfactant and milliQ water. The behavior of oil-water interfaces were evaluated by oscillatory pendant drop technique at different surfactant concentrations. The results of interfacial tension (IFT) showed that for a concentration above the CMC (at least 10 times), the diffusion of the surfactant to the interface is very fast at the beginning which leads to a decrease of the interfacial tension until a first equilibrium plateau is reached. Then a second decrease in IFT was observed until a new lower equilibrium value is reached. This behavior could be the result of the mixed kinetic-diffusion model which assumes that the surfactant diffuses from the bulk to the subsurface or of the formation of multilayer adsorption. The elastic and viscous moduli showed significant changes with surfactant concentration and interface aging time. It was possible to identify three regions during the time evolution. An initial plateau in which the elastic and the viscous moduli are almost equal and lower than the IFT, suggesting that the interfacial stress is isotropic. On the second region, the elastic modulus increases and becomes greater than the IFT, while the viscous modulus decreases. Finally, the third region initializes when the elastic modulus begins to decrease after reaching a maximum value while the viscous modulus tends towards a zero value. The formation of a solid-like interface was observed as the elastic modulus rises. However, the accuracy of the interface stress is compromised as the interfacial stress becomes anisotropic; the results above the maximum value of elastic moduli may not be accurate. The increase in elastic modulus also corresponds to the second drop in IFT. The structural change at the interface could be due to molecular interactions or rearrangements. Moreover, the interactions between the hydrophobic tails of the Span 80 and the satured hydrocarbons of Primol also play an important role on the interfacial surfactant organization and the viscoelastic properties.

In the Chapter 4 the coalescence between two water drops was investigated, correlating the results with the interfacial behavior of oil-water inter-

faces. In general, the data indicated that an excess of Span 80 is favorable in preventing coalescence as the film strength increases with the surfactant concentration. The results showed that the drainage time of the film between the drops, for the cases at which coalescence occurred, did not have relation with the aging time of the interfaces and coalescence was prevented by the formation of a solid-like interface with strong elastic modulus. Furthermore, coalescence was avoided when the elastic modulus predominated over the viscous modulus. The time for the formation of the interface structure is inversely proportional by the surfactant concentration, so the increase of the surfactant concentration reduces the interface structuring time. The phenomenon of non-coalescence was always observed when the aging time was longer than the time at which the storage modulus predominate over the loss modulus, for high surfactant concentration systems. After the study we could conclude that the coalescence process was better understood by comparing the aging times of the interface with the characteristic times obtained by the viscoelastic characterization of the interface.

Looking for a better comprehension of the behavior of this solid-like interface observed in Chapters 3 and 4, Chapter 5 presented a microscopic visualization study of the drop interface. It was possible to conclude that in fact it was not a skin presented at the interface but an agglomerate of microdroplets formed through spontaneous emulsification that interacts with each other and forms a network, maintaining the stability of the interface of the larger drop.

Finally, a way to destabilize the emulsions formed with the fluid system studied on this theses was proposed and tested in Chapter 6. The method is based on the removal of the interface structure formed by small droplets achieved during the flow of the drops through a constricted capillary.

During all this study, it was seen that the Span 80 concentration plays an important role on the dynamic of the interfacial rheology and consequently on the coalescence process. This observation is in concordance with studies at the literature that evaluating the amount of asphaltenes on the crude oil and presenting that the stability of emulsion will increase with the increase in the concentration of asphaltenes in the crude oil [115, 116].

For further investigations, it would be interesting to change the water phase to a saline water more compatible with the water produced in the oil industry, and to evaluate the interfacial behavior in this case. We used a non-ionic surfactant, so we expect to obtain similar behavior. About spontaneous emulsification, a deeper investigation into the growth rate of microdroplets at the interface as a function of surfactant concentration could provide a time

window in which it would still be possible to obtain the coalescence of the drops and consequent phase separation. Last of all, to improve the phases separation, it could be interesting to construct a device that allows us to evaluate a greater number of drops at the same time, simulating the flow of an emulsion in a pipe. It would basically be a mesh (filter) formed by several capillaries with constriction through which the emulsions pass before being collected.

Bibliography

[1] **Bp energy review, 2019**. https://www.bp.com/content/dam/bp/business-sites/en/global/corporate/pdfs/energy-economics/energy-outlook/bp-energy-outlook-2019.pdf. Accessed: 2022-07-18.

[2] RAYA, S.; SAAID, I.; AHMED, A. ; UMAR, A.. **A critical review of development and demulsification mechanisms of crude oil emulsion in the petroleum industry**. J. Petrol Explor. Prod. Technol., 10:1711–1728, 2020.

[3] **Ecologically compatible solution for the separation of crude oil from water**. https://www.clariant.com/en/Innovation/Innovation-Spotlight-Videos/Phasetreat. Accessed: 2022-07-18.

[4] PEÑA, A.; HIRASAKI, G. ; MILLER, C.. **Chemically induced destabilization of water-in-crude oil emulsions**. Industrial & Engineering Chemistry Research, 44(5):1139–1149, 2005.

[5] FINGAS, M.; FIELDHOUSE, B.; BOBRA, M. ; TENNYSON, E.. **The physics and chemistry of emulsions**. In: PROCEEDINGS OF THE WORKSHOP ON EMULSIONS, p. 11–19. Marine Spill Response Corporation Washington, DC, 1993.

[6] ARAÚJO, M.. **Estudo de Quebra de Emulsões de Petróleo Utilizando Microemulsões e Célula de Desidratação Eletrostática**. PhD thesis, Dissertação de Mestrado, UFRN. Natal: DEQ/PPGEQ, 2004.

[7] PAL, R.; RHODES, E.. **A novel viscosity correlation for non-newtonian concentrated emulsions**. Journal of Colloid and Interface Science, 107(2):301–307, 1985.

[8] JOHNSEN, E. E.; RØNNINGSEN, H. P.. **Viscosity of 'live'water-in-crude-oil emulsions: experimental work and validation of correlations**. Journal of Petroleum Science and Engineering, 38(1-2):23–36, 2003.

[9] LANGEVIN, D.; POTEAU, S.; HENAUT, I. ; ARGILLIER, J.-F.. **Crude oil emulsion properties and their application to heavy oil transportation**. Oil & gas science and technology, 59(5):511–521, 2004.

[10] DOL, S.; SEN, L.. **The effect of flow-induced oil-water emulsions on pressure drop**. International Journal of Theoretical and Applied Mechanics, 2:73–78, 2017.

[11] BENMEKHBI, M.; SIMON, S. ; SJÖBLOM, J.. **Dynamic and rheological properties of span 80 at liquid–liquid interfaces**. Journal of Dispersion Science and Technology, 35(6):765–776, 2014.

[12] ALVAREZ, G.; POTEAU, S.; ARGILLIER, J.-F.; LANGEVIN, D. ; SALAGER, J.-L.. **Heavy oil- water interfacial properties and emulsion stability: Influence of dilution**. Energy & Fuels, 23(1):294–299, 2009.

[13] PERLES, C.; GUERSONI, V. ; BANNWART, A.. **Rheological study of crude oil/water interface–the effect of temperature and brine on interfacial film**. Journal of Petroleum Science and Engineering, 162:835–843, 2018.

[14] RANE, J. P.; PAUCHARD, V.; COUZIS, A. ; BANERJEE, S.. **Interfacial rheology of asphaltenes at oil–water interfaces and interpretation of the equation of state**. Langmuir, 29(15):4750–4759, 2013.

[15] BOCHNER DE ARAUJO, S.; MEROLA, M.; VLASSOPOULOS, D. ; FULLER, G. G.. **Droplet coalescence and spontaneous emulsification in the presence of asphaltene adsorption**. Langmuir, 33(40):10501–10510, 2017.

[16] DAVIES, G.; NILSEN, F. ; GRAMME, P.. **The formation of stable dispersions of crude oil and produced water: the influence of oil type, wax & asphaltene content**. In: SPE ANNUAL TECHNICAL CONFERENCE AND EXHIBITION. OnePetro, 1996.

[17] YOUNG, G.; WAKLEY, W.; TAGGART, D.; ANDREWS, S. ; WORRELL, J.. **Oil-water separation using hydrocyclones: An experimental search for optimum dimensions**. Journal of petroleum science and engineering, 11(1):37–50, 1994.

[18] PLAT, R.. **Gravitational and centrifugal oil-water separators with plate pack internals.** 1995.

[19] **6 ways to separate an oil and water emulsion**. https://kimray.com/training/6-ways-separate-oil-and-water-emulsion. Accessed: 2022-07-18.

[20] LEE, H. S.. **SEPARATIONS OF WATER-IN-OIL EMULSIONS BY ELECTROSTATIC FIELD AT THE ELEVATED TEMPERATURE**. PhD thesis, 2019.

[21] KAVEHPOUR, H. P.. **Coalescence of drops**. Annual Review of Fluid Mechanics, 47:245–268, 2015.

[22] NARAYAN, S.; MAKHNENKO, I.; MORAVEC, D. B.; HAUSER, B. G.; DALLAS, A. J. ; DUTCHER, C. S.. **Insights into the microscale coalescence behavior of surfactant-stabilized droplets using a microfluidic hydrodynamic trap**. Langmuir, 36(33):9827–9842, 2020.

[23] SANTINI, E.; LIGGIERI, L.; SACCA, L.; CLAUSSE, D. ; RAVERA, F.. **Interfacial rheology of span 80 adsorbed layers at paraffin oil–water interface and correlation with the corresponding emulsion properties**. Colloids and Surfaces A: Physicochemical and Engineering Aspects, 309(1-3):270–279, 2007.

[24] PANDOLFINI, P.; LOGLIO, G.; RAVERA, F.; LIGGIERI, L.; KOVALCHUK, V.; JAVADI, A.; KARBASCHI, M.; KRÄGEL, J.; MILLER, R.; NOSKOV, B. ; OTHERS. **Dynamic properties of span-80 adsorbed layers at paraffin-oil/water interface: Capillary pressure experiments under low gravity conditions**. Colloids and Surfaces A: Physicochemical and Engineering Aspects, 532:228–243, 2017.

[25] DUGYALA, V. R.; ANJALI, T. G.; UPENDAR, S.; MANI, E. ; BASAVARAJ, M. G.. **Nano ellipsoids at the fluid–fluid interface: effect of surface charge on adsorption, buckling and emulsification**. Faraday Discuss., 186:419–434, 2016.

[26] GOODARZI, F.; ZENDEHBOUDI, S.. **A comprehensive review on emulsions and emulsion stability in chemical and energy industries**. The Canadian Journal of Chemical Engineering, 97(1):281–309, 2019.

[27] LIN, S.. **A computer simulation and molecular-thermodynamic framework to model the micellization of ionic branched surfactants in aqueous solution**. PhD thesis, Massachusetts Institute of Technology, 2008.

[28] SHENG, J.. **Modern chemical enhanced oil recovery: theory and practice**. Gulf Professional Publishing, 2010.

[29] GRIFFIN, W. C.. **Classification of surface-active agents by "hlb"**. Journal of Cosmetic Science, 1:311–326, 1949.

[30] DALTIN, D.. **Tensoativos: química, propriedades e aplicações**. Editora Blucher, 2011.

[31] BUTT, H.-J.; GRAF, K. ; KAPPL, M.. **Physics and chemistry of interfaces**. John Wiley & Sons, 2013.

[32] PATIST, A.; OH, S.; LEUNG, R. ; SHAH, D.. **Kinetics of micellization: its significance to technological processes**. Colloids and Surfaces A: Physicochemical and Engineering Aspects, 176(1):3–16, 2001.

[33] TADROS, T.. **Application of rheology for assessment and prediction of the long-term physical stability of emulsions**. Advances in colloid and interface science, 108:227–258, 2004.

[34] HU, Y.-T.; TING, Y.; HU, J.-Y. ; HSIEH, S.-C.. **Techniques and methods to study functional characteristics of emulsion systems**. Journal of food and drug analysis, 25(1):16–26, 2017.

[35] WASAN, D.. **Destabilization of water-in-oil emulsions**. In: EMULSIONS—A FUNDAMENTAL AND PRACTICAL APPROACH, p. 283–295. Springer, 1992.

[36] CASTAÑO, E. P. M. C.. **Linking the rheology of W/O crude emulsions with the droplet agreggation process**. PhD thesis, Pontifical Catholic University of Rio de Janeiro, 2020.

[37] THOMSON, J. J.; NEWALL, H. F.. **V. on the formation of vortex rings by drops falling into liquids, and some allied phenomena**. Proceedings of the royal society of London, 39(239-241):417–436, 1886.

[38] VENKATARAMANI, D.; SMAY, J. ; AICHELE, C.. **Transient stability of surfactant and solid stabilized water-in-oil emulsions**. Colloids and Surfaces A: Physicochemical and Engineering Aspects, 490:84–90, 2016.

[39] ARYAFAR, H.; KAVEHPOUR, H.. **Drop coalescence through planar surfaces**. Physics of Fluids, 18(7):072105, 2006.

[40] ARYAFAR, H.; LUKYANETS, A. ; KAVEHPOUR, H.. **Inertia-dominated coalescence of drops**. Applied Mathematics Research eXpress, 2006, 2006.

[41] BLANCHETTE, F.; MESSIO, L. ; BUSH, J. W.. **The influence of surface tension gradients on drop coalescence**. Physics of Fluids, 21(7):072107, 2009.

[42] WU, M.; CUBAUD, T. ; HO, C.-M.. **Scaling law in liquid drop coalescence driven by surface tension**. Physics of Fluids, 16(7):L51–L54, 2004.

[43] NOWAK, E.; KOVALCHUK, N. M.; CHE, Z. ; SIMMONS, M. J.. **Effect of surfactant concentration and viscosity of outer phase during the coalescence of a surfactant-laden drop with a surfactant-free drop**. Colloids and Surfaces A: Physicochemical and Engineering Aspects, 505:124–131, 2016.

[44] FENG, S.; YI, L.; ZHAO-MIAO, L.; REN-TUO, C. ; GUI-REN, W.. **Advances in micro-droplets coalescence using microfluidics**. Chinese Journal of Analytical Chemistry, 43(12):1942–1954, 2015.

[45] TAN, Y.-C.; FISHER, J. S.; LEE, A. I.; CRISTINI, V. ; LEE, A. P.. **Design of microfluidic channel geometries for the control of droplet volume, chemical concentration, and sorting**. Lab on a Chip, 4(4):292–298, 2004.

[46] TAN, Y.-C.; HO, Y. L. ; LEE, A. P.. **Droplet coalescence by geometrically mediated flow in microfluidic channels**. Microfluidics and Nanofluidics, 3(4):495–499, 2007.

[47] BREMOND, N.; THIAM, A. R. ; BIBETTE, J.. **Decompressing emulsion droplets favors coalescence**. Physical review letters, 100(2):024501, 2008.

[48] BAN, T.; KAWAIZUMI, F.; NII, S. ; TAKAHASHI, K.. **Study of drop coalescence behavior for liquid–liquid extraction operation**. Chemical engineering science, 55(22):5385–5391, 2000.

[49] THORODDSEN, S. T.; TAKEHARA, K.. **The coalescence cascade of a drop**. Physics of Fluids, 12(6):1265–1267, 2000.

[50] GILET, T.; MULLENERS, K.; LECOMTE, J.-P.; VANDEWALLE, N. ; DORBOLO, S.. **Critical parameters for the partial coalescence of a droplet**. Physical Review E, 75(3):036303, 2007.

[51] DUCHEMIN, L.; EGGERS, J. ; JOSSERAND, C.. **Inviscid coalescence of drops**. Journal of Fluid Mechanics, 487:167–178, 2003.

[52] THORODDSEN, S.; TAKEHARA, K. ; ETOH, T.. **The coalescence speed of a pendent and a sessile drop**. Journal of Fluid Mechanics, 527:85–114, 2005.

[53] WEHELIYE, W. H.; DONG, T. ; ANGELI, P.. **On the effect of surfactants on drop coalescence at liquid/liquid interfaces**. Chemical Engineering Science, 161:215–227, 2017.

[54] BŁAWZDZIEWICZ, J.; CRISTINI, V. ; LOEWENBERG, M.. **Near-contact motion of surfactant-covered spherical drops: ionic surfactant**. Journal of colloid and interface science, 211(2):355–366, 1999.

[55] DAI, B.; LEAL, L. G.. **The mechanism of surfactant effects on drop coalescence**. Physics of fluids, 20(4):040802, 2008.

[56] CHESTERS, A. K.; BAZHLEKOV, I. B.. **Effect of insoluble surfactants on drainage and rupture of a film between drops interacting under a constant force**. Journal of Colloid and Interface Science, 230(2):229–243, 2000.

[57] GHOSH, P.; JUVEKAR, V.. **Analysis of the drop rest phenomenon**. Chemical Engineering Research and Design, 80(7):715–728, 2002.

[58] YEO, L. Y.; MATAR, O. K.; DE ORTIZ, E. S. P. ; HEWITT, G. F.. **Film drainage between two surfactant-coated drops colliding at constant approach velocity**. Journal of colloid and interface science, 257(1):93–107, 2003.

[59] MARTIN, D. W.; BLANCHETTE, F.. **Simulations of surfactant effects on the dynamics of coalescing drops and bubbles**. Physics of Fluids, 27(1):012103, 2015.

[60] LIN, Y.-J.; PERRARD, A.; BISWAL, S. L.; HILL, R. M. ; TRABELSI, S.. **Microfluidic investigation of asphaltenes-stabilized water-in-oil emulsions**. Energy & Fuels, 32(4):4903–4910, 2018.

[61] DUDEK, M.; CHICAULT, J. ; ØYE, G.. **Microfluidic investigation of crude oil droplet coalescence: effect of oil/water composition and droplet aging**. Energy & Fuels, 34(5):5110–5120, 2019.

[62] NARAYAN, S.; MAKHNENKO, I.; MORAVEC, D. B.; HAUSER, B. G.; DALLAS, A. J. ; DUTCHER, C. S.. **Insights into the microscale coalescence behavior of surfactant-stabilized droplets using a microfluidic hydrodynamic trap**. Langmuir, 36(33):9827–9842, 2020.

[63] ARYAFAR, H.; KAVEHPOUR, P.. **Electrocoalescence**. Physics of Fluids, 19(9):091107, 2007.

[64] DERKACH, S.; KRÄGEL, J. ; MILLER, R.. **Methods of measuring rheological properties of interfacial layers (experimental methods of 2d rheology)**. Colloid journal, 71(1):1–17, 2009.

[65] LUCASSEN-REYNDERS, E. H.. **Interfacial viscoelasticity in emulsions and foams**. Food Struct., 12:1–12, 1993.

[66] RAVERA, F.; LOGLIO, G. ; KOVALCHUK, V. I.. **Interfacial dilational rheology by oscillating bubble/drop methods**. Current Opinion in Colloid & Interface Science, 15(4):217–228, 2010.

[67] JAENSSON, N.; VERMANT, J.. **Tensiometry and rheology of complex interfaces**. Current Opinion in Colloid & Interface Science, 37:136–150, 2018.

[68] FULLER, G. G.; VERMANT, J.. **Complex fluid-fluid interfaces: rheology and structure**. Annual review of chemical and biomolecular engineering, 3:519–543, 2012.

[69] MILLER, R.; FERRI, J. K.; JAVADI, A.; KRÄGEL, J.; MUCIC, N. ; WÜSTNECK, R.. **Rheology of interfacial layers**. Colloid and Polymer Science, 288(9):937–950, 2010.

[70] GIMÉNEZ-RIBES, G.; HABIBI, M. ; SAGIS, L. M.. **Interfacial rheology and relaxation behavior of adsorption layers of the triterpenoid saponin escin**. Journal of colloid and interface science, 563:281–290, 2020.

[71] FAN, Y.; SIMON, S. ; SJÖBLOM, J.. **Interfacial shear rheology of asphaltenes at oil–water interface and its relation to emulsion stability: Influence of concentration, solvent aromaticity and nonionic surfactant**. Colloids and Surfaces A: Physicochemical and Engineering Aspects, 366(1-3):120–128, 2010.

[72] RAVERA, F.; LOGLIO, G. ; KOVALCHUK, V. I.. **Interfacial dilational rheology by oscillating bubble/drop methods**. Current Opinion in Colloid & Interface Science, 15(4):217–228, 2010.

[73] GEORGIEVA, D.; SCHMITT, V.; LEAL-CALDERON, F. ; LANGEVIN, D.. **On the possible role of surface elasticity in emulsion stability**. Langmuir, 25(10):5565–5573, 2009.

[74] CHANDRAN SUJA, V.; RODRÍGUEZ-HAKIM, M.; TAJUELO, J. ; FULLER, G.. **Single bubble and drop techniques for characterizing foams and emulsions**. Advances in Colloid and Interface Science, 286:102295, 2020.

[75] YEUNG, A.; ZHANG, L.. **Shear effects in interfacial rheology and their implications on oscillating pendant drop experiments**. Langmuir, 22(2):693–701, 2006.

[76] OPAWALE, F. O.; BURGESS, D. J.. **Influence of interfacial properties of lipophilic surfactants on water-in-oil emulsion stability**. Journal of colloid and interface science, 197(1):142–150, 1998.

[77] USHIKUBO, F.; CUNHA, R.. **Stability mechanisms of liquid water-in-oil emulsions**. Food Hydrocolloids, 34:145–153, 2014.

[78] LOGLIO, G.; PANDOLFINI, P.; MILLER, R.; MAKIEVSKI, A.; RAVERA, F. ; LIGGIERI, L.. **Drop and bubble shape analysis as a tool for dilational rheological studies of interfacial layers**. In: Möbius, D.; Miller, R., editors, NOVEL METHODS TO STUDY INTERFACIAL LAYERS, volumen 11 de **Studies in Interface Science**, p. 439–483. Elsevier, 2001.

[79] PELTONEN, L.; HIRVONEN, J. ; YLIRUUSI, J.. **The behavior of sorbitan surfactants at the water–oil interface: Straight-chained hydrocarbons from pentane to dodecane as an oil phase**. Journal of Colloid and Interface Science, 240(1):272–276, 2001.

[80] NARAYAN, S.; BARMAN, S.; MORAVEC, D. B.; HAUSER, B. G.; DALLAS, A. J.; ZASADZINSKI, J. A. ; DUTCHER, C. S.. **Dilatational rheology of water-in-diesel fuel interfaces: effect of surfactant concentration and bulk-to-interface exchange**. Soft Matter, 17:4751–4765, 2021.

[81] AGRAWAL, M.; NEUMAN, R. D.. **Surface diffusion in monomolecular films: Ii. experiment and theory**. Journal of Colloid and Interface Science, 121(2):366–380, 1988.

[82] BAUGET, F.; LANGEVIN, D. ; LENORMAND, R.. **Dynamic Surface Properties of Asphaltenes and Resins at the Oil–Air Interface**. Journal of Colloid and Interface Science, 239(2):501–508, jul 2001.

[83] POLITOVA, N.; TCHOLAKOVA, S. ; DENKOV, N.. **Factors affecting the stability of water-oil-water emulsion films**. Colloids and Surfaces A: Physicochemical and Engineering Aspects, 522:608–620, 2017.

[84] POLITOVA, N. I.; TCHOLAKOVA, S.; TSIBRANSKA, S.; DENKOV, N. D. ; MUELHEIMS, K.. **Coalescence stability of water-in-oil drops: Effects of drop size and surfactant concentration**. Colloids and Surfaces A: Physicochemical and Engineering Aspects, 531:32–39, 2017.

[85] FREER, E.; SVITOVA, T. ; RADKE, C.. **The role of interfacial rheology in reservoir mixed wettability**. Journal of Petroleum Science and Engineering, 39(1-2):137–158, 2003.

[86] BENJAMINS, J.; CAGNA, A. ; LUCASSEN-REYNDERS, E.. **Viscoelastic properties of triacylglycerol/water interfaces covered by proteins**. Colloids and Surfaces A: Physicochemical and Engineering Aspects, 114:245–254, 1996.

[87] FREER, E. M.; YIM, K. S.; FULLER, G. G. ; RADKE, C. J.. **Interfacial Rheology of Globular and Flexible Proteins at the Hexadecane/Water Interface: Comparison of Shear and Dilatation Deformation**. Journal of Physical Chemistry B, 108(12):3835–3844, 2004.

[88] YEUNG, A.; DABROS, T. ; MASLIYAH, J.. **Dissipative interfaces and departures from the young- laplace equation**. Langmuir, 13(24):6597–6606, 1997.

[89] HUTIN, A.. **Static Multiple Light Scattering (SMLS)**, July 2022.

[90] CHEN, J.-D.. **A model of coalescence between two equal-sized spherical drops or bubbles**. Journal of Colloid and Interface Science, 107(1):209–220, 1985.

[91] EDWARDS, D. A.; BRENNER, H. ; WASAN, D. T.. **Thin liquid film hydrodynamics**. In: Edwards, D. A.; Brenner, H. ; Wasan, D. T., editors, INTERFACIAL TRANSPORT PROCESSES AND RHEOLOGY, p. 280–302. Butterworth-Heinemann, Boston, 1991.

[92] CRISTINI, V.; BLANWZDZIEWICZ, J. ; LOEWENBERG, M.. **Near-contact motion of surfactant-covered spherical drops**. Journal of Fluid Mechanics, 366:259–287, 1998.

[93] GHOSH, P.; JUVEKAR, V.. **Analysis of the drop rest phenomenon**. Chemical Engineering Research and Design, 80(7):715–728, 2002.

[94] DRELICH, A.; GOMEZ, F.; CLAUSSE, D. ; PEZRON, I.. **Evolution of water-in-oil emulsions stabilized with solid particles: Influence of added emulsifier**. Colloids and Surfaces A: Physicochemical and Engineering Aspects, 365(1-3):171–177, 2010.

[95] JERIBI, M.; ALMIR-ASSAD, B.; LANGEVIN, D.; HENAUT, I. ; ARGILLIER, J.. **Adsorption kinetics of asphaltenes at liquid interfaces**. Journal of colloid and interface science, 256(2):268–272, 2002.

[96] POTEAU, S.; ARGILLIER, J.-F.; LANGEVIN, D.; PINCET, F. ; PEREZ, E.. **Influence of ph on stability and dynamic properties of asphaltenes and other amphiphilic molecules at the oil- water interface**. Energy & Fuels, 19(4):1337–1341, 2005.

[97] DUKHIN, A.; GOETZ, P.. **Ionic properties of so-called "non-ionic" surfactants in non-polar liquids**. Dispersion Technology Inc, Bedford Hills, New York, 15:151–157, 2005.

[98] GUO, Q.; SINGH, V. ; BEHRENS, S. H.. **Electric charging in nonpolar liquids because of nonionizable surfactants**. Langmuir, 26(5):3203–3207, 2010.

[99] LEE, J.; ZHOU, Z.-L. ; BEHRENS, S. H.. **Interfaces charged by a non-ionic surfactant**. The Journal of Physical Chemistry B, 122(22):6101–6106, 2018.

[100] WU, T.; FIROOZABADI, A.. **Surfactant-enhanced spontaneous emulsification near the crude oil–water interface**. Langmuir, 37(15):4736–4743, 2021.

[101] GONZÁLEZ-OCHOA, H.; ARAUZ-LARA, J. L.. **Spontaneous two-dimensional spherical colloidal structures**. Langmuir, 23(10):5289–5291, 2007.

[102] SCHMITT, M.; TOOR, R.; DENOYEL, R. ; ANTONI, M.. **Spontaneous microstructure formation at water/paraffin oil interfaces**. Langmuir, 33(49):14011–14019, 2017.

[103] SANTANA-SOLANO, J.; QUEZADA, C. M.; OZUNA-CHACÓN, S. ; ARAUZ-LARA, J. L.. **Spontaneous emulsification at the water/oil interface**. Colloids and Surfaces A: Physicochemical and Engineering Aspects, 399:78–82, 2012.

[104] BOCHNER DE ARAUJO, S.; REYSSAT, M.; MONTEUX, C. ; FULLER, G.. **Ablation of water drops suspended in asphaltene/heptol solutions due to spontaneous emulsification**. Science advances, 5(10):eaax8227, 2019.

[105] LÓPEZ-MONTILLA, J. C.; HERRERA-MORALES, P. E.; PANDEY, S. ; SHAH, D. O.. **Spontaneous emulsification: Mechanisms, physicochemical aspects, modeling, and applications**. Journal of dispersion science and technology, 23(1-3):219–268, 2002.

[106] LI, Z.; XU, D.; YUAN, Y.; WU, H.; HOU, J.; KANG, W. ; BAI, B.. **Advances of spontaneous emulsification and its important applications in enhanced oil recovery process**. Advances in Colloid and Interface Science, 277:102119, 2020.

[107] SOLANS, C.; MORALES, D. ; HOMS, M.. **Spontaneous emulsification**. Current Opinion in Colloid & Interface Science, 22:88–93, 2016.

[108] RUSCHAK, K. J.; MILLER, C. A.. **Spontaneous emulsification in ternary systems with mass transfer**. Industrial & Engineering Chemistry Fundamentals, 11(4):534–540, 1972.

[109] GREINER, R. W.; EVANS, D. F.. **Spontaneous formation of a water-continuous emulsion from aw/o microemulsion**. Langmuir, 6(12):1793–1796, 1990.

[110] RODRÍGUEZ-HAKIM, M.; ANAND, S.; TAJUELO, J.; YAO, Z.; KANNAN, A. ; FULLER, G. G.. **Asphaltene-induced spontaneous emulsification: Effects of interfacial co-adsorption and viscoelasticity**. Journal of Rheology, 64(4):799–816, 2020.

[111] MILLER, C. A.. **Spontaneous emulsification produced by diffusion—a review**. Colloids and surfaces, 29(1):89–102, 1988.

[112] MICHELON, M.; LEOPÉRCIO, B. C. ; CARVALHO, M. S.. **Microfluidic production of aqueous suspensions of gellan-based microcapsules containing hydrophobic compounds**. Chemical Engineering Science, 211:115314, 2020.

[113] SHAH, R. K.; SHUM, H. C.; ROWAT, A. C.; LEE, D.; AGRESTI, J. J.; UTADA, A. S.; CHU, L.-Y.; KIM, J.-W.; FERNANDEZ-NIEVES, A.; MARTINEZ, C. J. ; OTHERS. **Designer emulsions using microfluidics**. Materials Today, 11(4):18–27, 2008.

[114] BASHEVA, E. S.; GURKOV, T. D.; IVANOV, I. B.; BANTCHEV, G. B.; CAMPBELL, B. ; BORWANKAR, R. P.. **Size dependence of the stability of emulsion drops pressed against a large interface**. Langmuir, 15(20):6764–6769, 1999.

[115] ZAKI, N.; SCHORIING, P.-C. ; RAHIMIAN, I.. **Effect of asphaltene and resins on the stability of water-in-waxy oil emulsions**. Petroleum science and technology, 18(7-8):945–963, 2000.

[116] AGUILERA, B.; DELGADO, J. ; CÁRDENAS, A.. **Water-in-oil emulsions stabilized by asphaltenes obtained from venezuelan crude oils**. Journal of Dispersion Science and Technology, 31(3):359–363, 2010.